UNIVERSITY OF CALIFORNIA
RIVERSIDE

Design of Robust Feedback Networks From Ultrasensitive Modules

A Dissertation submitted in partial satisfaction
of the requirements for the degree of

Doctor of Philosophy

in

Mechanical Engineering

by

Christian Erik Cuba Samaniego

June 2017

Dissertation Committee:

Dr. Elisa Franco, Chairperson
Dr. Lorenzo Mangolini
Dr. Victor G.J. Rodgers

The Dissertation of Christian Erik Cuba Samaniego is approved:

Committee Chairperson

University of California, Riverside

Acknowledgments

The result of this work is the effort of the many people I have met during my journey at UC Riverside.

I am deeply grateful to my advisor Elisa Franco for coaxing the best out of me by her invaluable guidance on this journey. Without her help, I would not have been here. I am very grateful to Fabio Pasqualetti, who let me join his lab meetings and expand my understanding of control theory in complex networks. I would also like to express my gratitude to Mustafa Khammash for kindly hosting me as a visitor scholar at ETH-Zurich and motivating me to study control systems in living cells. I would also like to thank Lorenzo Mangolini and Victor Rodgers for being on my thesis committee.

I would like to thank Hari Subramanian, Leopold Green and Jaimie Stewart for having the patience to teach me biology during their experiments. I am also thankful to all the members of Khammas' lab, especially to Gabriele Lillacci, Timothy Frei and Briat Corentin for introducing to me several techniques for synthetic biology in bacteria and their valuable analytical feedback during my time in Basel.

I am thankful to all the members of Franco's lab, especially to the BIOMOD team. Their curiosity into synthetic circuits and their inner workings inspired me to learn and understand more so that I could teach them.

I am glad to have met Mika Lai, Damiano La Manna, Gianluca Bianchin, Shiyu Zhao and Rajasekhar Anguluri for our constant discussions of biology and control theory, trips and meetings for lunch.

Finally, I wish to thank my family for their encouragement and support during

this time. I am especially grateful to my parents, sister and aunts for their love and being with me when I need them.

A la memoria de mi madre Celina y familia for todo su apoyo.

ABSTRACT OF THE DISSERTATION

Design of Robust Feedback Networks From Ultrasensitive Modules

by

Christian Erik Cuba Samaniego

Doctor of Philosophy, Graduate Program in Mechanical Engineering
University of California, Riverside, June 2017
Dr. Elisa Franco, Chairperson

Synthetic biology promise to provide solution to many challenges in energy, agriculture, and health by reprogramming cells to execute new tasks in the host organism. In order to do that, it requires (1) the understanding of the design principles that underlie complex dynamics in biology, (2) the development of computational tools that support the identification those principles and (3) the use of those principles and computational tools to guide the experimental implementation of novel biomolecular programs. The main motivation of this thesis is to describe my current progress and future plans to expand (1)-(3).

We incorporate a new design principle, known as ultrasensitivity response, to design robust biomolecular dynamical system. We show that molecular titration in the context of feedback circuits enhance the emergence of oscillations and bistable behavior in the parameter space. We also propose and analyze a new molecular network, termed Brink motif, which exhibits an ultrasensitive input-output response similar to a zero-order ultrasensitive switch. We discuss the Brink motif in the context of robust feedback circuits as a suitable mechanism to build (1) reliable circuits, oscillatory and bistable dynamical behaviors, un-

der parameters uncertainty, downstream load effects and shared resources and (2) robust closed loop controllers that overcome the limitation of unidirectional action controllers. Ultrasensitivity is achieved by combining molecular titration and an activation/deactivation cycle and requires fast titration and switching rates. Additionally, the response of the Brink motif has a precisely tunable threshold, which can be determined by an external input to the motif. We assess the robustness of feedback circuits with numerical simulations and mathematical analysis.

Contents

List of Figures

List of Tables

Chapter 1

Introduction

In 1992, Eric Drexler wrote of tiny molecular robots that could travel inside the body, repair living cells, treat diseases, reverse aging, and make our bodies faster and stronger than before. The scale of those tiny intelligent robots ranged from nanometers to hundreds of microns. Although it sounds as though it belongs to the realm of science fiction, it has become fact. Now it is actually possible to program cells to sense their environment and react by producing specific molecules for biomedical applications.

Ten years later, the new fields of synthetic and systems biology emerged. Engineering intelligent biomolecular systems has enabled the development of many solutions to challenges in agriculture, energy and health, beginning with the implementation of the first three well-known synthetic circuits. In 2000, a toggle switch (memory device) [46], repressilator (autonomous oscillator) [35] and negative feedback [6] (enhance the stability of a circuit in a noisy environment), were all implemented in genetic circuits. A great deal of progress has been made in bacterial and mammalian cells, but lack practical applications

in most cases [33].

Engineering these autonomous and intelligent biomolecular systems (molecular robots) requires (1) the understanding of the design principles that underlie the complex dynamics in biology, (2) the development of computational tools that support the identification of these principles and (3) the use of these principles and computational tools to guide the experimental implementation of novel biomolecular programs. The main motivation of this thesis is to describe my current progress and future plans to expand (1)-(3).

My work aims to understand the feedback principles in biology by designing a variety of simple and detail synthetic circuits that produce dynamical behavior such as oscillations (negative feedback), bistability (positive feedback), a frequency divider (negative/positive feedback) and a robust biomolecular controller (special negative feedback). To do this, I combine different tools from control theory, nonlinear systems, systems biology, and synthetic biology to model, analysis and interpret those principles to address questions such as: How do we automate an oscillator? What are the conditions that raise bistability in a positive feedback loop? What are the working conditions for a frequency divider and its input/output rating to work as such? How can we build robust biomolecular controllers?

In order to build robust biomolecular controllers, we look to digital circuits. Transistors are the key to reliability in digital circuits, applicable to many implementations. A sharp transition is present in the transistor's input/output mapping, known in engineering as a high gain and in biology as an ultrasensitive response. Inspired by this principle, we introduce a new design principle in biomolecular circuits: ultrasensitivity. Our results show that in oscillatory and bistable biomolecular systems, the desired dynamical behavior in-

creases in the parameter space and is robust to parameter variability. Chapter 2 will discuss this in detail.

Mechanisms to incorporate ultrasensitivity into these systems include cooperativity, molecular sequestration and zero-order ultrasensitivity. Although incorporating the first two mechanisms improve the robustness of dynamical circuits, it is not yet reliable enough for use in applications. Zero-order ultrasensitive mechanisms are also ideal for designing circuits and are present in a variety of dynamical circuits found in nature. However, it is very challenging to work with synthetic circuits, and so we introduce a new network motif, named the Brink Motif. In Chapters 2 and 3, we use the Brink Motif to produce an ultrasensitive response and analyze it in the context of oscillatory and bistable biomolecular networks. Our results show very robust dynamical circuits with respect to parameter variability and perform reliably under shared resource conditions.

Synthetic Biology has the potential to deliver valuable real-world applications and requires biomolecular feedback controllers to do so. In Chapters 4 and 5, we propose the use of the Brink Controller to design a robust closed loop control for biomolecular systems. Our results suggest that the key requirement for robust tracking and constant disturbance rejection in the system is an ultrasensitive steady state.

1.1 Contribution

Chapter 2: Elisa Franco developed the initial design idea. Christian Cuba Samaniego executed the analysis and numerical simulations. Franco Blanchini and Giulia Giordano focused on the technical results. Jongmin Kim discussed the result in a biological

context [28].

Chapter 3: Franco Blanchini and Giulia Giordano suggested the oscillator. Christian Cuba Samaniego executed the analysis and numerical simulations. Elisa Franco focused on the technical results [26].

Chapter 4: Christian Cuba Samaniego developed the initial design idea and executed the analysis and numerical simulations. Elisa Franco and Christian Cuba Samaniego focused on the technical results. Hari Subramanian provided feedback on the CRISPR/Cas system. Christian Cuba Samaniego interpreted the results in a biological context [30].

Chapter 5: Christian Cuba Samaniego developed the initial design idea and executed the analysis and numerical simulations. Elisa Franco and Christian Cuba Samaniego focused on the technical results and interpreted the result in a biological context [25].

Chapter 6: Christian Cuba Samaniego developed the initial design idea and executed the analysis and numerical simulations. Elisa Franco and Christian Cuba Samaniego focused on the technical results and interpreted the results in a biological context.

1.2 Support

My graduate studies at U.C. Riverside were supported by Dean's Distinguished Fellowship Award, National Science Foundation through grant CMMI-1266402 and the Department of Energy under grant DE-SC0010595.

Chapter 2

Molecular titration enhances robustness to parameter variability in oscillatory and bistable minimal networks

2.1 Results

In this chapter we show that biomolecular processes driven by monomeric regulators can be combined to obtain oscillations and bistability. We consider minimal systems whose output can be repressed or activated by an increase in input monomers. These monomers bind to and control the production rate of a target molecule that represents the module output; the monomer input can be titrated by competing species that serve as

constitutive activators or inhibitors. By modulating the parameters of the titration process we can control the steady state and the temporal response of the modules. In particular, we show the total concentration of titrating species modulates the steady state response threshold (or "dead-zone") and the delay in the temporal response; the titration reaction rate speed influences the steepness of the on/off transitions in the steady state and transient response.

We interconnect modules to form canonical signal generators in biomolecular systems. Oscillators are important in biological organisms because they drive and synchronize the activity of downstream pathways [47]. Timing signals are needed for synthetic molecular systems as well, and many artificial oscillators have been built *in vivo* [36, 5, 45, 85, 89, 31] and *in vitro* [51, 42, 65]. Bistable systems are equally relevant as they achieve robust on-off behaviors and serve as memory elements in signal transduction and developmental networks[38, 2], as well as being important components in artificial systems[46, 5, 53, 70].

Our approach combines numerical simulations and rigorous mathematical analysis. The models we consider have many parameters, and it is desirable to establish what their admissible dynamic behaviors are in a wide range of parameter variability, or – ideally – for arbitrary parameter choices. We employ control and dynamical systems methods and identify stability and monotonicity[2, 4] properties of the inhibited and activated modules; we say these properties are structural because they do not depend on the specific parameters chosen[10]. When these modules are interconnected to form a negative or a positive feedback loop, we can conclude that they can exclusively admit instability of oscillatory or bistable nature (respectively). Simulations are required to identify parameter values yielding the

desired dynamics: we numerically integrate the models of the candidate dynamic networks and study the parameter range in which the desired behavior is achieved. The simulations reveals that direct titration is not necessary to achieve oscillations and bistability, but it significantly enhances their robustness to parameter variability.

2.1.1 Minimal inhibited and activated modules

We consider molecular modules where monomeric activators and inhibitors compete to determine the fraction of a target that is in an active (X_T) or inactive (X_T^*) state. We say that our models are minimal because activators and repressors are monomeric, and regulatory reactions are solely uni- and bi-molecular. In the rest of this paper we indicate a chemical species with an uppercase letter, and its concentration with the corresponding lowercase letter (*e.g.* species A has concentration a).

An inhibited module is composed of the target X_T, a constitutive activator X_A, and is regulated by the inhibiting species R_I (2.1 A). Similarly, an activated module is composed of the target X_T, a constitutive inhibitor X_I, and an activator R_A (2.1 F). We assume that the total concentration of target is constant: $x_T + x_T^* = x_T^{tot}$ at any point in time. This assumption is reasonable if the target is, for instance, a gene whose copy number is constant. Similarly, we assume that the total concentration of constitutive inhibitor and constitutive activator are constant in each module; in other words, we assume that the timescale of their production and degradation is much slower than the regulatory reactions within the modules, and can thus be neglected for the purpose of our analysis. Like the target X_T, the constitutive inhibitor X_I and activator X_A switch between a functional and inert state while their total concentrations remain constant. This assumption is handy

because it allows us to examine the behavior of each system treating the total concentration of constitutive activator/inhibitor species as a design parameter. The inert constitutive activators/inhibitors are converted back to their active form at a constant rate. Finally, we assume that the activators and inhibitors R_A and R_I are produced by "input" species U_A and U_I respectively, and are degraded at a constant rate.

The regulators R_I and R_A bind directly to their target X_T controlling the amount of its active fraction. In addition, we also consider the case where regulators can bind to the constitutive inhibitor or activator: these interactions result in titration of the regulators available for direct target binding. Inhibitor R_I binds to active target X_T, converting it to inactive target X_T^* and releasing inert constitutive activator X_A^*; however, R_I also binds to free X_A, yielding an inert complex X_A^* where R_I is sequestered. A large amount of free X_A in solution can thus titrate R_I, delaying inhibition of the target. The activated module works in a similar manner. In practice, X_I and X_A could be proteins or RNA species designed to bind to and titrate the input regulators R_A and R_I respecitvely[**?**, 41]. We refer to these reactions as "direct titration" or simply titration. The reactions between regulators R_I and R_A, and the complexes X_A and X_I bound to targets X_T^* and X_T, respectively, can be classified as titration reactions as well, but in this context we refer to them as "indirect titration". Molecular titration is a well known mechanism to generate ultrasensitivity and delays [19, 18]; we will describe how these properties can be achieved and tuned by controlling the direct titration reaction.

The reactions defining each module are listed below. (For simplicity we denote

reaction rates with the same symbols when they have the same function in the two modules.)

	Inhibited module		**Activated module**
Activator:	$X_T^* + X_A \xrightarrow{\alpha} X_T$	Inhibitor:	$X_T + X_I \xrightarrow{\delta} X_T^*$
Inhibitor:	$U_I \xrightarrow{\beta} U_I + R_I$	Activator:	$U_A \xrightarrow{\beta} U_A + R_A$
Inhibition:	$X_T + R_I \xrightarrow{\delta} X_T^* + X_A^*$	Activation:	$X_T^* + R_A \xrightarrow{\alpha} X_T + X_I^*$
Direct titration:	$X_A + R_I \xrightarrow{\nu} X_A^*$	Direct titration:	$X_I + R_A \xrightarrow{\nu} X_I^*$
Recovery:	$X_A^* \xrightarrow{\kappa} X_A$	Recovery:	$X_I^* \xrightarrow{\kappa} X_I$
Degradation:	$R_I \xrightarrow{\phi} \emptyset$	Degradation:	$R_A \xrightarrow{\phi} \emptyset$

Because the total concentration of species X_T, X_I, and X_A is constant, we can write the following mass conservation equalities: $x_T^{tot} = x_T + x_T^*$, $x_I^{tot} = x_I + x_I^* + x_T^*$, and $x_A^{tot} = x_A + x_A^* + x_T$. 2.1 A and F show a graphical representation of the two modules and their reactions. Using the law of mass action and the mass conservation equalities, we obtain the following model for the inhibited module:

$$\dot{x}_T = \alpha(x_T^{tot} - x_T)x_A - \delta x_T r_I \tag{2.1}$$

$$\dot{x}_A = \kappa(x_A^{tot} - x_A - x_T) - \alpha(x_T^{tot} - x_T)x_A - \boxed{\nu x_A r_I} \tag{2.2}$$

$$\dot{r}_I = \beta u_I - \phi r_I - \delta x_T r_I - \boxed{\nu x_A r_I}. \tag{2.3}$$

The differential equations describing the activated module are:

$$\dot{x}_T = \alpha(x_T^{tot} - x_T)r_A - \delta x_T x_I \tag{2.4}$$

$$\dot{x}_I = \kappa(x_I^{tot} - x_I - (x_T^{tot} - x_T)) - \delta x_T x_I - \boxed{\nu x_I r_A} \tag{2.5}$$

$$\dot{r}_A = \beta u_A - \phi r_A - \alpha(x_T^{tot} - x_T)r_A - \boxed{\nu x_I r_A}. \tag{2.6}$$

Boxes highlight terms associated with the titration reactions between constitutive activators/inhibitors and the input regulators. Before exploring numerically the behavior of these differential equations, we point out some important properties of the stationary and transient behavior of these systems.

Boundedness of the solutions, monotonicity of the equilibrium input/output maps, monotonicity of the linearized dynamics, and unconditional stability are all important properties when considering these modules in the context of larger circuits[3, 10]. The fact that these properties hold for (nearly) arbitrary choices of parameters indicates that our minimal systems may be treated as input/output "gray box" modules. These modules can be interconnected creating predictable, robust feedback loops whose net positive or negative sign does not depend on the parameters. More detail can be found in [28].

2.1.2 The concentration of titrating species modulates the dose response threshold and the delay of the time response.

Using the parameters reported in Table 2.1, we numerically solved the differential equations describing the inhibited and the activated modules, examining their steady state (Fig. 2.1 B, C, G, H) and their transient response (Fig. 2.1 D, E, I and J). The steady state fraction of active target x_T/x_T^{tot} shows a Hill-type dose response to the concentration of species U_A or U_I that produce the regulator; the response threshold can be increased by increasing the total concentration of constitutive activator or inhibitor (titrating species). For example, Fig. 2.1 B shows that the steady state fraction of active target decreases as the concentration of U_I (the species producing inhibitor) increases; as the concentration of

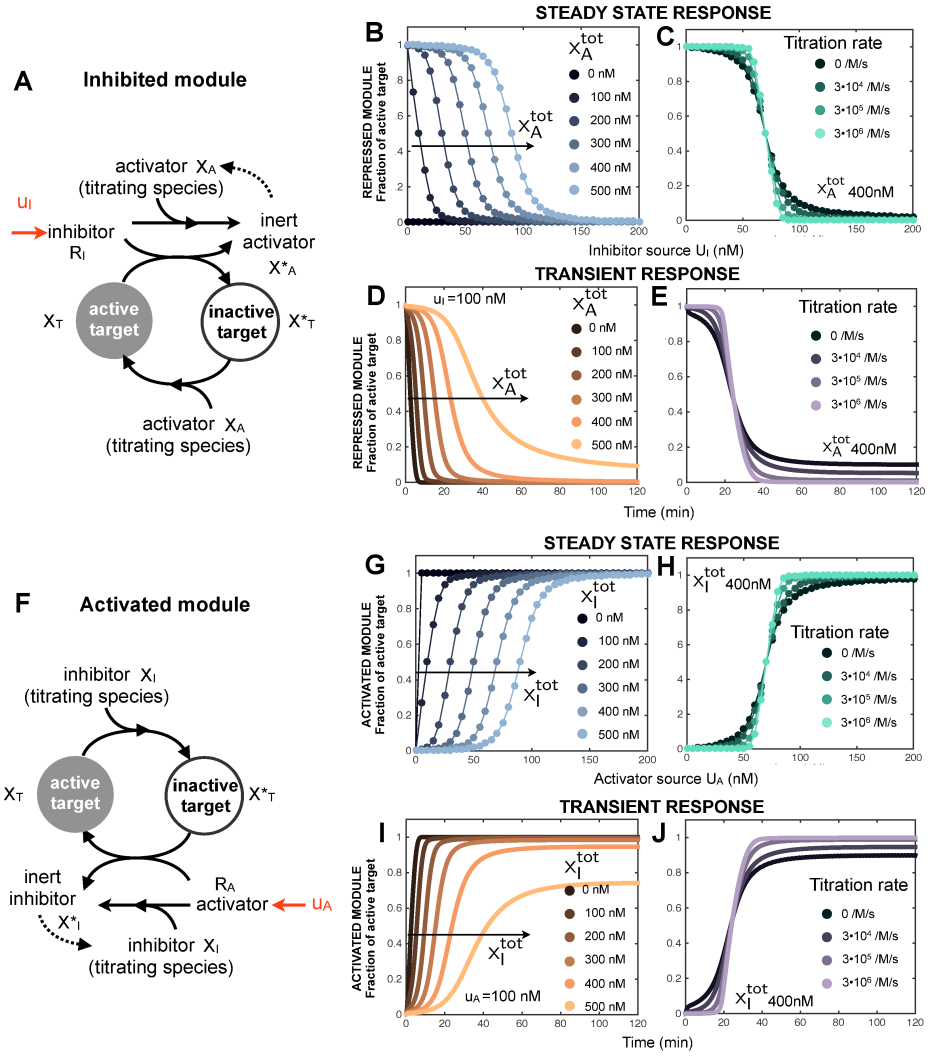

Figure 2.1: Stationary and transient behavior of the inhibited and activated modules described in 2.1.1. A: Scheme of the inhibited module. B: Steady state fraction of target X_T as a function of the input u_I (source of inhibitor R_I), for varying amounts of total constitutive activator X_A. By increasing x_A^{tot} we move the "dead zone" of the response to the right. C: Steady state fraction of active target as the titration rate ν varies, for $x_A^{tot} = 400$ nM; a large titration rate corresponds to a sharper on-off transition. D: Transient response of the active fraction of x_T for varying amounts of x_A^{tot}; large x_A^{tot} introduces a delay in the time it takes for the system to reach steady state. E: The transient response of the activated module (active fraction of x_T) shows a sharper transition for large titration rate ν. F: Scheme of the activated module. G: Steady state fraction of target x_T as a function of u_A, for varying amounts of x_I^{tot}. H: Steady state response of the inhibited module, with increasing titration rate ν, and $x_I^{tot} = 400$ nM. I: Transient response of the active fraction of x_T in the inhibited module as a function of x_I^{tot}, showing how delay is increased. J: Transient response of the inhibited module (active fraction of x_T); the transition is sharper as the titration rate ν increases.

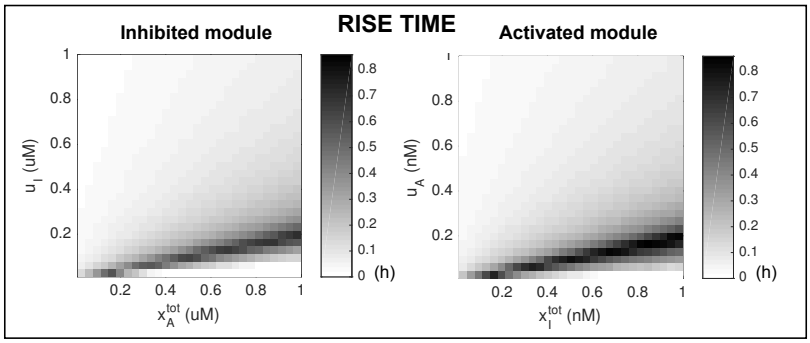

Figure 2.2: Rise time of the active fraction of target in the inhibited and activated module. A significant increase in rise time occurs for low values of the input source, and large concentration of constitutive activator/inhibitor. Below a certain concentration threshold of u_I and u_A, the rise time is small because the target is not affected by activation and inhibition reactions.

constitutive activator (titrating species) is increased up to 500 nM, the inhibition threshold moves to the right reaching about 100 nM. A similar behavior is observed for the activated module in Fig. 2.1 G. The dynamical effect of an increase in titrating species concentration is a temporal delay in reaching steady state, as shown in Fig. 2.1 D and I; for the reaction rates chosen in this example, the delay can reach 25-30 minutes. We numerically explored the role of the titration reaction rate, whereby constitutive activators and inhibitors sequester available regulator input. While the titration reactions are not required to obtain the qualitative threshold-dependent dose response and the time delay, their presence sharpens both responses. As shown in Fig. 2.1 C and H, the larger the titration rate the sharper is the transition between on and off modules at steady state, once a certain U_I or U_A input threshold is reached. Fig. 2.1 E and J show that the temporal switch between fully on and fully off states of the target becomes sharper as the titration rate increases. We remark that in the absence of titration ($\nu = 0$) the systems still exhibit a dose response threshold and a delay in the time response; large values of ν yield sharper nonlinear behaviors, in

Table 2.1: Parameters for the inhibited system equations (2.1)-(2.3) and for the activated system equations (2.4)-(2.6)

Rate	Description	Value	Other studies
α (/M/s)	Activation	$3 \cdot 10^5$	Bimolecular reactions
δ (/M/s)	Inhibition	$3 \cdot 10^5$	Nucleic acids: $10^4 - 10^6$ Refs.[53, 97]
ν (/M/s)	Titration rate	$3 \cdot 10^5$	Protein/Protein: $10^4 - 10^6$ Refs.[79, 80]
β (/s)	Production of regulator	$5 \cdot 10^{-3}$	RNA: $10^{-3} - 1$ Refs.[91, 22] Proteins: $3 \cdot 10^{-3} - 1$ Refs.[19]
κ (/s)	Recovery of titrating	$1 \cdot 10^{-3}$	RNA: $10^{-5} - 10^{-2}$ Refs.[7, 22]
ϕ (/s)	Degradation of regulator	$1 \cdot 10^{-3}$	Proteins: $10^{-4} - 10^{-3}$ Refs.[19]

particolar increased ultrasensitivity and faster temporal switch in activity.

To characterize the dynamic response of the modules we integrated the differential equations varying the signal source, target and titrating species concentration. As a measure of the delay, we then quantified the rise time of the target response, defined as the time it takes for the target concentration to reach 60% of its steady state value. Results are shown in Fig. 2.2: the rise time is most dramatically influenced by the concentration of titrating species, and increases proportionally to it; as expected, the rise time is reduced by increasing the concentration of source signal.

In summary, by modulating the concentration of titrating species and the titration rate, we can control the characteristics of both the dynamic and the steady state response of each modules. Specifically, we can determine the threshold and steepness of the steady state nonlinearity, and we can modulate the delay of the temporal response. These features are essential to build complex dynamical systems using the titration-based modules as components.

2.1.3 The feedback interconnection of inhibitor and activator modules creates a negative feedback loop and is a structural oscillator

By interconnecting the inhibited and the activated module described in the previous sections, we create a negative feedback loop circuit and explore its capacity to exhibit oscillations. A scheme of the interconnection is shown in Fig. 2.3 A. The differential equations of the oscillator are:

$$\dot{z}_T = \alpha_z(z_T^{tot} - z_T)x_{R,A} - \delta_z z_T\, z_I, \tag{2.7}$$

$$\dot{z}_I = \kappa_z(z_I^{tot} - z_I - (z_T^{tot} - z_T)) - \delta_z z_T\, z_I - \nu_z x_{R,A}\, z_I, \tag{2.8}$$

$$\dot{x}_{R,A} = \beta_x x_T - \alpha_z(z_T^{tot} - z_T)\, x_{R,A} - \nu_z x_{R,A}\, z_I - \phi_x x_{R,A}, \tag{2.9}$$

$$\dot{x}_T = \alpha_x(x_T^{tot} - x_T)x_A - \delta_x x_T\, z_{R,I}, \tag{2.10}$$

$$\dot{x}_A = \kappa_x(x_A^{tot} - x_A - x_T) - \alpha_x(x_T^{tot} - x_T)\, x_A - \nu_x x_A\, z_{R,I}, \tag{2.11}$$

$$\dot{z}_{R,I} = \beta_z z_T - \delta_x x_T\, z_{R,I} - \nu_x x_A\, z_{R,I} - \phi_z z_{R,I}. \tag{2.12}$$

The equations are ordered to highlight two groups of variables: z_T, z_I, $x_{R,A}$ and x_T, x_A, $z_{R,I}$. The first group represents the inhibited subsystem, the second group represents the activated subsystem (Fig. 2.3 A). First, we establish mathematically that this system has the correct structure to oscillate, and that its only admissible transition to instability is oscillatory. Second, we characterize the circuit behavior as a function of the concentration of titrating species (constitutive activator and inhibitor), of titration reaction rate, and production rate of regulators.

Structural analysis

The oscillator is designed to have a negative feedback loop, which is generally a necessary (not sufficient) condition for oscillations. However, equations (2.7)–(2.12) are nonlinear ODEs with 16 parameters, which makes the system quite complex: it is reasonable to ask what dynamic behaviors are admissible when the parameter values are varied. In addition to verifying that the system can oscillate with numerical analysis (shown in the next section), it is possible to establish analytically that – depending on the chosen parameters – this model either behaves as an oscillator, or as a system with a unique, stable equilibrium point. We can exclude multiple equilibria. We can reach this conclusion following different routes.

In the absence of titration reactions, the system is the negative feedback interconnection of two unconditionally stable monotone subsystems (Section 3 of the SI). In Fig. 2.3 A, the monotone subsystems are highlighted by gray boxes; the target species x_T and z_T generate a single negative loop between the modules (orange lines). The equilibrium conditions (derived analytically for each module) intersect in a single point for arbitrary choices of the parameters. Due to the boundedness of the solution of each subsystem, the solution of ODEs (2.7)–(2.12) is also bounded and we can identify a "box" in the space of concentrations where the solution is trapped. These properties (together with other mild assumptions listed in Sections 1 and 2 of the SI in [28]), imply that the only type of transition to instability admitted by this system is oscillatory: in other words, by changing one or more parameters (reaction rates or total concentrations), we can push the only equilibrium admitted by the system to become unstable, and this transition is driven by a pair of com-

plex conjugate eigenvalues which correspond to an oscillating solution. This is a behavior akin to the well-known Hopf bifurcation. We say that this is a strong candidate oscillator (Proposition 17, Section 3.1 of the SI in [28]), because the only admissible transition to instability is oscillatory [10]. This is a structural property, in the sense that it does not depend on the chosen system parameters.

When titration reactions are present the system is still a strong candidate oscillator, even though the inhibited and activated module lose their structural monotonicity properties (Section 3.2 of the SI in [28]). This can be demonstrated by computing explicitly the characteristic polynomial of the Jacobian matrix: because its coefficients are all positive (for any value of the parameters and equilibria), it cannot have positive real roots (Proposition 18, Section 3.2 of the SI in [28]). Thus, unstable eigenvalues must be complex conjugate and this implies that transitions to instability can only be oscillatory. (This approach can be also applied to the system in the absence of titration reactions.)

Numerical analysis

We integrate the differential equations (2.7)–(2.12) numerically, and we test the capacity of the system to oscillate when certain parameters are varied. First, we randomly varied reaction rates and total concentrations of species[24, 15] (Section 3.3.1 of the SI), and we used that infomation to identify a nominal set of parameters (Table 2.2) that yields oscillations with a period of roughly one hour, as shown in Fig. 2.3 B. Equilibrium conditions intersect at a single equilibrium point, as expected based on our analytical derivations (Fig. 2.3 C).

Varying the concentration of titrating species affects both the amplitude and the

frequency of oscillation (Fig. 2.3 B): in particular, the higher x_A^{tot} and z_I^{tot}, the larger the amplitude of oscillations. This is likely a consequence of two phenomena: the first is the temporal delay observed when the titrating species concentration increases in each module (Fig. 2.1 D, I and Fig. 2.2 A and B); the the second is the steady state response threshold directly proportional to the titrating species concentration (Fig. 2.1 B, G). We explored systematically period and amplitude as a function of x_A^{tot} and z_I^{tot} in Fig. 3.8 A, for varying strength of the titration rate which we assumed for simplicity to be identical in both subsystems ($\nu = \nu_x = \nu_z$). All the other parameters are chosen as in Table 2.2. In this figure, we computed period and amplitude numerically from trajectories integrated for 20 hours. These plots include also slowly damped oscillations; the region where oscillations are sustained (found as the area where the eigenvalues of the Jacobian are complex with positive real part) is inside the cyan contour. In the space x_A^{tot} and z_I^{tot}, the region where oscillations are detected becomes larger as the titration rate is increased. This is likely caused by the fact that a large titration rate sharpens the stationary and dynamic response of each module. It is worth noting that the concentration of titrating species promotes oscillations only in a certain range, which may change depending on the nominal operating point; both excess or lack of x_A^{tot} and z_I^{tot} can cause loss of oscillations.

We also varied the total concentration of targets x_T^{tot} and z_T^{tot}, and observed that the system is very sensitive to variations in the total concentration of inhibited target x_T^{tot}, which is the species responsible for creating negative feedback; in contrast, the system is robust to variations in the total concentration of activated target z_T^{tot}, as shown in Fig. 3.8 B.

The production rate of each regulator species is another particularly important parameter: the feedback interconnection of the two linearized subsystems is defined primarily by β_x and β_z, which can be thought of as parameters that control the "loop gain" of the system. This is evident from the Jacobian matrix of the system, where two blocks are interconnected precisely by β_x and β_z (SI Section 3.1.2 and 3.2.2 in [28]). The oscillatory region in the β_x-β_z space is also increased when the titration rate is higher.

While the period is only moderately affected by the variations we considered, the amplitude changes more significantly. A complete analysis of the oscillatory regions as a function of all the system parameters is presented in the SI, Section 3.3.2 in [28]. Increasing the titration rate always expands the parameter areas where oscillations are observed (Figures S2 and S3 in [28]).

Table 2.2: Nominal parameters for the oscillator

Rate	Value	Rate	Value
α_z (/M/s)	$75 \cdot 10^3$	α_x (/M/s)	$3 \cdot 10^5$
δ_z (/M/s)	$3 \cdot 10^5$	δ_x (/M/s)	$3 \cdot 10^5$
ν_z (/M/s)	$3 \cdot 10^5$	ν_x (/M/s)	$3 \cdot 10^5$
β_z (/s)	$5 \cdot 10^{-3}$	β_x (/s)	$2 \cdot 10^{-2}$
κ_z (/s)	$1 \cdot 10^{-3}$	κ_x (/s)	$1 \cdot 10^{-3}$
ϕ_z (/s)	$1 \cdot 10^{-3}$	ϕ_x (/s)	$1 \cdot 10^{-3}$
z_T^{tot} (nM)	250	x_T^{tot} (nM)	120
z_I^{tot} (nM)	700	x_A^{tot} (nM)	300

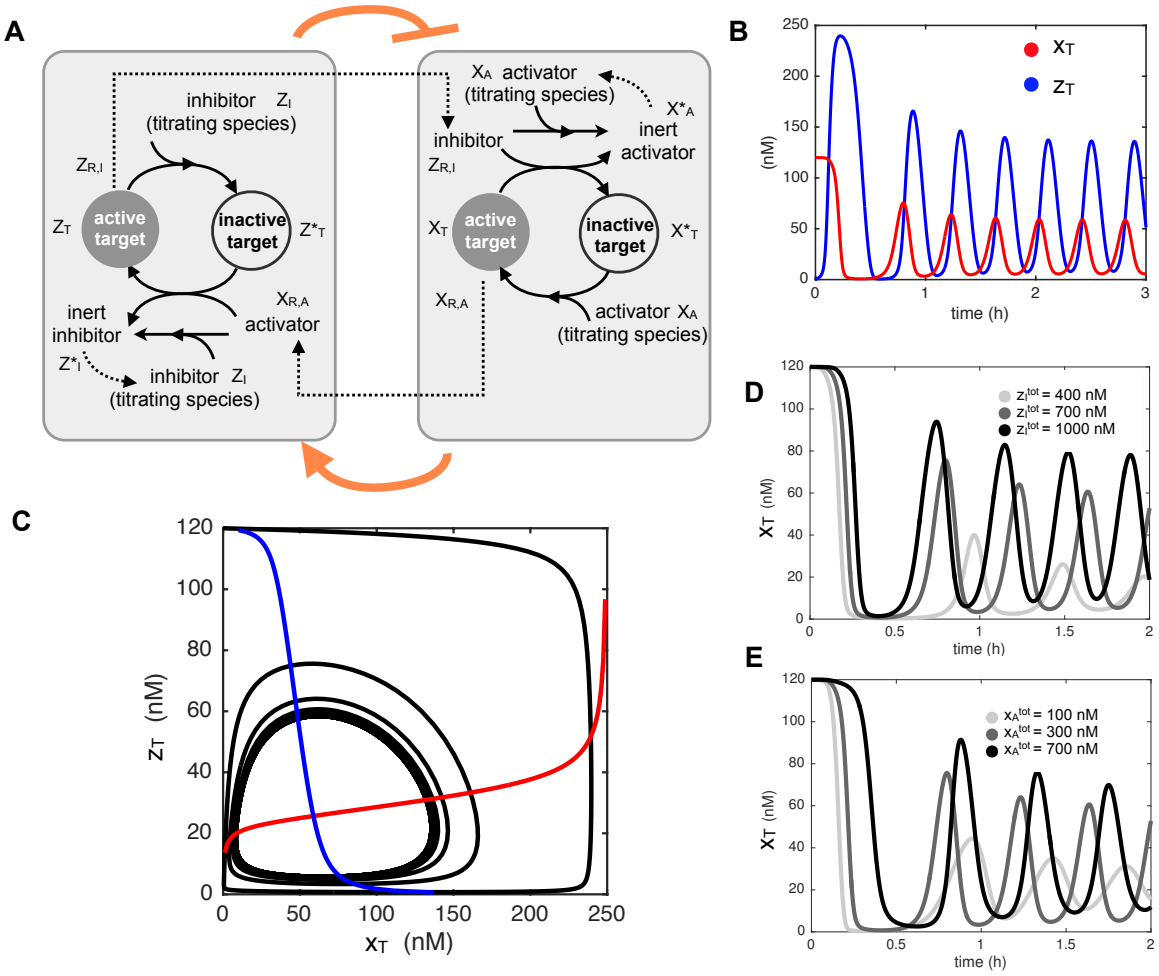

Figure 2.3: A: Schematic of the oscillator system built by interconnecting an inhibited and an activated module. B: Trajectories of the target species when equations (2.7)–(2.12) are integrated using nominal parameters (Table 2.2). C: Trajectories in panel B overlapped with the system equilibrium equations (Section 3.2 of the SI file [28]). D and E: Trajectories of the target species for variable concentrations of constitutive activators and inhibitors, obtained by integrating equations (2.7)–(2.12) using nominal parameters (Table 2.2). The concentration of titrating species affect primarily the amplitude of the oscillations.

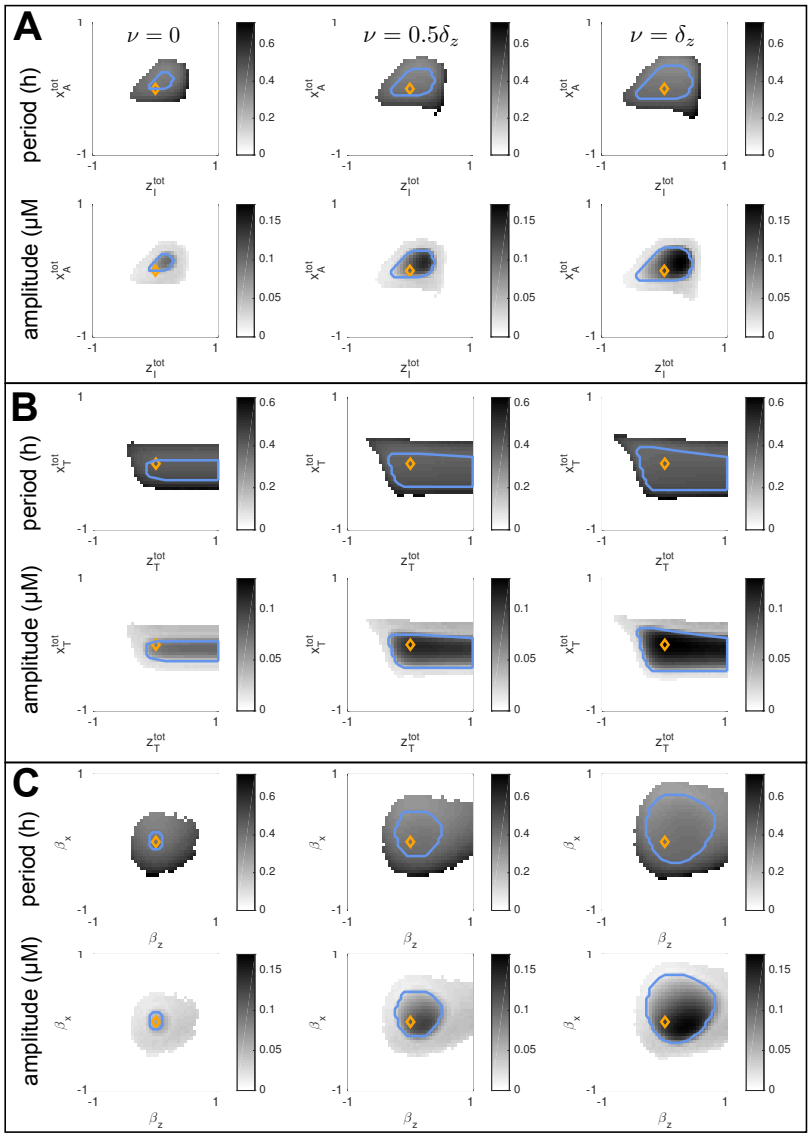

Figure 2.4: Period and amplitude of the oscillations when key parameters are varied near their nominal value (2.2), for increasing value of the titration rates. Axes are in log scale; parameters are varied between one tenth and ten times their nominal value. Oscillations (sustained or damped) occur in the gray areas; the cyan contour indicates the region of sustained oscillations (the linearized system has dominant unstable complex conjugate eigenvalues); the orange diamond indicates the nominal value of the parameters. A: Variation of the concentration of constitutive activators and inhibitors x_A^{tot} and z_I^{tot}. B: Variations of total target concentrations x_T^{tot} and z_T^{tot}. The system is robust to variations in the target molecule of the activated subsystem. C: Variations of the production rates of regulators, which control primarily the strength of the feedback loop. In all cases, a larger titration rate expands the oscillatory regions.

2.1.4 Mutually inhibiting modules create a positive feedback loop and a structural bistable system

Two inhibited modules can be mutually interconnected by designing the output of one module to be the inhibitor input of the other, as sketched in Fig. 2.5 A. The differential equations are:

$$\dot{z}_T = \alpha_z(z_T^{tot} - z_T)z_A - \delta_z z_T x_{R,I}, \tag{2.13}$$

$$\dot{z}_A = \kappa_z(z_A^{tot} - z_A - z_T) - \alpha_z(z_T^{tot} - z_T)z_A - \nu_z x_{R,I} z_A, \tag{2.14}$$

$$\dot{x}_{R,I} = \beta_x x_T - \delta_z z_T x_{R,I} - \phi_x x_{R,I} - \nu_z x_{R,I} z_A, \tag{2.15}$$

$$\dot{x}_T = \alpha_x(x_T^{tot} - x_T)x_A - \delta_x x_T z_{R,I}, \tag{2.16}$$

$$\dot{x}_A = \kappa_x(x_A^{tot} - x_A - x_T) - \alpha_x(x_T^{tot} - x_T)x_A - \nu_x x_A z_{R,I}, \tag{2.17}$$

$$\dot{z}_{R,I} = \beta_z z_T - \delta_x x_T z_{R,I} - \phi_z z_{R,I} - \nu_x x_A z_{R,I}. \tag{2.18}$$

As done for the oscillator, the variables have been grouped as z_T, z_A, $x_{R,I}$ and x_T, x_A, $z_{R,I}$ to separate the two inhibited subsystems (Fig. 2.5 A). The list of chemical reactions is reported in the SI, Section 4. In the next sections, first we establish if this system has the capacity to exhibit multistationary behaviors. Then, we explore the bistability regions as a function of various species concentrations and of the titration rate. Fast titration reaction rates always yield larger bistability regions, although this effect is less prominent than in the oscillator.

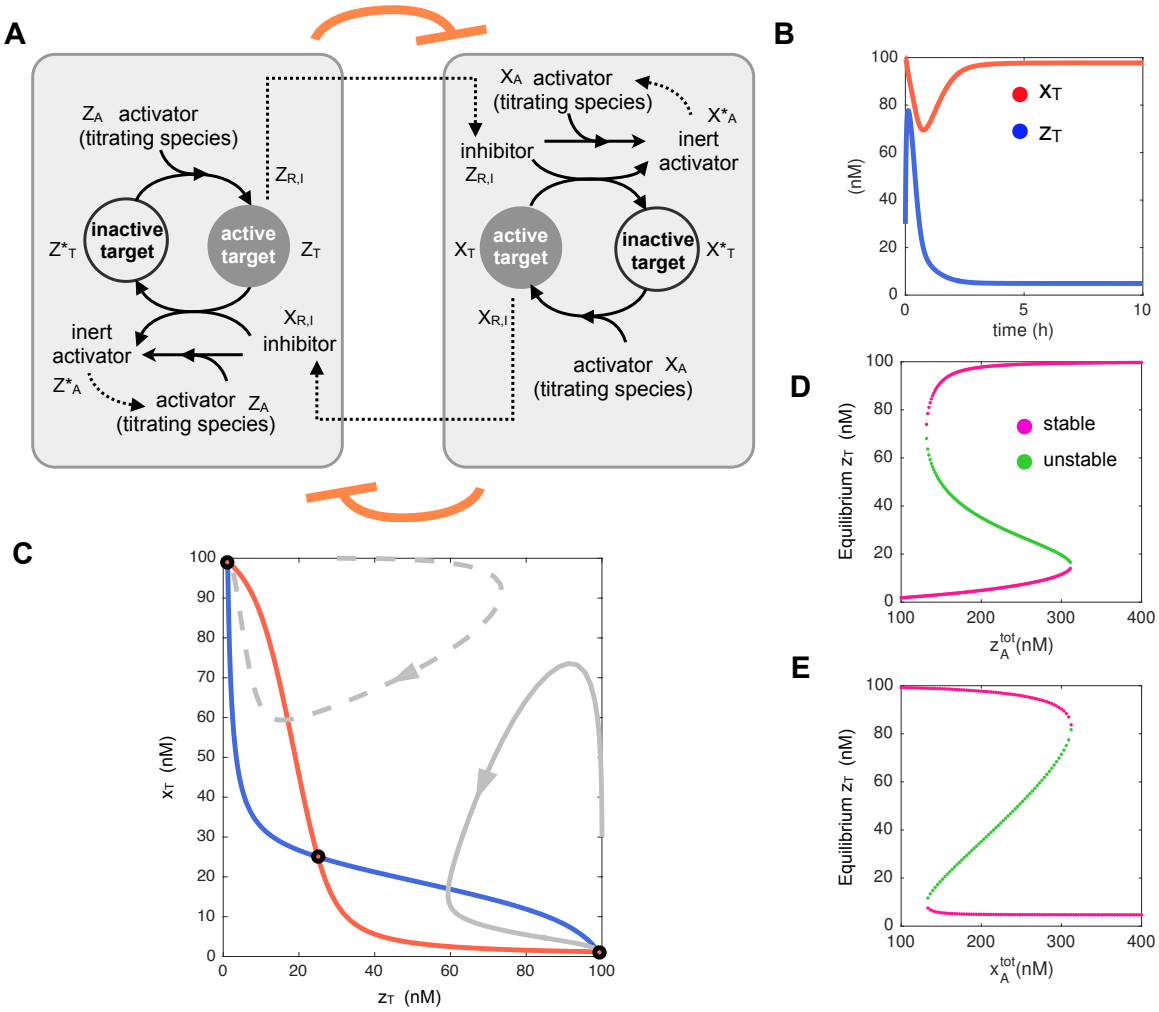

Figure 2.5: A: Schematic of the bistable system built by interconnecting two inhibited modules. B: Trajectories of the target species when equations (2.13)–(2.18) are integrated using nominal parameters (Table 2.3). C: Trajectories in panel B (solid grey lines) overlapped with the system equilibrium equations (Section 4.2 of the SI file [28]). D and E: Bifurcation diagram of equations (2.13)–(2.18) using nominal parameters (Table 2.3) for varying concentrations of the two constitutive activators.

Structural analysis

As for the oscillator circuit, model (2.13)–(2.18) is quite complex: nevertheless, we can establish mathematically that for appropriate choices of parameters, the system either presents a single stable equilibrium or more than one stable equilibrium (accompanied by the emergence of unstable equilibria) where the dominant eigenvalue is real. There is no choice of the parameters that will make the system oscillate. In fact, the two inhibited modules in the absence of titration reactions are both unconditionally stable, their solutions are bounded, and they are input-output monotone systems (SI Section 2.1 and 2.2 [28]). The two monotone modules are connected via a single positive feedback loop; in Fig. 2.5 A, the modules are represented by components in the gray boxes; the positive feedback loop is generated by the target species and is highlighted with the orange lines. The properties satisfied by the modules imply that their interconnection (2.13)–(2.18) can only undergo real transitions to instability [10]; this kind of instability is related to the well-known saddle-node bifurcation. We say that this system is a strong candidate bistable system (Proposition 20 in the SI, Section 4.1.2 [28]): no matter how its reaction rates and total component concentrations are varied, the system dynamics are restricted to be either bistable or monostable.

In the presence of titration reactions, we cannot reach the same analytical conclusions without making assumptions on the region where the system equilibria fall (which depends on the specific choice of parameters). However, numerical simulations presented in the next section show that the presence of titration reactions expands the bistability region of the system significantly.

Numerical analysis

We identified a set of nominal parameters (Table 2.3) via a preliminary randomized exploration[24, 15] of the parameter space (SI Section 4.3.1 [28]), where for simplicity we assumed the two subsystems have the same parameters. The trajectories of x_T and z_T obtained with the nominal parameter set are shown in Fig. 2.5 B, and their behavior in phase space is shown in Fig. 2.5 C. When we vary the concentration of the titrating species near their nominal values, we obtain bifurcation diagrams that clearly show the coexistence of three equilibria, of which two are stable and one is unstable, as shown in Fig. 2.5 D and E.

We then explored bistability trends in the region near the nominal parameters (Table 2.3). Bistability regions were computed by numerically finding the intersections of the equilibrium conditions, and then checking the magnitude of the eigenvalues of the Jacobian matrix computed at the equilibrium (see SI, Section 4.3.2 for further details [28]). In Fig. 2.6 we vary the concentration of titrating species, of targets, and the regulator production rates (all other parameters are kept constant as in Table 2.3). First of all, we note that in the absence of titration reactions ($\nu_x = \nu_z = 0$), the system becomes very sensitive to variations in the concentration of titrating species, and the region of bistability is very narrow; this limitation can be relaxed by increasing the titration rate (Fig. 2.6 A). In contrast, the concentration of target species can significantly vary without affecting bistability, and again a fast titration rate expands the bistable region. Similarly, changes in the regulator production rates (which determine the strength of the feedback loop) are tolerated in a reasonably large range, as long as the rates remain large. As in the oscillator,

increasing the titration rate always broadens the bistable regime; this is verified numerically for all other parameters in the system (SI, Section 4.3.2, Figures S5 and S6 [28]).

Table 2.3: Nominal parameters for the bistable system

Rate	Value
$\alpha_z = \alpha_x$ (/M/s)	$3 \cdot 10^4$
$\delta_z = \delta_x$ (/M/s)	$3 \cdot 10^4$
$\nu_z = \nu_x = \delta_z$ (/M/s)	$3 \cdot 10^4$
$\beta_z = \beta_x$ (/s)	0.0021
$\kappa_z = \kappa_x$ (/s)	$3 \cdot 10^{-4}$
$\phi_z = \phi_x$ (/s)	$1 \cdot 10^{-3}$
$z_T^{tot} = x_T^{tot}$ (nM)	100
$z_A^{tot} = x_A^{tot}$ (nM)	200

2.2 Discussion and Conclusions

We have demonstrated that biomolecular modules regulated by monomeric inputs can be successfully interconnected to build two essential circuit components: an oscillator and a bistable switch. We considered deterministic ODE models of these modules, which are composed by a target molecule and by its constitutive regulators (activators or inhibitors); input regulators compete with the constitutive regulators, which act as titrating species for the input, to determine the active or inactive state of the target. The steady state and transient response of the target molecule concentration can be finely tuned by appropriate design of the titration rate and the concentration of the titrating species. Specifically, these parameters determine the "dead-zone" and steepness of the on/off transitions in the steady state dose response, and the speed and delay of the dynamic response, which promote the emergence of oscillations and bistability when modules are interconnected in feedback loops.

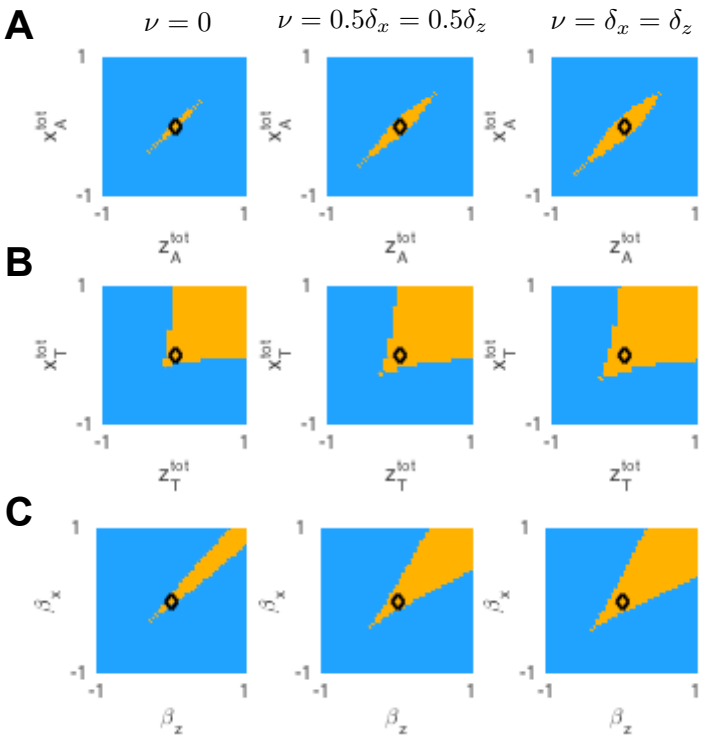

Figure 2.6: Regions of bistability near the nominal parameters (2.3) for increasing value of the titration rates; we assume the two inhibited subsystems have identical parameters for simplicity. Axes are in log scale; parameters are varied between one tenth and ten times their nominal value. A: Variations in the concentration of constitutive activators; the bistability region is very narrow, but can be expanded by increasing the titration rate. B: Bistability region as a function of the total target concentration. C: Bistability region as a function of the regulator production rates β_x and β_z which control the strength of the feedback loop (Section 4 of the SI [28]).

One important finding is that, although direct titration reactions significantly increase the probability of the circuits to oscillate or have multiple steady states, they are not strictly necessary to provide the systems with the capacity for these complex behaviors.

Our numerical simulations are accompanied by rigorous mathematical analysis: we show that the modules and their interconnections have many important properties that do not depend on the model parameters (reaction rates and total concentrations of components). We say our analysis is structural precisely because it allows us to establish properties of the systems that hold for arbitrary parameter values; this approach can yield useful insights in nonlinear systems with many parameters. In particular, we show that in the absence of direct titration the modules are bounded, unconditionally stable input-output monotone systems[2, 4] under very mild assumptions (the concentration of constitutive regulators should be larger than the concentration of their target molecule). These properties guarantee that when a positive or negative feedback loop is generated by their interconnection, the admissible bifurcations in the system are either exclusively multistationary (positive feedback) or exclusively oscillatory (negative feedback). These results build on previous theoretical work[10] where a complete classification of oscillatory and multistationary systems is proposed based on Jacobian cycles. The presence of titration reactions weakens these structural properties, making them dependent on the location of the equilibria and on the strength of the titration rate. However, numerical simulations show that titration increases the probability of bistability and oscillations, because it sharpens the stationary and temporal response of the modules, and increases the delay in the system.

In addition to the concentration of titrating species and to the titration rates, key

parameters in the modules are the production rates of the regulators β_x and β_z. These rates primarily influence the strength of the feedback loops both in the oscillator and in the bistable system, as can be seen from the linearization of the modules' ODEs shown in the SI Sections 3 and 4. High gain in a feedback loop can generally destabilize a dynamical system; however, β_x and β_z influence other parts of the linearized dynamics as well, thus their increase does not guarantee that the desired bifurcation will occur.

While it is well known (experimentally and theoretically) that molecular titration can be tuned to generate nonlinear ultrasensitive responses and delays[19, 18, 73], to our knowledge very few attempts have been made to build complex dynamic networks using this mechanism. Experimentally, molecular titration obtained via RNA polymerase sigma factors was used *in vivo* to build a bistable switch with tunable domain boundaries and the capacity for state toggling[21]. *In vitro*, titration pathways very similar to those we describe here were used to build a bistable switch[53] and an oscillator[51, 42]. In these systems, the target molecules are DNA templates that produce RNA outputs acting as mutual template regulators; template activity is switched on and off via a partial promoter displacement reaction, whose speed is determined by sequence and length of toehold domains on the nicked promoter (**??** B). In these systems, templates are constitutively activated or repressed depending on the presence of DNA activators (which complete the promoter) and DNA inhibitors (which displace the activators). RNA regulators either inhibit (by displacing DNA activators) or activate (by displacing DNA inhibitors) the templates, generating inert activator or inhibitor complexes which can be recovered by RNase H-mediated degradation of RNA bound to DNA. By increasing the concentration of titrating species

(DNA activators/inhibitors) within certain bounds, the oscillatory or bistable behavior of the systems is significantly enhanced[42]. The molecular oscillator is also highly sensitive to the concentration of RNA polymerase, which in the system determines the production rates. These experimental findings are consistent with the results of our analysis.

A common feature of existing dynamic systems built using molecular titration[21, 53, 51, 42] is that the domains in parameter space where oscillations or bistability are achieved is generally narrow. Recently, this was clearly highlighted in a series of experiments where the *in vitro* oscillator by Kim and Winfree was encapsulated in microdroplets[92]; the droplet production process causes a perturbation of the nominal operating point of the system (in particular, there is a loss of enzymes activity), and results in a striking dynamical diversity and often a loss of oscillations in droplets. This is consistent with our numerical analysis, and we speculate that this might be a consequence of the monomeric nature of the regulators in the system. In a regime where stochastic effects are predominant, however, the lack of cooperativity may not be a significant limitation to achieve complex behaviors, depending on the system architecture[90, 58].

We expect that our analysis of molecular titration in the context of feedback systems will be useful to build circuits with new classes of monomeric regulators such as the CRISPR-Cas system . Logic circuits based on CRISPR-Cas have been recently characterized[68, 9], however feedback loops with bistable or oscillatory responses have not yet been obtained, presumably due to the difficulty in obtaining sharp nonlinear responses required for these behaviors. While building circuits with multiple, interconnected feedback loops may prove helpful[56], we speculate that titration of the guide RNA with over

expressed titrating RNA species might be an effective strategy.

Chapter 3

Stability analysis of an artificial biomolecular oscillator with non-cooperative regulatory interactions

3.1 Introduction

All organisms require timing circuits to orchstrate processes related to their life cycle, such as cell growth, metabolism, and division [93]. By building molecular timers from the bottom up, we have an opportunity to understand the design requirements to program periodic biochemical behaviours. In addition, synthetic oscillators are useful components to direct autonomous molecular operations *in vivo* and *in vitro* [36, 85, 89, 31, 92].

In vitro nucleic acid oscillators can be built with a small number of parts, and their behaviour is quantitatively predictable [51, 42, 65, 44, 92]. Nucleic acids have become molecular building blocks for a variety of logic and dynamic circuits, because their thermodynamic and kinetic interactions can be programmed by choosing their sequence content with rational optimisation algorithms. Existing nucleic acid oscillators however cannot be ported to the cellular environment, because they rely on the presence of multiple single-stranded or partially single-stranded DNA species, which are incompatible with the cellular machinery [51, 42, 65, 44]. Here we describe a new nucleic acid oscillator architecture that has the potential to overcome this limitation, as it does not require single stranded DNA molecules. A particularly interesting aspect of our model is that it does not include Hill-type nonlinearities, present in the majority of models for molecular oscillators. All regulatory interactions in this circuit are non-cooperative.

Our molecular oscillator comprises three polymerases, two of which mutually regulate each other (Fig 3.1 A). The interactions among enzymes are defined by four synthetic genes and four RNA species (Fig 3.1 B). The activity of two of the enzymes is modulated by RNA species that serve as inhibitors or activators. The third enzyme species controls the baseline production of two of the RNA species, and has a net effect of counteracting the mutual regulation of the other two enzymes. For instance, let us consider the pathway by which enzyme E_2 is inhibited by enzyme E_1 and activated by enzyme E_3. E_1 produces RNA species R_1 by transcribing gene g_1; R_1 binds to and inhibits enzyme E_2, converting it to inactive enzyme E_2^* (a reaction experimentally demonstrated, for instance, in [69, 67]). RNA species R_4 (transcribed by E_3) counteracts this pathway and causes reactivation of

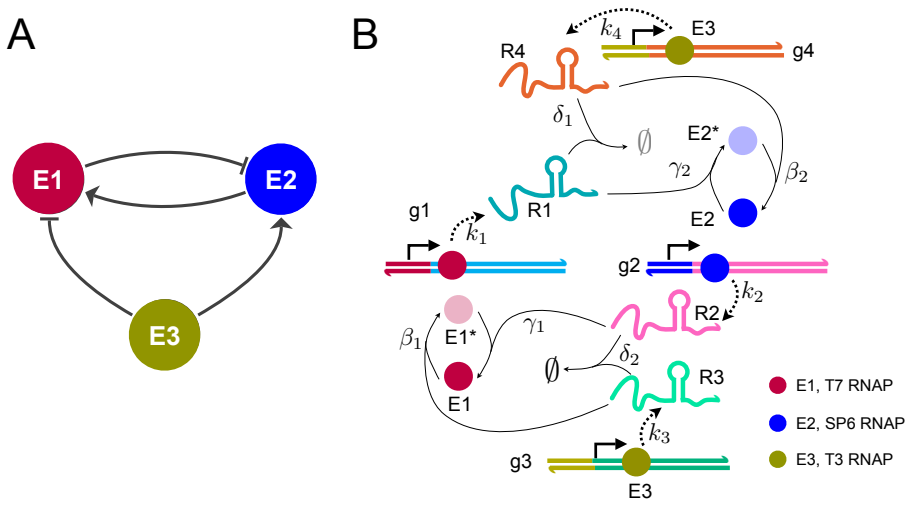

Figure 3.1: A: Architecture of the three-node oscillator: enzymes E_1 and E_2 mutually regulate their concentration (arrows indicate activation, flat arrows indicate repression) generating a negative feedback loop; enzyme E_3 counteracts the loop regulation. B: Schematic of the chemical reactions underlying the oscillator architecture. Different enzyme species are indicated as circles of different color; bright color indicates active enzyme, and dim color indicates inactive enzyme. RNA species are transcribed (dashed arrows) from synthetic genes present at constant concentration; enzymes are activated or inhibited by a given RNA species according to the illustrated reactions and corresponding rates. The full set of reactions is listed in Section 2, and result in ODE systems (3.1) and (3.2).

E_2 (conversion of E_2^* to E_2), because it is designed to displace R_1 bound to E_2, and to titrate free R_1 as well. Similar reactions generate inhibition and activation pathways for E_1 (due to E_3 and to E_2, respectively). Overall, these interactions contribute to creating a negative feedback loop. This system can be experimentally implemented using T7, T3, and SP6 bacteriophage RNA polymerases [86, 62, 55], which can be purchased off-the-shelf from many vendors. RNA sequences (known as aptamers [34]) that bind to bacteriophage RNA polymerases and work as inhibitors have been experimentally characterised [67, 69]. RNA activators can be designed as strands whose sequence are complementary to the sequences of the inhibitors via the mechanism of strand displacement and strand titration [94, 53].

We describe this system by means of ordinary differential equations (ODEs) built using the law of mass action, starting from a list of chemical reactions reported in Section 2. We demonstrate that the system is a candidate oscillator due to the sign pattern of its Jacobian matrix [10, 14]; in particular we show that the system admits transitions to instability that are exclusively oscillatory.

Our analysis relies on monotone systems theory (background is provided in Section 3) and the theory of invariant sets. In Section 4 we study the capacity of this dynamical system to *structurally* exhibit sustained oscillations whenever it becomes unstable, in view of its particular Jacobian structure; this approach can be applied to a variety of chemical reaction networks, as we have shown, for instance, in the context of other titration-based regulatory networks [77]. Structural (namely, parameter-free) results can greatly help unravel the functioning of biological systems, which are affected by intrinsic uncertainties and variabilities in their parameters, but can nonetheless exhibit an extraordinary robustness and resilience [12]. We conclude with a numerical bifurcation analysis and study of period and amplitude as a function of variations in individual parameters, showing that for realistic reaction rates the system exhibits oscillatory behaviours (Section 5). We previously described a two-enzyme oscillator relying on RNA aptamers [15, 29]; we claim that a three-enzyme system is more tunable, and simulation results indicate that in a certain region of parameter space its amplitude can be modulated independently from the period.

3.2 A three-enzyme oscillator regulated by first and second order reactions

In the following, capital letters represent chemical species and the corresponding lowercase letters represent species concentrations (*e.g.*, species A has concentration a). Our three node oscillator is described by the biochemical reactions below. Reactions are grouped in two sets corresponding to functional modules (Fig. 3.2), whose common external input is E_3. For simplicity we assume a common degradation rate for all products R_i, $i = 1, ..., 4$.

Module 1:		Module 2:	
$E_1 \xrightarrow{\alpha_1} E_1 + R_1$	Production	$E_2 \xrightarrow{\alpha_2} E_2 + R_2$	Production
$E_3 \xrightarrow{\alpha_3} E_3 + R_3$		$E_3 \xrightarrow{\alpha_4} E_3 + R_4$	
$E_2 + R_1 \xrightarrow{\beta_1} E_2^*$	Inhibition	$E_1 + R_4 \xrightarrow{\beta_2} E_1^*$	Inhibition
$E_2^* + R_3 \xrightarrow{\gamma_1} E_2$	Conversion	$E_1^* + R_2 \xrightarrow{\gamma_2} E_1$	Conversion
$R_1 + R_3 \xrightarrow{\delta_1} 0$	Titration	$R_2 + R_4 \xrightarrow{\delta_2} 0$	Titration
$R_1 \xrightarrow{\phi} 0$	Degradation	$R_2 \xrightarrow{\phi} 0$	Degradation
$R_3 \xrightarrow{\phi} 0$		$R_4 \xrightarrow{\phi} 0$	

The differential equations describing Module 1 are:

$$\begin{aligned} \dot{r_1} &= \alpha_1 e_1 - \beta_1 r_1 e_2 - \delta_1 r_1 r_3 - \phi r_1, \\ \dot{r_3} &= \alpha_3 e_3 - \gamma_1 r_3 e_2^* - \delta_1 r_1 r_3 - \phi r_3, \\ \dot{e_2} &= \gamma_1 r_3 e_2^* - \beta_1 r_1 e_2. \end{aligned} \tag{3.1}$$

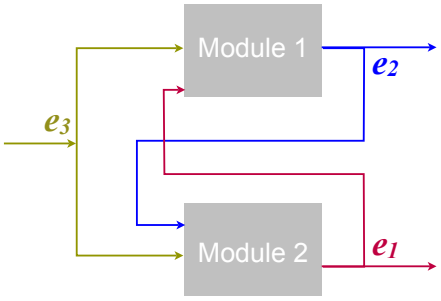

Figure 3.2: Schematic of the interconnections between reaction Modules 1 and 2, with enzyme concentrations as inputs and outputs.

The differential equations describing Module 2 are:

$$\begin{aligned} \dot{r_2} &= \alpha_2 e_2 - \gamma_2 r_2 e_1^* - \delta_2 r_2 r_4 - \phi r_2, \\ \dot{r_4} &= \alpha_4 e_3 - \beta_2 r_4 e_1 - \delta_2 r_2 r_4 - \phi r_4, \\ \dot{e_1} &= \gamma_2 r_2 e_1^* - \beta_2 r_4 e_1. \end{aligned} \tag{3.2}$$

The total concentration of E_1 and E_2 is assumed to be constant, and equal to e_1^{tot} and e_2^{tot} respectively; hence, mass conservation laws yield $e_1^* = e_1^{tot} - e_1$ and $e_2^* = e_2^{tot} - e_2$. The two modules are interconnected and form a feedback loop: Module 1 (associated with variables r_1, r_3 and e_2) receives input e_1 from Module 2; in turn, Module 2 (associated with variables r_2, r_4 and e_1) receives input e_2 from Module 1. Both modules receive input e_3, which we assume is constant (Fig. 3.2); we assume that the timescale at which e_3 binds to a gene and transcribes RNA is fast relative to the other timescales in the system, so that it can be neglected; this assumption is sensible for short transcripts (30-60 bases). In the next sections we demonstrate that transitions to instability in this system can occur exclusively due to a pair of complex conjugate eigenvalues crossing the imaginary axis, hence sustained oscillations necessarily arise whenever the system is driven to instability.

From numerical simulations it is apparent that the system can actually be destabilised, for suitable parameter choices, and is therefore a good candidate oscillator.

3.3 Background

We summarise several background notions that are required to introduce our main results in Section 3.4. Additional information can be found in references [10, 14]. Consider a system:

$$\dot{x}(t) = f(x(t), \mu), \qquad x \in \mathbb{R}^n, \tag{3.3}$$

where μ is a real-valued parameter and $f(\cdot, \cdot)$ is a sufficiently smooth function, continuous in μ, satisfying the following Assumptions *for every admissible value of* μ.

Assumption 1 *All the solutions of* (3.3) *are globally uniformly asymptotically bounded in the compact set* $\mathcal{S} \subset \mathbb{R}^n$.

Hence, system (3.3) admits an equilibrium $\bar{x}$ in $\mathcal{S}$ ([83, 74, 75]).

Assumption 2 $\partial f_i / \partial x_j$ *is either always positive, always negative, or always null in the considered domain.*

Assumption 3 *For all* i, $\partial f_i / \partial x_i < 0$, i.e., *the system is non-autocatalytic.*

Due to the monotonicity of $f_i(\cdot)$ with respect to each argument x_j, the Jacobian matrix $\mathbf{J}$ of system (3.3) is sign definite.

Definition 1 *Given a system with a sign-definite Jacobian* $\mathbf{J}$, *its* structure *is the sign pattern matrix* $\Sigma = sign[\mathbf{J}]$.

The structure Σ of system (3.3) is assumed to be invariant with respect to μ. Assumption 1 ensures that an equilibrium exists; all the following definitions refer to this equilibrium, which is, in general, a function of μ: $f(\bar{x}_\mu, \mu) = 0$. We assume that $\bar{x}_\mu$ depends continuously on μ. Note that a suitable change of coordinates always allows us to shift the equilibrium to the origin, without affecting our analysis.

Definition 2 *System* (3.3) *undergoes a* Transition to Instability (TI) *at* $\mu = \mu^*$ *iff its Jacobian matrix* $\mathbf{J}(\bar{x}_\mu)$ *is asymptotically stable in a left neighborhood of* μ^**, and unstable in a right neighborhood*[1]*. A TI is* simple *if at most a single real eigenvalue or a single pair of complex conjugate eigenvalues crosses the imaginary axis.*

Definition 3 *System* (3.3) *undergoes an* Oscillatory Transition to Instability (OTI) *at* $\mu = \mu^*$ *iff its Jacobian matrix* $\mathbf{J}(\bar{x}_{\mu^*})$ *has a single pair of pure imaginary eigenvalues, while all the other eigenvalues have negative real part:*

$$\sigma\left(\mathbf{J}(\bar{x}_{\mu^*})\right) = \{\lambda_1, \lambda_2, \ldots, \lambda_n\}, \quad \textit{where} \quad \lambda_{1,2} = \pm j\omega,$$

with $Re(\lambda_k) < 0$ *for* $k > 2$ *and* $Re(\lambda_k) > 0$ *for* $k = 1, 2$ *in a right neighborhood of* μ^**.*

We now provide general definitions for candidate oscillatory and multistationary systems. We consider system (3.3), with its given structure Σ (invariant with respect to μ), under Assumptions 1, 2 and 3.

Definition 4 *A system of the form* (3.3)*, with structure* Σ*, is structurally a candidate*

1. oscillator in the weak sense *iff it admits an OTI for some* $\mu = \mu^*$*;*

[1] The definition holds as well for systems transitioning to instability from the right to the left neighborhood of μ^*: just take $\hat{\mu} = \mu^* - \mu$ as the bifurcation parameter.

2. oscillator in the strong sense *iff every simple TI (if any) is an OTI;*

Necessary and sufficient conditions characterizing strong and weak oscillators/ multistationary systems are provided in [10] in terms of cycles in the structure graph. We associate matrix Σ with a directed n-node graph, whose arcs are positive $(+1)$, negative (-1), or zero depending on the sign of the corresponding matrix entries.

Definition 5 *Given a graph, a* cycle *is an oriented, closed sequence of distinct nodes connected by distinct directed arcs. A cycle is* negative *(*positive*) if the number of negative arcs is odd (even). The* order *of a cycle is the number of arcs involved in the cycle. We say a system is* critical *when all negative cycles (if any) are of order two.*

Proposition 6 *A non-critical system is a candidate oscillator in the weak sense if and only if its structure has at least one negative cycle (necessarily of order greater than two).*

Proposition 7 *A non-critical system is a candidate oscillator in the strong sense if and only if its structure has only negative cycles.*

Proofs for Propositions 6 and 7 can be found in [10].

Remark 8 *The results above are verified as well if we drop Assumption 1 and we restrict our analysis to solutions that belong to a compact positively invariant set $\mathcal{S}$, with a non-empty interior and with no equilibrium points on the boundary.*

The graph-based results in [10] have been generalised in [14] to the case of systems composed of the sign definite interconnection of subsystem that are either monotone or anti-monotone. We provide below the definitions of monotone and anti-monotone system.

Definition 9 *A system*

$$\dot{x}(t) = f(x(t), u(t)), \tag{3.4}$$

where $u(\cdot) \in \mathbb{R}$ *is a scalar, time varying input, is* input-to-state monotone *if, denoting as* $x_1(t)$ *and* $x_2(t)$ *the solutions of the system corresponding to inputs* $u_1(t)$ *and* $u_2(t)$*, the fact that* $x_2(0) \geq x_1(0)$ *and* $u_2(t) \geq u_1(t)$ *for* $t > 0$ *implies that* $x_2(t) \geq x_1(t)$ *for* $t > 0$*, where inequalities are intended to hold componentwise. The system is* input-to-state anti-monotone *if the input has the opposite effect on the state, i.e., if* $x_2(0) \geq x_1(0)$ *and* $u_2(t) \leq u_1(t)$ *for* $t > 0$*, then* $x_2(t) \geq x_1(t)$ *for* $t > 0$*. If the system includes an output* $y = g(x)$*, the system is* input-output monotone (anti-monotone) *if it is input-to-state monotone (anti-monotone) and if* $x_2 \geq x_1$ *implies* $g(x_2) \geq g(x_1)$*.*

A simple characterisation of input-to-state monotonicity and anti-monotonicity [2, 82] can be provided by exploiting the concept of Metzler matrix: a matrix is Metzler if its elements satisfy $a_{ij} \geq 0$, $\forall (i, j)$ such that $i \neq j$.

Theorem 10 *System* (3.4) *is input-to-state monotone if its Jacobian matrix* $\mathbf{J} = \partial f / \partial x$ *is a Metzler matrix and* $\partial f / \partial u \geq 0$ *componentwise. Conversely, system* (3.4) *is input-to-state anti-monotone if its Jacobian matrix* $\mathbf{J} = \partial f / \partial x$ *is a Metzler matrix and* $\partial f / \partial u \leq 0$ *componentwise.*

A more general concept, which we will use in the following, is given by monotonicity (or anti-monotonicity) with respect to a given signature tuple $(s_1, \ldots, s_n)$, where $s_i = 1$ or -1 for all i [37]: this amounts to requiring that, after changing the sign of the state variables as $\hat{x}_i = s_i x_i$ for all i, the system becomes monotone (or anti-monotone). Hence, Theorem 10 applies to the system in the new coordinates.

3.4 Analytical results

3.4.1 Existence of equilibria

First, we show that this system always admits a steady state (equilibrium).

Proposition 11 *Consider the interconnection of systems* (3.1) *and* (3.2)*. For any constant* $e_3 > 0$*, there exists a suitably large* $\rho \in \mathbb{R}^+$ *such that the compact set*

$$\mathcal{S}_\rho = \left\{ r_1, r_2, r_3, r_4, e_1, e_2 \geq 0 : \quad r_1 + r_3 \leq \rho, \quad r_2 + r_4 \leq \rho, \quad e_1 \leq e_1^{tot}, \quad e_2 \leq e_2^{tot} \right\}$$

is positively invariant. Moreover, all of the solutions of the system are globally uniformly asymptotically bounded in $\mathcal{S}_\rho$*, hence the interconnection of systems* (3.1) *and* (3.2) *satisfies Assumption 1.*

Proof. The inequalities $e_1(t) \leq e_1^{tot}$ and $e_2(t) \leq e_2^{tot}$ are always satisfied by construction. Consider the constraint $r_1 + r_3 \leq \rho$ and assume that at some point $r_1 + r_3 = \rho$. Then

$$\begin{aligned} \frac{d}{dt}(r_1 + r_3) &= \alpha_1 e_1 - \beta_1 r_1 e_2 - \delta_1 r_1 r_3 - \phi r_1 + \alpha_3 e_3 - \gamma_1 r_3 e_2^* - \delta_1 r_1 r_3 - \phi r_3 \\ &\leq \alpha_1 e_1^{tot} + \alpha_3 e_3 - \phi r_1 - \phi r_3 = \alpha_1 e_1^{tot} + \alpha_3 e_3 - \phi\rho < 0 \end{aligned}$$

for ρ large enough: $\rho > \frac{\alpha_1 e_1^{tot} + \alpha_3 e_3}{\phi}$. Hence, the constraint $r_1 + r_3 \leq \rho$ cannot be violated. Analogously, the constraint $r_2 + r_4 \leq \rho$ cannot be violated because, if at some point $r_2 + r_4 = \rho$, then

$$\frac{d}{dt}(r_2 + r_4) \leq \alpha_2 e_2^{tot} + \alpha_4 e_3 - \phi r_2 - \phi r_4 = \alpha_2 e_2^{tot} + \alpha_4 e_3 - \phi\rho < 0$$

for $\rho > \frac{\alpha_2 e_2^{tot} + \alpha_4 e_3}{\phi}$. Then, any value $\rho > \max\left\{ \frac{\alpha_1 e_1^{tot} + \alpha_3 e_3}{\phi}, \frac{\alpha_2 e_2^{tot} + \alpha_4 e_3}{\phi} \right\}$ ensures that $\mathcal{S}_\rho$ is positively invariant. Also, since $\frac{d}{dt}(r_1 + r_3)$ is negative whenever $r_1 + r_3 \geq \rho$ and $\frac{d}{dt}(r_2 + r_4)$

is negative whenever $r_2 + r_4 \geq \rho$, any trajectory of the system is uniformly asymptotically bounded in $\mathcal{S}_\rho$ (indeed, $V_1 = r_1 + r_3$ and $V_2 = r_2 + r_4$ can be taken as Lyapunov-like functions for modules 1 and 2, respectively, to show that all the trajectories of the system are uniformly ultimately bounded in the compact set $\mathcal{S}_\rho$ [11]). ■

Proposition 12 *The dynamical system defined by the interconnection of systems* (3.1) *and* (3.2) *always admits the existence of a steady state.*

Proof. The existence of the compact invariant set $\mathcal{S}_\rho$ where the solutions of the system are globally uniformly asymptotically bounded (Proposition 11) implies the existence of a steady state [83, 74, 75]. ■

We later demonstrate that this steady state is unique.

Remark 13 *The presence of degradation reactions (at rate $\phi > 0$) is essential to have structural boundedness. In fact, if we set $\phi = 0$ and we consider the function $\psi = -r_1 + r_3 + e_2$, we have*

$$\dot{\psi} = -\dot{r_1} + \dot{r_3} + \dot{e_2} = -\alpha_1 e_1 + \alpha_3 e_3 \geq -\alpha_1 e_1^{tot} + \alpha_3 e_3,$$

which may grow unbounded for a large value of e_3.

3.4.2 Monotonicity properties and uniqueness of equilibrium point

Now we show that the overall system is the feedback interconnection of two subsystem, corresponding to the modules defined earlier, that are respectively *anti-monotone* and *monotone*. This property further implies that the system admits a unique equilibrium.

We individually linearise subsystems (3.1) and (3.2) around an equilibrium point (which is guaranteed to exist), and we begin by studying each subsystem in isolation.

$$\text{Module 1:} \qquad \dot{z} = \mathbf{A_1} z + \mathbf{B_1} \delta e_1, \tag{3.5}$$

$$\text{Module 2:} \qquad \dot{w} = \mathbf{A_2} w + \mathbf{B_2} \delta e_2, \tag{3.6}$$

where the linearised state variables of each subsystems are $z = [\delta r_1 \ \delta r_3 \ \delta e_2]^\top$ and $w = [\delta r_2 \ \delta r_4 \ \delta e_1]^\top$. We denote equilibrium values of each variable with a $^-$ symbol (*e.g.*, $\bar{e}_1$ is the equilibrium of e_1). The linearised dynamics are defined by matrices:

$$\mathbf{A_1} = \begin{bmatrix} -\beta_1 \bar{e}_2 - \delta_1 \bar{r}_3 - \phi & -\delta_1 \bar{r}_1 & -\beta_1 \bar{r}_1 \\ -\delta_1 \bar{r}_3 & -\gamma_1 \bar{e}_2^* - \delta_1 \bar{r}_1 - \phi & \gamma_1 \bar{r}_3 \\ -\beta_1 \bar{e}_2 & \gamma_1 \bar{e}_2^* & -\beta_1 \bar{r}_1 - \gamma_1 \bar{r}_3 \end{bmatrix}, \quad \mathbf{B_1} = \begin{bmatrix} \alpha_1 \\ 0 \\ 0 \end{bmatrix}$$

and

$$\mathbf{A_2} = \begin{bmatrix} -\gamma_2 \bar{e}_1^* - \delta_2 \bar{r}_4 - \phi & -\delta_2 \bar{r}_2 & \gamma_2 \bar{r}_2 \\ -\delta_2 \bar{r}_4 & -\beta_2 \bar{e}_1 - \delta_2 \bar{r}_2 - \phi & -\beta_2 \bar{r}_4 \\ \gamma_2 \bar{e}_1^* & -\beta_2 \bar{e}_1 & -\gamma_2 \bar{r}_2 - \beta_2 \bar{r}_4 \end{bmatrix}, \quad \mathbf{B_2} = \begin{bmatrix} \alpha_2 \\ 0 \\ 0 \end{bmatrix}.$$

The two linearised subsystems are stable, and the matrices defining their dynamics (Jacobian matrices of the nonlinear systems) are Metzler up to changes in the sign of some variables. This can be easily shown by changing sign to the first component of z and to the second component of w: $z_1 := -z_1$ and $w_2 := -w_2$. This is equivalent to changing sign to the variables r_1 and r_4 in the original system and provides matrices

$$\hat{\mathbf{A}}_\mathbf{1} = \begin{bmatrix} -\beta_1 \bar{e}_2 - \delta_1 \bar{r}_3 - \phi & +\delta_1 \bar{r}_1 & +\beta_1 \bar{r}_1 \\ +\delta_1 \bar{r}_3 & -\gamma_1 \bar{e}_2^* - \delta_1 \bar{r}_1 - \phi & \gamma_1 \bar{r}_3 \\ +\beta_1 \bar{e}_2 & \gamma_1 \bar{e}_2^* & -\beta_1 \bar{r}_1 - \gamma_1 \bar{r}_3 \end{bmatrix} \hat{\mathbf{B}}_\mathbf{1} = \begin{bmatrix} -\alpha_1 \\ 0 \\ 0 \end{bmatrix} \tag{3.7}$$

and

$$\hat{\mathbf{A}}_{\mathbf{2}} = \begin{bmatrix} -\gamma_2\bar{e}_1^* - \delta_2\bar{r}_4 - \phi & +\delta_2\bar{r}_2 & \gamma_2\bar{r}_2 \\ +\delta_2\bar{r}_4 & -\beta_2\bar{e}_1 - \delta_2\bar{r}_2 - \phi & +\beta_2\bar{r}_4 \\ \gamma_2\bar{e}_1^* & +\beta_2\bar{e}_1 & -\gamma_2\bar{r}_2 - \beta_2\bar{r}_4 \end{bmatrix} \hat{\mathbf{B}}_{\mathbf{2}} = \begin{bmatrix} \alpha_2 \\ 0 \\ 0 \end{bmatrix} \tag{3.8}$$

Proposition 14 *Matrices* $\hat{\mathbf{A}}_{\mathbf{1}}$ *in* (3.7) *and* $\hat{\mathbf{A}}_{\mathbf{2}}$ *in* (3.8) *are Metzler and are Hurwitz stable. Moreover, their inverse matrices are (element-wise) negative.*

Proof. Consider systems (3.5) and (3.6), which after the sign change have matrices (3.7) and (3.8). Since all of their off-diagonal entries are non-negative, $\hat{\mathbf{A}}_{\mathbf{1}}$ and $\hat{\mathbf{A}}_{\mathbf{2}}$ are Metzler matrices. They are also irreducible[2]. Hurwitz stability (all the eigenvalues of the Jacobian $\mathbf{J} = \partial f/\partial x(\bar{x})$ have a negative real part) immediately follows from the fact that $\hat{\mathbf{A}}_{\mathbf{1}}$ and $\hat{\mathbf{A}}_{\mathbf{2}}$ are Metzler and diagonally dominant, with negative diagonal entries (this is a consequence of Gershgorin's circle theorem). Finally, any stable and irreducible Metzler matrix has an element-wise negative inverse (see [11] for details). ■

We are now ready to demonstrate monotonicity properties of the two nonlinear modules.

Proposition 15 *Systems* (3.1) *and* (3.2) *are respectively input-to-state anti-monotone and monotone after the sign change in the variables:*

$$\hat{r}_1 = -r_1 \quad \textit{and} \quad \hat{r}_4 = -r_4. \tag{3.9}$$

Proof. This follows from Theorem 10, since the state matrices $\hat{\mathbf{A}}_{\mathbf{1}}$ and $\hat{\mathbf{A}}_{\mathbf{2}}$ are Metzler, while the input matrices $\hat{\mathbf{B}}_{\mathbf{1}}$ and $\hat{\mathbf{B}}_{\mathbf{2}}$ are respectively nonpositive and nonnegative. ■

[2]A matrix is irreducible if there does not exist a permutation of its rows or columns that transforms it into a block triangular matrix.

Monotonicity and stability have important consequences on the static input-state and input-output characteristics (input-output equilibrium conditions) and on uniqueness of the equilibrium point. Indeed, the feedback of two systems that are either monotone or anti-monotone always admits a single equilibrium point (if any).

We have shown in Proposition 12 that an equilibrium always exists; we prove below, for completeness, that the static input-output characteristics of the two modules are monotonic, hence such an equilibrium point is unique.

Proposition 16 *We assume that inputs e_1 and e_2 in systems* (3.1) *and* (3.2) *are constant. Then, the steady-state values of the modules, $\bar{r}_1(e_1)$, $\bar{r}_3(e_1)$, $\bar{e}_2(e_1)$ and $\bar{r}_2(e_2)$, $\bar{r}_4(e_2)$, $\bar{e}_1(e_2)$, depend monotonically on the inputs. Precisely, $\bar{r}_2(e_2)$, $\bar{r}_4(e_2)$ and $\bar{e}_1(e_2)$ monotonically increase as a function of e_2, while $\bar{r}_1(e_1)$, $\bar{r}_3(e_1)$ and $\bar{e}_2(e_1)$ monotonically decrease as a function of e_1.*

Proof. We recall that, for a generic system $\dot{x} = f(x, u)$, the steady-state characteristic $\bar{x}(u)$ is implicitly defined by

$$0 = f(\bar{x}, u).$$

We can apply the implicit function theorem to find its derivative:

$$\frac{d}{du}\bar{x}(u) = \left(-\frac{\partial f}{\partial \bar{x}}\right)^{-1} \frac{\partial f}{\partial u}.$$

Consider Module 1, after the sign change in the variables at equation (3.9):

$$\frac{d}{de_1}\bar{z}(e_1) = -(\hat{\mathbf{A}}_\mathbf{1})^{-1}\hat{\mathbf{B}}_\mathbf{1} < 0.$$

The inequality holds componentwise (Proposition 14), hence after the sign change equilibria $\bar{r}_1(e_1)$, $\bar{r}_3(e_1)$ and $\bar{e}_2(e_1)$ are monotonically decreasing functions of e_1.

As for Module 2, after the sign change at equation (3.9):

$$\frac{d}{de_2}\bar{w}(e_2) = -(\hat{\mathbf{A}}_\mathbf{2})^{-1}\hat{\mathbf{B}}_\mathbf{2} > 0$$

componentwise, hence after the sign change $\bar{r}_2(e_2)$, $\bar{r}_4(e_2)$ and $\bar{e}_1(e_2)$ are monotonically increasing functions of input e_2. ■

Proposition 17 *The interconnection of systems* (3.1) *and* (3.2) *admits a unique equilibrium.*

Proof. The system always admits a steady state, as shown in Proposition (12). Due to Proposition 16, $\bar{e}_2(e_1)$ is a decreasing function and $\bar{e}_1(e_2)$ is an increasing function. Thus, the system of equations:

$$\begin{cases} e_2 = \bar{e}_2(e_1), \\ e_1 = \bar{e}_1(e_2), \end{cases}$$

has a unique solution. ■ It is possible to demonstrate that this unique equilibrium is strictly positive, and there cannot be equilibria with zero components. This claim can be proved by showing that the two equilibrium equations intersect for positive values of e_1 and e_2. Then, we can show that all other variables have a positive steady state from their equilibrium conditions, which are all derived analytically in Appendix **??**.

3.4.3 The interconnected system admits exclusively oscillatory transitions to instability

Based on the properties demonstrated in the previous sections, we establish that our three-enzyme network has the appropriate structure to exhibit sustained oscillations,

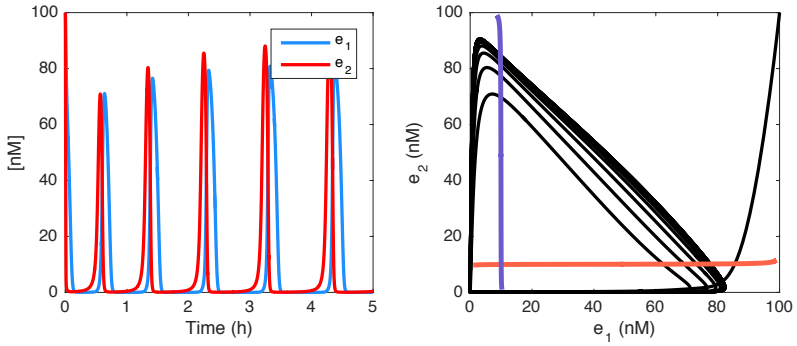

Figure 3.3: Left: Time evolution of e_1 and e_2 when parameters are chosen as in Table 3.2. Right: Trajectories in the plane e_1-e_2 (black) and equilibrium conditions (red and blue).

whenever it is driven to instability. More precisely, the network admits *exclusively* oscillatory transitions to instability.

Proposition 18 *The interconnection of systems* (3.1) *and* (3.2) *is a strong candidate oscillator.*

Proof. The Jacobian of the overall system, with variables ordered as (r_1, r_3, e_2, r_2, r_4, e_1) and with the variable sign change $\hat{r}_1 = -r_1$ and $\hat{r}_4 = -r_4$, highlights that the system is the negative feedback interconnection of two monotone subsystems:

$$J = \begin{bmatrix} -\beta_1 e_2 - \delta_1 r_3 - \phi & \delta_1 r_1 & \beta_1 r_1 & 0 & 0 & -\alpha_1 \\ \delta_1 r_3 & -\gamma_1 e_2^* - \delta_1 r_1 - \phi & \gamma_1 r_3 & 0 & 0 & 0 \\ \beta_1 e_2 & \gamma_1 e_2^* & -\beta_1 r_1 - \gamma_1 r_3 & 0 & 0 & 0 \\ 0 & 0 & \alpha_2 & -\gamma_2 e_1^* - \delta_2 r_4 - \phi & \delta_2 r_2 & \gamma_2 r_2 \\ 0 & 0 & 0 & \delta_2 r_4 & -\beta_2 e_1 - \delta_2 r_2 - \phi & \beta_2 r_4 \\ 0 & 0 & 0 & \gamma_2 e_1^* & \beta_2 e_1 & -\gamma_2 r_2 - \beta_2 r_4 \end{bmatrix} \tag{3.10}$$

Due to Proposition 11, the system satisfies Assumption 1. By inspecting the Jacobian matrix, it is apparent that Assumptions 2 and 3 are also satisfied. Therefore, the system is a strong candidate oscillator [10, 14]. This means that the system can transition to instability

exclusively due to a pair of complex conjugate eigenvalues crossing the imaginary axis (OTI) and yielding oscillatory dynamics. ■

3.5 Numerical analysis

Model (3.1)-(3.2) was integrated using the MATLAB routine `ode23`. Bifurcation analysis, period and amplitude computation was also done writing MATLAB scripts *ad hoc*.

In the numerical analysis that follows, we choose nominal parameters (Table 3.2) that are compatible with reaction rates measured in nucleic acid strand displacement reactions and *in vitro* transcription. An example solution trajectory for Model (3.1)-(3.2), integrated with the nominal parameters, is shown in Fig. 3.3

3.5.1 Randomised parameter sampling

First, we selected random values for the parameters sampling from a uniform distribution in the interval 10^{-2} to 10^{2} times the nominal parameter value (Table 3.2). We locate peaks and wells of the oscillations and compute period and amplitude as averaged over all the measured peaks and wells. A trajectory is classified as oscillatory if at least three oscillations are measured, if the period of the trajectory is between 0.5h to 40h, and its amplitude is larger than 1nM. This plot highlights that high degradation rates and low concentrations of e_1 and e_2 are associated with loss of oscillations.

3.5.2 Bifurcation analysis

Using analytical equilibrium conditions, we find equilibria numerically and compute the eigenvalues of Jacobian (3.10) at the equilibria. If at least one pair of complex conjugate eigenvalues with non-negative real part is found, the equilibrium is classified as oscillatory. We vary two parameters simultaneously, while all others are kept constant as in Table 3.2. Oscillatory regions are shown in orange in Fig. 3.5, while stable regions are shown in blue.

3.5.3 Period and amplitude

We focus on the influence of reaction rates and total concentrations of e_i on the period and amplitude. Parameters α_1, α_2, α_3, α_4, e_3, e_1^{tot} and e_2^{tot} are particularly relevant because they are experimentally easy to change (Fig 3.1 B): α_i, $i = 1, ..., 4$, are transcription rates, which can be tuned by mutating the promoter region; e_1^{tot}, e_2^{tot} and e_3 can be chosen by the experimenter.

We compute the period and amplitude from integrated solutions to the ODEs. As done in Section 3.5.1, we locate peaks and wells of the oscillations and compute period and amplitude as averaged over all the measured peaks and wells. We require at least three oscillations, and amplitude larger than 1 nM.

From Figs. 3.6 and 3.7 we observe that the period can be tuned from 0 to 5 hours. Also, the parameters related to the kinetics rate can change the period up to 3 hours in the range of one tenth to ten times their nominal value.

These plots show that when varying e_3 in a range between 0.1-10 times its nominal

value, the period remains flat. In that same range, amplitude varies significantly. We also observe that varying δ_1 between 0.1-10 times its nominal value, amplitudes stays flat while the period varies between 0-3 hours. It is worth noting that the titration rates δ_1 and δ_2 do not affect drastically neither amplitude nor period, which indicates that the system performance is robust relative to variations in the titration rates.

We observe that there is a range in which parameters α_2 and α_4 could be varied to tune exclusively the period, while the amplitude remains nearly constant. Alternatively, there is a range in which parameters e_1^{tot} and e_3 could be varied to modulate exclusively the amplitude, keeping the period nearly unchanged (and slow). Correlation between period and amplitude is shown in Fig. 3.8.

3.6 Conclusion

We have described an artificial three-enzyme biochemical network that has the capacity to oscillate. The network is designed for *in vitro* implementation with nucleic acid components and bacteriophage RNA polymerases, but has the potential to be implemented *in vivo* as well. The polymerases transcribe synthetic genes whose RNA transcripts in turn regulate enzyme activity, generating a negative feedback loop that is necessary for oscillations (the famous Thomas' conjecture [88, 81]). We analytically demonstrated that this architecture can exclusively undergo oscillatory transitions to instability, due to the structure of its Jacobian matrix. Numerical analysis shows that in a range of realistic parameters the system oscillates; simulations are useful to direct the experimental implementation of

Table 3.1: Nominal simulation parameters

Parameter	α_1	α_2	α_3	α_4	β_1	β_2	ϕ
Units	$1/s$	$1/s$	$1/s$	$1/s$	$1/M.s$	$1/M.s$	$1/s$
Value	0.1	0.1	0.1	0.1	5×10^5	5×10^5	5×10^{-5}
Parameter	γ_1	γ_2	δ_1	δ_2	e_3	e_1^{tot}	e_2^{tot}
Units	$1/M.s$	$1/M.s$	$1/M.s$	$1/M.s$	nM	nM	nM
Value	10^5	10^5	4×10^4	4×10^4	10	100	100

Table 3.2: Nominal simulation parameters

Rate	Description	Value	Other studies
$\alpha_{1,2,3,4}$ (/s)	Production	0.1	RNA: $10^{-3} - 1$ Refs.[91, 22]
$\beta_1 = \beta_2$ (/M/s)	Inhibition	$5 \cdot 10^5$	Nucleic acids: $10^4 - 10^6$ Refs.[53, 97]
$\gamma_1 = \gamma_2$ (/M/s)	Activation	10^5	Nucleic acids: $10^4 - 10^6$ Refs.[53, 97]
$\delta_!1 = \delta_2$ (/M/s)	Titration	$4 \cdot 10^4$	Nucleic acids: $10^4 - 10^6$ Refs.[53, 97]
ϕ (/s)	Degradation	$5 \cdot 10^{-5}$	Proteins: $10^{-4} - 10^{-3}$ Refs.[19]
$e_1(nM)$	Concentration	100	
$e_2(nM)$	Concentration	100	
$e_3(nM)$	Concentration	10	

this circuit, which is currently being pursued.

Figure 3.4: We randomly choose parameters in the interval 10^{-2} to 10^2 times their nominal value. Each black dot in this plot indicates that the (randomly) chosen parameter vector results in oscillations. Axes are in log scale. Orange diamonds represent the nominal value of each parameter (Table 3.2).

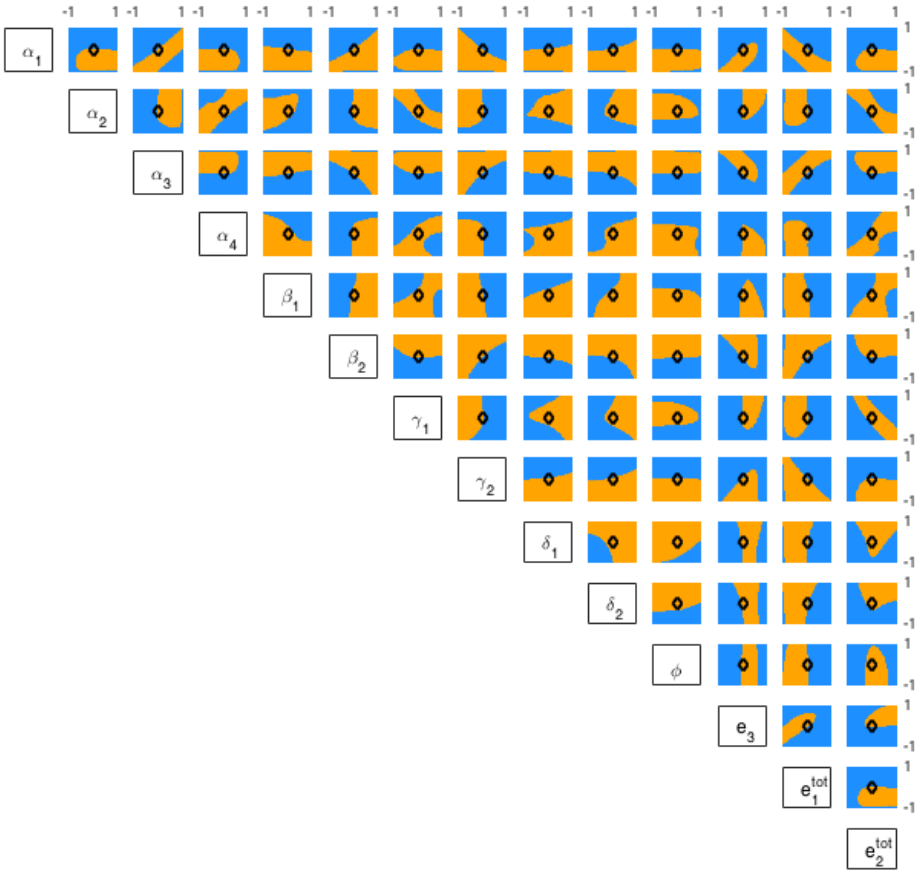

Figure 3.5: Log plots showing how varying pairs of parameters influences the stability of the equilibrium. Each parameter was varied between one tenth to ten times its nominal value (black diamond). Orange regions indicate oscillatory behaviour; blue regions indicate a single stable equilibrium.

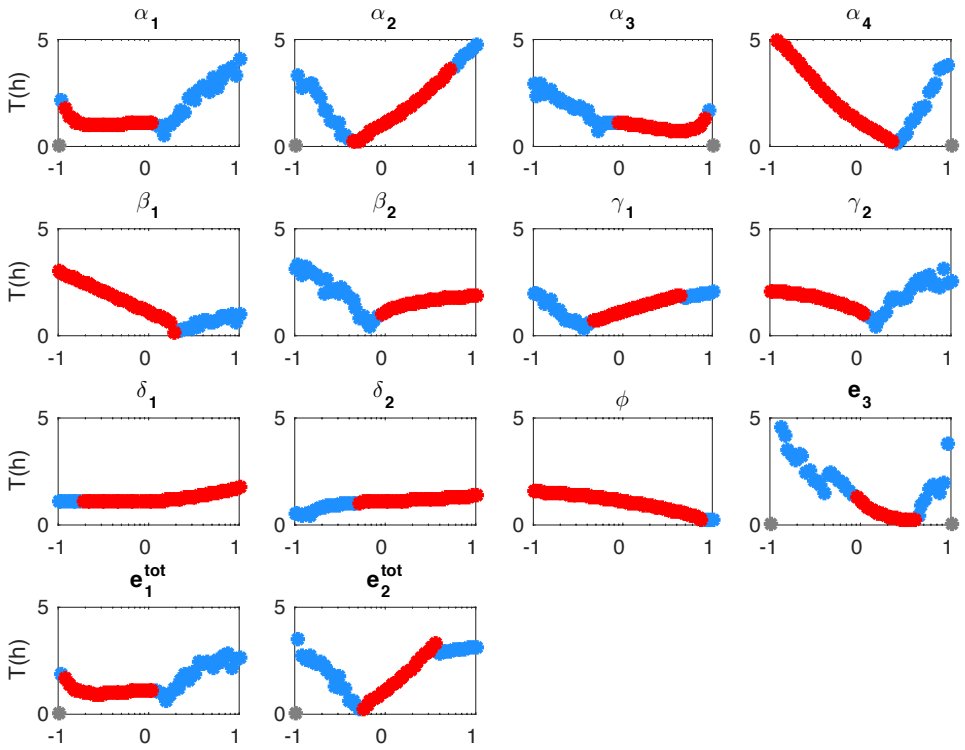

Figure 3.6: Period (h) as a function of each parameter (x axis in log scale). Blue circles represent when the Jacobian has at least one pair of complex eigenvalue with negative real part. The red circles represent when Jacobian has at least one pair of complex eigenvalue with positive real part. The grey circles represent when all eigenvalues are negative. The parameters were changed in the range of one tenth to ten times their nominal values.

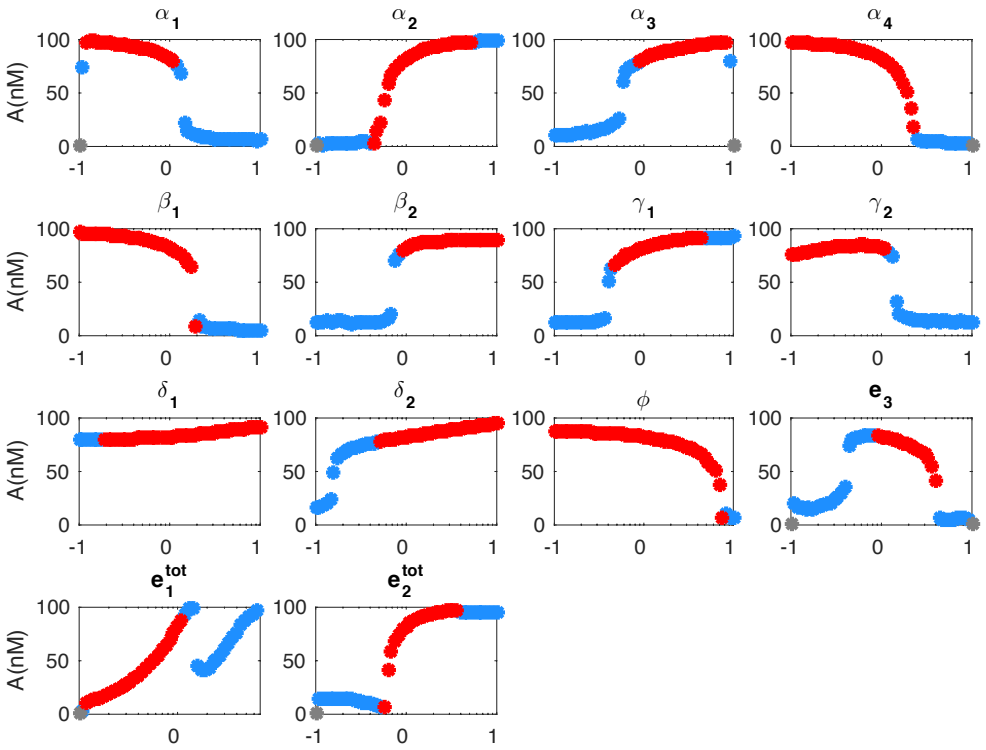

Figure 3.7: Amplitude (nM) as a function of each parameter (x axis in log scale). Blue circles represent when the Jacobian has at least one pair of complex eigenvalue with negative real part. The red circles represent when Jacobian has at least one pair of complex eigenvalue with positive real part. The grey circles represent when all eigenvalues are negative. The parameters were changed in the range of one tenth to ten times their nominal values.

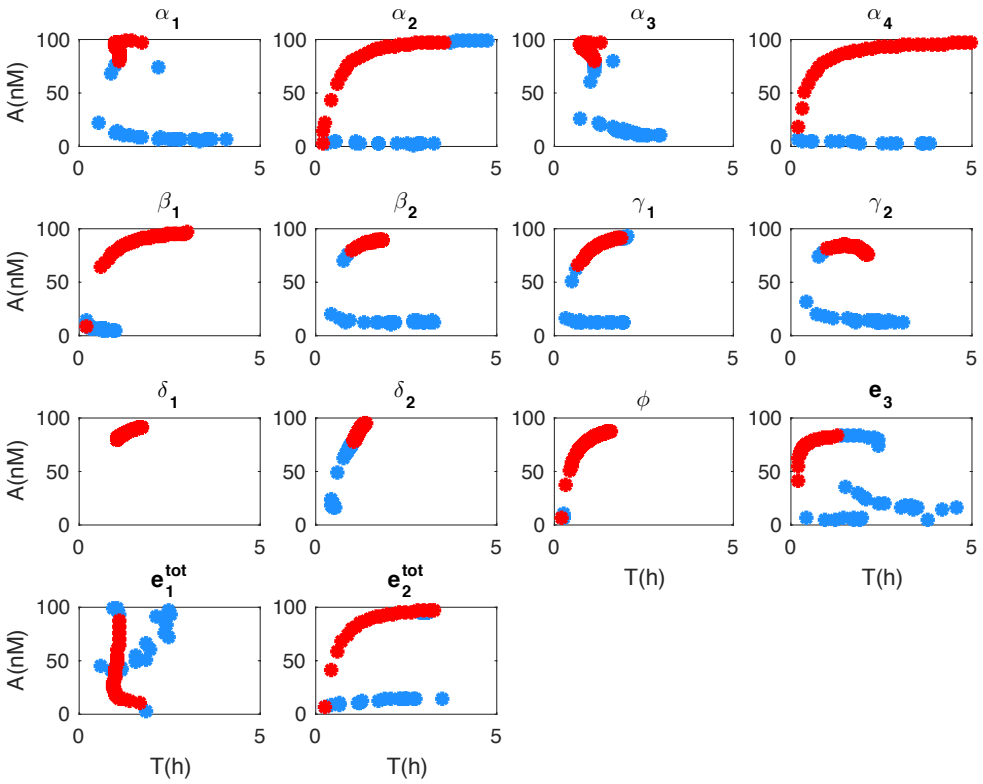

Figure 3.8: Period (h) and amplitude (nM) correlation. Blue circles represent when the Jacobian has at least one pair of complex eigenvalue with negative real part. The red circles represent when Jacobian has at least one pair of complex eigenvalue with positive real part. The grey circles represent when all eigenvalues are negative. The parameters were changed in the range of 0.1 to 10 times its nominal values.

Chapter 4

Design of a biomolecular bistable network using the CRISPR/Cas system

4.1 Introduction

The ability to engineer biomolecular circuits is essential to add desired functionality in cells and it has wide-ranging applications from personalized medicine to making designer organisms for materials production. While there exist many strategies to build biomolecular circuits, it is still difficult to systematically scale them up. For example, an approach using transcription factors for building genetic circuits is often limited in scale due a limited number of orthogonal transcription factors. Recently, the CRISPR/Cas based gene editing and gene regulation tools have provided a revolutionary way to control virtually any gene

inside the cell [71]. The CRISPR system was first found in a bacterial immune system [64]. This system was then successfully engineered into a tool to edit mammalian genes at will [23, 50]. It consists of a DNA endonuclease enzyme (Cas9), which cleaves the DNA and a guide RNA (gRNA), which recognizes the target DNA and localizes the enzyme on the target. Later, researchers also engineered Cas9 into a catalytically inactive form called dead Cas9 (dCas9) [71], which binds to the target site of the gRNA without cutting the DNA. Binding of dCas9 in the promoter region of a gene can inactivate the gene by blocking transcription.

In this paper, using analysis and simulations, we discuss a novel approach which use the dCas9-gRNA system to build biomolecular circuits. First, we present a regulatory module that achieves tunable input/output ultrasensitivity by combining molecular titration and an activation/deactivation cycle. Second, we use this module to build a multi-gene bistable switch, where the transcription product of each gene directs activation or inactivation of other genetic components of the circuit. Gene inhibition is accomplished by the dCas9-gRNA system; for reactivation of genes inhibited by dCas9, we propose to reverse the binding of dCas9 to the target gene using an anti-gRNA molecule.

In previous work, we proposed RNA-regulated genetic circuits that relied on RNA aptamers to modulate activity of RNA polymerases [61, 16, 59, 78, 76, 60]. In these systems, to reverse the aptamer-target binding pathway in a programmable manner, we developed anti-aptamer strands, which are DNA or RNA strands that are complementary to the aptamers. We also experimentally demonstrated the feasibility of using anti-aptamers to reactivate the aptamer-inhibited enzymes [1]. In the system presented in this manuscript, we

propose to use a similar idea to reactivate the gene inhibited by the dCas9-gRNA complex using an anti-gRNA species. The anti-gRNA is designed to be partly complementary to the gRNA and is expected to displace it from the target and the dCas9. While the feasibility of this approach is yet to be demonstrated experimentally, we postulate that this is feasible if the gRNA is designed to have single stranded "toehold" domains [53] at the target binding end, to facilitate displacement using the anti-gRNA species.

4.2 Circuit description and modeling

4.2.1 A CRISPR/CAS9 regulatory module

We describe a basic module, shown in Fig. 4.1 that will be used as the building block to design more complex circuits systematically. It consists of three genes: a target gene G_T, an inhibitor gene G_I and an activator gene G_A.

The inhibitor gene G_I transcribes RNA species R_I, which works as a gRNA that associates with dCas9 C_f forming a complex CR_I; this complex binds to the target gene G_T, thereby inhibiting it and converting it to species G_T^*. The activator gene G_A produces the anti gRNA species R_A, which displaces the gRNA R_I form the target gene G_T^* and the dCas9-R_I complex CR_I, thereby reactivating the target gene G_T. In the equations given below, free dCas9 concentration is denoted as C_f , the dCas9-R_I complex is denoted as CR_I and the inactive gene is represented by G_T^*. Species R_A and R_I bind to each other to produce a waste product which does not interfere with rest of the circuit. In the following, chemical species are indicated with capital letters (*e.g.* G_I) and their concentration with

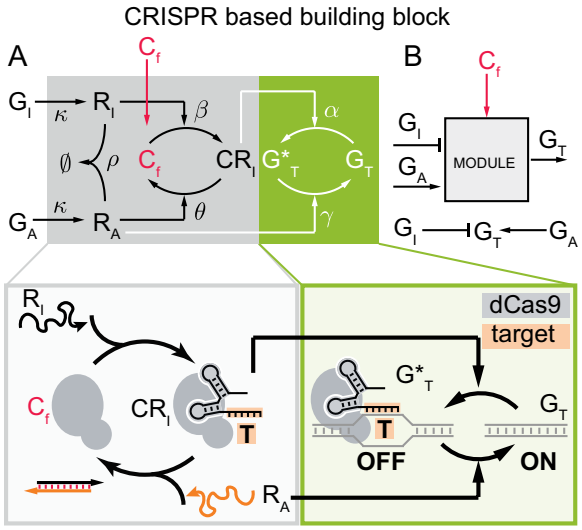

Figure 4.1: **Ultrasensitive regulatory module based on CRISPR/Cas system** A) Top: Schematic summary of the reactions defining the module. "G" stands for gene and "R" stands for RNA; subscript "I" stands for inhibitor, "A" stands for activator and "T" stands for target. Bottom: depiction of the proposed implementation using the CRISPR/Cas system and anti-gRNA. B) Inputs and output of the building block.

the corresponding lowercase letters (*e.g.* g_I).

Inhibitor process

$G_I \xrightarrow{\kappa} G_I + R_I$	gRNA Production
$R_I \xrightarrow{\phi} 0$	Degradation
$R_I + C_f \xrightarrow{\beta} CR_I$	dCas9 Activation
$G_T + CR_I \xrightarrow{\alpha} G_T^*$	Gene Inhibition

Activator process

$G_A \xrightarrow{\kappa} G_A + R_A$	Anti-gRNA Production
$R_A \xrightarrow{\phi} 0$	Degradation
$R_A + CR_I \xrightarrow{\theta} C_f$	dCas9 Inhibition
$G_T^* + R_A \xrightarrow{\gamma} G_T + C_f$	Gene Inhibition
$R_A + R_I \xrightarrow{\rho} 0$	Waste

The total concentration of species G_T and C_f are constant, as captured by the following mass conservation equations:

$$\begin{cases} g_T^{tot} = g_T + g_T^* \\ c^{tot} = c_f + cr_I + g_T^*. \end{cases} \tag{4.1}$$

Using the law of mass action and the mass conservation equalities, we obtain the

following model for the regulatory module:

$$\dot{r}_I = \kappa g_I - \beta r_I c_f - \phi r_I - \rho r_A r_I \tag{4.2}$$

$$\dot{r}_A = \kappa g_A - \gamma g_T^* r_A - \phi r_A - \rho r_I r_A - \theta c r_I r_A \tag{4.3}$$

$$\dot{g}_T = \gamma g_T^* r_A - \alpha c r_I g_T \tag{4.4}$$

$$\dot{cr}_I = \beta r_I c_f - \alpha c r_I g_T - \theta c r_I r_A. \tag{4.5}$$

4.2.2 Equilibrium conditions for the regulatory module

Here we derive expressions for the unique equilibrium of system (4.2)-(4.4). From $\dot{r}_I = \dot{r}_A$, we obtain:

$$\kappa g_I - \beta r_I c_f - \phi r_I = \kappa g_A - \gamma g_T^* r_A - \phi r_A - \theta c r_I r_A. \tag{4.6}$$

From $\dot{cr}_I = \dot{g}_T$, we obtain:

$$\beta r_I c_f = \theta c r_I r_A + \gamma r_A g_T^*. \tag{4.7}$$

Substituting expression (4.7) in (4.6), we obtain:

$$\kappa g_I - \phi r_I = \kappa g_A - \phi r_A. \tag{4.8}$$

Replacing (4.7) in $\dot{r}_A = 0$ and finding r_A:

$$r_A = \frac{\kappa g_A - \beta r_I c_f}{\phi + \rho r_I}. \tag{4.9}$$

Combining (4.8) and (4.9), we obtain the polynomial:

$$P(r_A) = a_r r_A^2 + b_r r_A + c_r = 0, \tag{4.10}$$

where

$$\begin{aligned} a_r &= \phi\rho, \\ b_r &= \phi^2 + \kappa\rho(g_I - g_A) + \beta\phi c_f, \\ c_r &= \beta\kappa(g_I - g_A)c_f - \phi\kappa g_A. \end{aligned}$$

If c_r is positive, both solutions are negative; one positive solution appears when c_r is negative, *i.e.* $g_I < \frac{\beta c_f + \phi}{\beta c_f} g_A$. In this case the unique positive solution of the polynomial is:

$$\bar{r}_A(g_I, g_A) = \frac{-b_r + \sqrt{b_r^2 - 4a_r c_r}}{2a_r}. \tag{4.11}$$

Then, we can obtain $\bar{r}_I$ from epxression (4.8):

$$r_I = \frac{\kappa(g_I - g_A) + \phi r_A}{\phi}. \tag{4.12}$$

We can obtain cr_I by combining $\dot{cr}_I = 0$ and $\dot{g}_T = 0$:

$$cr_I = \frac{\beta r_I c_f}{\alpha g_T + \theta r_A} = \frac{\gamma r_A (g_T^{tot} - g_T)}{\alpha g_T}. \tag{4.13}$$

We derive a polynomial:

$$P(g_T) = a_g g_T^2 + b_g g_T + c_g = 0, \tag{4.14}$$

where

$$\begin{aligned} a_g &= \alpha\gamma r_A, \\ b_g &= \alpha\beta r_I c_f - \alpha\gamma g_T^{tot} r_A + \gamma\theta r_A^2, \\ c_g &= -\gamma\theta g_T^{tot} r_A^2. \end{aligned}$$

The sign of c_g is always negative. Then the unique solution of the polynomial is:

$$g_T(g_I, g_A) = \frac{-b_g + \sqrt{b_g^2 - 4a_g c_g}}{2a_g} \tag{4.15}$$

4.2.3 Ultrasensitivity input-output relationship

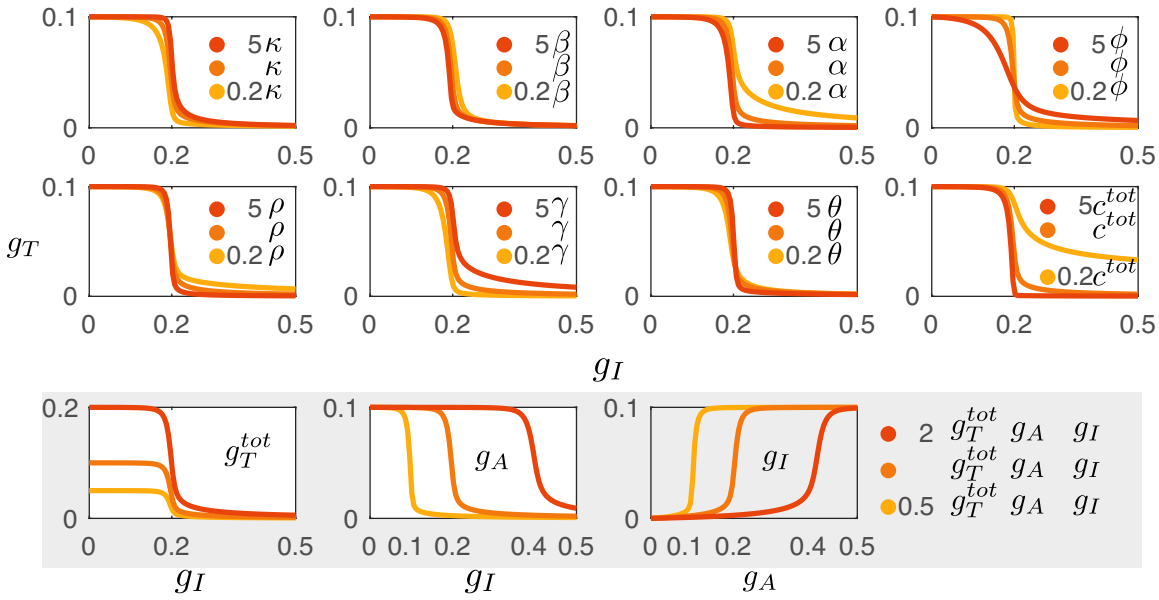

Figure 4.2: **Ultrasensitive characterization.** Stationary behavior of our regulatory module. Input-output equilibrium conditions from equations (4.2)-(4.5) as parameters are changed. Nominal parameters are in Table 4.1.

Fig. 4.2 shows numerical simulations of the steady state behavior of g_T and g_I, which highlight the ultrasensitive steady state response of the module. We numerically solve equations (4.2)-(4.5) and find the steady state values to find the input-output relationship. In every panel, a single parameter is varied as specified in the legend relative to its nominal value listed Table 4.1. We note that smaller values for the degradation rate ϕ boost ultrasensitivity, while smaller values of c^{tot} can reduce the ultrasensitive response. For larger parameter values, the system resemble a zero-order ultrasensitive response [39].

Titration of R_I and R_A enables precise tuning of threshold of the ultrasensitive response by varying either the input g_A or g_I, as shown inside the grey box in Fig. 4.2.

This result agrees with our previous detailed studies of the isolated mechanism inside the grey box in Fig. 4.1, where exploited this tunability to design a robust oscillator [27] and biomolecular feedback control [25].

4.2.4 Effects of loading and shared resources

We now examine two important phenomena that are known to affect molecular circuits: first, the influence of downstream processes on the performance of the regulatory module (loading [63, **?**]); second, the influence of Cas9 sharing with other circuits that may be present in solution (resource sharing [**?**, **?**]). To consider the first problem, we introduce additional reactions by which G_T is coupled to a downstream process; for example, the gene may become bound to a polymerase or a transcription factor. If the gene is depleted due to the binding to other molecules, we want to quantify the effect of this sequestration on the module. We consider the downstream process:

Downstream process

$G_T + E \underset{\kappa^-}{\overset{\kappa^+}{\rightleftharpoons}} C_E$	Binding/unbinding of the load E

Then, equation (4.4) becomes

$$\dot{g}_T = \gamma g_T^* r_A - \alpha c r_I g_T + \underbrace{\kappa^- c_e - \kappa^+ g_T e}_{\text{load}} \tag{4.16}$$

If we assume that binding/unbinding (κ^+/κ^-) are fast with respect to the time scale of the module, at steady state we find that $c_e = \frac{e}{e+\kappa_M} g_T$, where $\kappa_M = \frac{\kappa^+}{\kappa^-}$. We define the effective load on the system as $\lambda = e/\kappa_M$. Then, we update equation (6.6):

$$g^{tot} = g_T + g_T^* + \frac{\lambda}{1+\lambda} g_T \tag{4.17}$$

We plot the module input/output response as a function of the effective load λ in Fig. 4.3A; the results indicate that the presence of a load does not affect ultrasensitivity. This suggests that this regulatory network could be used within complex networks and maintain the ultrasensitivity observed when the circuit is in isolation.

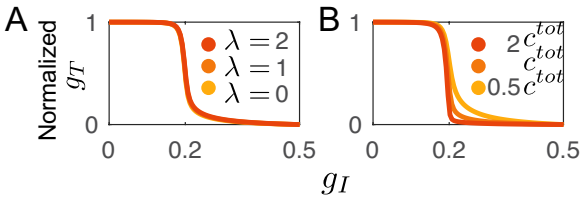

Figure 4.3: **Retroactivity and shared resources analysis** A) Shows the input-output mapping for different values of available Cas9 c_f. B) Shows for different loads of the module. Nominal parameters are in Table 4.1.

We now examine how competition for Cas9 available in the system affects the input/output mapping of the circuit. Fig. 4.3B shows the numerical analysis when we titrate the total amount of Cas9, suggesting that the ultrasensitive behavior is maintained up to a critical amount of enzyme. This result suggests that in the presence of a limited amount of Cas9, the module can maintain its ultrasensitive response. Therefore, we believe that this is a robust module to build synthetic circuits because it maintains its ultrasensitive behavior under loading and resource limitation.

4.3 Interconnecting ultrasensitive modules to build a bistable swtich based on CRISPR/CAS9

We now combine two modules ($G_1 - G_2 - G_4$ and $G_2 - G_1 - G_3$) to create a bistable system, schematically represented in Fig. 4.4. We create a positive feedback loop circuit

with two external inputs. In the rest of this section, we explore its capacity to exhibit bistability.

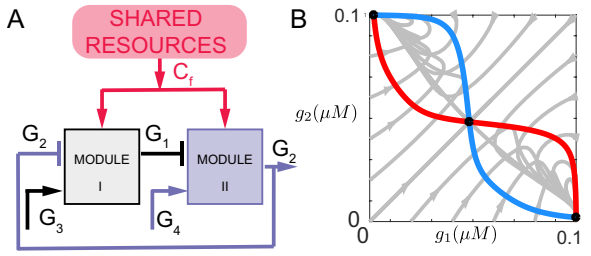

Figure 4.4: **Bistable system** A) Schematic of the interconnected inhibition and activation modules used to build the bistable network. B) Equilibrium conditions for system $g_1 = F1$ (red), equation (4.33), and $g_2 = F_2$ (blue), equation (4.29), and trajectories with different initial conditions (grey).

The differential equations of the bistable system are:

$$\dot{r_1} = \kappa g_1 - \beta r_1 c_f - \phi r_1 - \rho r_1 r_4 \tag{4.18}$$

$$\dot{r_4} = \kappa g_4 - \gamma r_4 g_2^* - \phi r_4 - \rho r_1 r_4 - \theta r_4 c r_1 \tag{4.19}$$

$$\dot{g_2} = \gamma r_4 g_2^* - \alpha g_2 c r_1 \tag{4.20}$$

$$c\dot{r}_1 = \beta r_1 c_f - \alpha g_2 c r_1 - \theta r_4 c r_1 \tag{4.21}$$

$$\dot{r_2} = \kappa g_2 - \beta r_2 c_f - \phi r_2 - \rho r_2 r_3 \tag{4.22}$$

$$\dot{r_3} = \kappa g_3 - \gamma r_3 g_1^* - \phi r_3 - \rho r_2 r_3 - \theta r_3 c r_2 \tag{4.23}$$

$$\dot{g_1} = \gamma r_3 g_1^* - \alpha g_1 c r_2 \tag{4.24}$$

$$c\dot{r}_2 = \beta r_2 c_f - \alpha g_1 c r_2 - \theta r_3 c r_2. \tag{4.25}$$

We assume there is mass conservation for the following components:

$$g_1^* = g_1^{tot} - g_1 \tag{4.26}$$

$$g_2^* = g_2^{tot} - g_2 \tag{4.27}$$

$$c_f = c^{tot} - cr_1 - g_1^* - cr_2 - g_2^*. \tag{4.28}$$

Additionally, $g_3 < g_2^{tot}$ and $g_4 < g_1^{tot}$.

4.3.1 Stability analysis

First, we derive equilibrium conditions for the circuits. Then, we demonstrate that the structure of this circuit is appropriate to obtain a bistable behavior; our proofs are modeled on previous work characterizing robust transitions to instability [13], where we need to demonstrate that each regulatory module is monotone and dissipative.

Equilibrium conditions

First, we derive the equilibrium conditions by setting each ODE in the model (4.18-4.25) equal to zero. The equilibrium conditions for a single building module are shown in Appendix A. Module I consist of $(G_1 - G_2 - G_4)$, where the target gene is G_2, the inhibitor gene is G_1 and the activator gene is G_4. Then, from (4.15) we can find $\bar{g}_2$ on function of g_1, g_4 and c_f. We obtain:

$$\bar{g}_2 = F_2(g_1, g_4, c_f) = \frac{-b_2 + \sqrt{b_2^2 - 4a_2c_2}}{2a_2}, \tag{4.29}$$

where

$$\begin{aligned} a_2 &= \alpha\gamma\bar{r}_4, \\ b_2 &= \alpha\beta\bar{r}_1\bar{c}_f - \alpha\gamma g_2^{tot}\bar{r}_4 + \gamma\theta\bar{r}_4^2, \\ c_2 &= -\gamma\theta g_2^{tot}\bar{r}_4^2. \end{aligned}$$

From (4.11) we obtain:

$$\bar{r}_4(g_1, g_4, c_f) = \frac{-b_1 + \sqrt{b_1^2 - 4a_1c_1}}{2a_1}, \tag{4.30}$$

where,

$$\begin{aligned} a_1 &= \phi\rho, \\ b_1 &= \phi^2 + \kappa\rho(\bar{g}_1 - g_4) + \beta\phi\bar{c}_f, \\ c_1 &= \beta\kappa(\bar{g}_1 - g_4)\bar{c}_f - \phi\kappa g_4. \end{aligned}$$

From (4.12) we obtain:

$$\bar{r}_1(g_1, g_4, c_f) = \frac{\kappa(\bar{g}_1 - g_4) + \phi\bar{r}_4}{\phi}, \tag{4.31}$$

and from (4.13) we obtain:

$$\bar{c}r_1 = \frac{\gamma\bar{r}_4\bar{g}_2^*}{\alpha\bar{g}_2}. \tag{4.32}$$

Similarly, Module II consist of $(G_2 - G_1 - G_3)$, where the target gene is G_1, the inhibitor gene is G_2 and the activator gene is G_3. Then, from (4.15) we can find $\bar{g}_1$ as a function of g_2, g_3 and c_f, and we get:

$$\bar{g}_1 = F_1(g_2, g_3, c_f) = \frac{-b_4 + \sqrt{b_4^2 - 4a_4c_4}}{2a_4}, \tag{4.33}$$

where

$$\begin{aligned} a_4 &= \alpha\gamma\bar{r}_3, \\ b_4 &= \alpha\beta\bar{r}_2\bar{c}_f - \alpha\gamma g_1^{tot}\bar{r}_3 + \gamma\theta\bar{r}_3^2, \\ c_4 &= -\gamma\theta g_1^{tot}\bar{r}_3^2. \end{aligned}$$

From (4.11) we obtain:

$$\bar{r}_3(g_2, g_3, c_f) = \frac{-b_3 + \sqrt{b_3^2 - 4a_3c_3}}{2a_3}, \tag{4.34}$$

where

$$\begin{aligned} a_3 &= \phi\rho, \\ b_3 &= \phi^2 + \kappa\rho(\bar{g}_2 - g_3) + \beta\phi\bar{c}_f, \\ c_3 &= \beta\kappa(\bar{g}_2 - g_3)\bar{c}_f - \kappa\phi g_3. \end{aligned}$$

From (4.12) we derive:

$$\bar{r}_2(g_2, g_3, c_f) = \frac{\kappa(\bar{g}_2 - g_3) + \phi\bar{r}_3}{\phi}, \tag{4.35}$$

and from (4.13) we obtain:

$$\bar{c}r_2 = \frac{\gamma\bar{r}_3\bar{g}_1^*}{\alpha\bar{g}_1}. \tag{4.36}$$

Then, we derive expressions for c_f as a function of g_1, g_2, g_3 and g_4. An expression for cr_1 can be obtained form $\dot{r_4} = 0$ and $\dot{g_2} = 0$, where we get:

$$cr_1 = \frac{\kappa g_4 - \gamma r_4 g_2^* - \phi r_4 - \rho r_1 r_4}{\theta r_4} = \frac{\gamma r_4 g_2^*}{\alpha g_2}. \tag{4.37}$$

By combining (4.31) and (4.37), we obtain the polynomial:

$$P(r_4) = a_5 r_4^2 + b_5 r_4 + c_5 = 0, \tag{4.38}$$

where

$$\begin{aligned} a_5 &= \phi(\alpha\rho g_2 + \gamma\theta g_2^*), \\ b_5 &= \alpha g_2(\gamma\phi g_2^* + \phi^2 + \kappa\rho(g_1 - g_4)), \\ c_5 &= -\alpha\phi\kappa g_4 g_2. \end{aligned}$$

The sign of c_5 is negative for any parameter set, therefore there is a unique solution:

$$r_4 = F_4(g_1, g_2) = \frac{-b_5 + \sqrt{b_5^2 - 4a_5c_5}}{2a_5}. \tag{4.39}$$

Similarly, we find expression for cr_2 from $\dot{r_3} = 0$ and $\dot{g_1} = 0$, we get:

$$cr_2 = \frac{\kappa g_3 - \gamma r_3 g_1^* - \phi r_3 - \rho r_2 r_3}{\theta r_3} = \frac{\gamma r_3 g_1^*}{\alpha g_1}. \tag{4.40}$$

By combing (4.35) and (4.40), we obtain a polynomial:

$$P(r_3) = a_6 r_3^2 + b_6 r_3 + c_6 = 0, \tag{4.41}$$

where

$$\begin{aligned} a_6 &= \phi(\alpha\rho g_1 + \gamma\theta g_1^*), \\ b_6 &= \alpha g_1(\gamma\phi g_1^* + \phi^2 + \kappa\rho(g_2 - g_3)), \\ c_6 &= -\alpha\phi\kappa g_1 g_3. \end{aligned}$$

The sign of c_6 is negative for arbitrary values of the parameters, therefore the unique solution is:

$$r_3 = F_3(g_1, g_2) = \frac{-b_6 + \sqrt{b_6^2 - 4a_6c_6}}{2a_6 t}. \tag{4.42}$$

Finally, we can express c_f as a function of g_1 and g_2 only:

$$c_f = F_5(g_1, g_2) = c^{tot} - cr_1 - cr_2 - g_1^* - g_2^*. \tag{4.43}$$

Substituting expression (4.43) into expressions (4.29) and (4.33), we can find $g_2 = F_2(g_1, g_2)$ and $g_1 = F_1(g_1, g_2)$, where g_3 and g_4 are the inputs of the system. Because it is difficult to express in a close form the equilibrium conditions $g_1 = f_2(g_2)$ and $g_2 = f_2(g_1)$, we solve them numerically. Fig 4.4 shows example equilibrium conditions obtained with the parameters in Table 4.1.

Monotonicity

Lemma 19 *System* (4.18)–(4.25) *is the positive feedback interconnection of two monotone subsystems.*

Proof The Jacobian matrix J of the system is shown at equation (4.45). All the elements of J are sign definite. We can apply a state transformation T to J as follow $J^* = TJT^{-1}$.

$$T = diag(1, -1, -1, 1, 1, -1, -1, 1) \tag{4.44}$$

Two block diagonal matrices in matrix (4.46) are Metzler matrices, and the only off diagonal elements are negative. Overall, the interconnected system is the positive feedback interconnection of two monotone subsystems (two negative interconnections result in an overall positive interconnection). ■

$$J = \begin{bmatrix} j_{1,1} & -\rho\bar{r}_1 & 0 & 0 & 0 & 0 & \kappa & 0 \\ -\rho\bar{r}_4 & j_{2,2} & \gamma\bar{r}_4 & -\theta\bar{r}_4 & 0 & 0 & 0 & \\ 0 & \gamma\bar{g}_2^* & -\alpha\bar{c}r_1 - \gamma\bar{r}_4 & -\alpha\bar{g}_2 & 0 & 0 & 0 & 0 \\ \beta\bar{c}_f & -\theta\bar{c}r_1 & -\alpha\bar{c}r_1 & -\alpha\bar{g}_2 - \theta\bar{r}_4 & 0 & 0 & 0 & 0 \\ 0 & 0 & \kappa & 0 & j_{5,5} & -\rho\bar{r}_2 & 0 & 0 \\ 0 & 0 & 0 & 0 & -\rho\bar{r}_3 & j_{6,6} & \gamma\bar{r}_3 & -\theta\bar{r}_3 \\ 0 & 0 & 0 & 0 & 0 & \gamma\bar{g}_1^* & -\alpha\bar{c}r_2 - \gamma\bar{r}_3 & -\alpha\bar{g}_1 \\ 0 & 0 & 0 & 0 & \beta\bar{c}_f & -\theta\bar{c}r_2 & -\alpha\bar{c}r_2 & -\alpha\bar{g}_1 - \theta\bar{r}_3 \end{bmatrix} \tag{4.45}$$

Where $j_{1,1} = -\beta c_f - \phi - \rho\bar{r}_4$, $j_{2,2} = -\gamma\bar{g}_2^* - \phi - \rho\bar{r}_1 - \theta\bar{c}r_1$, $j_{5,5} = -\beta\bar{c}_f - \phi - \theta\bar{r}_3$ and $j_{6,6} = -\gamma\bar{g}_1^* - \phi - \rho\bar{r}_2 - \theta\bar{c}r_2$

$$J^* = \begin{bmatrix} j_{1,1}^* & \rho\bar{r}_1 & 0 & 0 & 0 & 0 & -\kappa & 0 \\ \rho\bar{r}_4 & j_{2,2}^* & \gamma\bar{r}_4 & \theta\bar{r}_4 & 0 & 0 & 0 & \\ 0 & \gamma\bar{g}_2^* & -\alpha\bar{c}r_1 - \gamma\bar{r}_4 & \alpha\bar{g}_2 & 0 & 0 & 0 & 0 \\ \beta\bar{c}_f & \theta\bar{c}r_1 & \alpha\bar{c}r_1 & -\alpha\bar{g}_2 - \theta\bar{r}_4 & 0 & 0 & 0 & 0 \\ 0 & 0 & -\kappa & 0 & j_{5,5}^* & \rho\bar{r}_2 & 0 & 0 \\ 0 & 0 & 0 & 0 & \rho\bar{r}_3 & j_{6,6}^* & \gamma\bar{r}_3 & \theta\bar{r}_3 \\ 0 & 0 & 0 & 0 & 0 & \gamma\bar{g}_1^* & -\alpha\bar{c}r_2 - \gamma\bar{r}_3 & \alpha\bar{g}_1 \\ 0 & 0 & 0 & 0 & \beta\bar{c}_f & \theta\bar{c}r_2 & \alpha\bar{c}r_2 & -\alpha\bar{g}_1 - \theta\bar{r}_3 \end{bmatrix} \tag{4.46}$$

Where $j_{1,1}^* = -\beta c_f - \phi - \rho\bar{r}_4$, $j_{2,2}^* = -\gamma\bar{g}_2^* - \phi - \rho\bar{r}_1 - \theta\bar{c}r_1$, $j_{5,5}^* = -\beta\bar{c}_f - \phi - \theta\bar{r}_3$ and $j_{6,6}^* = -\gamma\bar{g}_1^* - \phi - \rho\bar{r}_2 - \theta\bar{c}r_2$

4.3.2 Admissible transitions to instability

We show that the system can only undergo real transitions to instability, thus any simple bifurcation yields a multistationary behavior. We begin recalling some definitions from [49] and [13].

Definition 20 (Dissipative system) *A system $\dot{x} = f(x)$, $x \in \mathbb{R}^n$ is dissipative if its solu-*

tions are eventually uniformly bounded, i.e., there exists a constant $k > 0$ such that:

$$\lim_{t \to +\infty} \sup x_j(t) \leq k, \quad j = 1, ..., n.$$

Lemma 21 *System* (4.18)–(4.25) *is dissipative.*

Proof Variables g_i and cr_i, $i = 1, 2$ are globally bounded because the total concentrations g_i^{tot} (genes) and c_f^{tot} (dCas9) are constant. We show that variables r_i,$i = 1 : 4$, which represent the concentration of RNA species, are asymptotically bounded using the comparison principle. The dynamics of r_i can be upper-bounded by a linear time invariant, asymptotically stable ODE.

$$\dot{r}_i \leq \kappa g_i^{tot} - \phi_i x_i, \quad i = 1 : 4,$$

thus as $t \to \infty$, $r_i(t) \leq (\kappa/\phi) y^{tot} = r_i^+$. (At all times, $r_i(t) \leq r_i^+ + (r_i(0) - r_i^+)e^{-\phi t}$.) ■

We recall that a simple transition to instability occurs when at most a single real eigenvalue or a single pair of complex conjugate eigenvalues crosses the imaginary axis.

Definition 22 (Real transition to instability [13]) *A system $\dot{x} = f(x, \mu)$ that is continuously differentiable with equilibrium $\bar{x}_\mu$, undergoes a* real transition to instability *at $\mu = \mu^*$ if and only if its Jacobian matrix $J(\bar{x}_{\mu^*})$ has a single zero eigenvalue, while all the other eigenvalues have negative real part:*

$$\sigma\left(J(\bar{x}_{\mu^*})\right) = \{\lambda_1, \ldots, \lambda_n\}, \quad \textit{where} \quad \lambda_1 = 0,$$

with $Re(\lambda_k) < 0$ for $k > 1$ and $Re(\lambda_1) > 0$ in a right neighborhood of μ^*.

Definition 23 (Strong candidate multistationary system [13]) *A continuosly differentiable, dissipative system $\dot{x} = f(x, \mu)$, presenting sign definite derivatives, is a candidate* multistationary system in the strong sense *iff, for any alteration of parameter μ, every simple transition to instability is a real transition to instability.*

Lemma 24 *System* (4.18)–(4.25) *admits exclusively real transitions to instability. Thus, it is a strong candidate multistationary system.*

Proof System (4.18)–(4.25) is dissipative (Lemma 21).The system is also the positive feedback interconnection of two input-output monotone systems with respect to the orthant $\Sigma = (+, -, -, +, +, -, -, +)$ (Lemma 19). Because all the cycles in the Jacobian matrix (4.46) are positive, the linearized system is monotone overall. Thus, the Jacobian (4.46) presents a real dominant eigenvalue. We conclude that any simple transition to instability must be a real transition to instability and the system is a strong candidate multistationary system. ■

Lemma 25 *If a simple transition to instability occurs at an equilibrim point $\bar{x}$ of system* (4.18)–(4.25)*, then at least two additional equilibria appear. If exactly two equilibria appear, then they are asymptotically stable.*

The proof of Lemma 25 is analogous to the proof of Corollary 2 in [13] and is thus omitted. The proof uses index theory and relies on monotonicity and boundedness of the system, and the fact that it is a strong candidate multistationary system.

Lemma 25 indicates that if a transition to instability is characterized by the emergence of exactly two additional equilibria, then the system near the transition is bistable.

Table 4.1: Nominal parameters used in numerical integration of equations (4.18)-(4.25)

Rate	Description	Value	Other studies
κ (/s)	Production	$1.3 \cdot 10^{-3}$	RNA: $10^{-3} - 1$ Refs. [91, 22] Proteins: $3 \cdot 10^{-3} - 1$ Ref. [19]
β (/M/s)	dCas9 activation	$1 \cdot 10^4$	NA
θ (/M/s)	dCas9 inhibition	$1 \cdot 10^4$	NA
γ (/M/s)	Gene activation	$1 \cdot 10^4$	NA
α (/M/s)	Gene inhibition	$1 \cdot 10^4$	Cas9/dCas9 $3 \cdot 10^4 - 3 \cdot 10^5$ Ref. [84].
ϕ (/s)	Degradation	$1 \cdot 10^{-4}$	Proteins: $10^{-4} - 10^{-3}$ Ref.[19]
ρ (/M/s)	RNA hybridization	$1 \cdot 10^4$	$10^2 - 10^6$ Ref. [41]

Thus, the system we designed has the appropriate structure to be a bistable switch. In the next section we numerically explore the parameter range in which bistability can be achieved.

4.4 Numerical analysis

MATLAB scripts were used to identify the bistability regions, by varying the parameters around their nominal values reported in Table 4.1. For simplicity we assumed that the nominal parameters of the two subsystems are identical, and are realistic for nucleic acid hybridization and transcription [42]. Kinetic binding rates of gRNA and Cas9, together with the gRNA displacement rates, have not been experimentally measured to the authors' knowledge; we assumed that these rates are comparable to nucleic acid hybridization rates.

Figs. 4.5 and 4.6 shows a logarithmic plot of the result of our simulations. Parameters were varied one order of magnitude around their nominal values. The system is bistable (*i.e.* has 3 equilibrium points, one of which is unstable and the other two are stable) in the

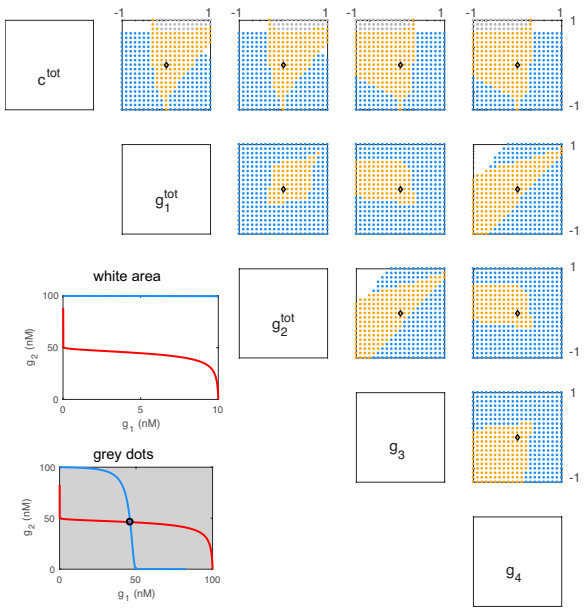

Figure 4.5: **Bifurcation analysis of experimentally tunable parameters.** Bistability regions were computed evaluating the Jacobian at each of three equilibria, which were calculated using the expressions at Section 4.3.1. Nominal parameters are in Table 4.1. White regions indicate when our algorithm fails to find the intersection due to a numerical discontinuity of the nullcline expression (example shown in the white box). The grey dots shows a single intersection. However, the algorithm fails to detect the other two equilibrium, an example of it is shown in the second figure with a grey background.

orange regions; the system is monostable in the cyan regions.

4.5 Conclusion

We have described an approach to design CRISPR-based ultrasensitive regulatory modules, and we demonstrated how these modules can be interconnected to build a bistable network. The regulatory building block can behave either as an activator or an inhibitor depending on the relative concentration of certain components. This module may be used as in more complex systems, since one can target virtually any gene using an appropriate

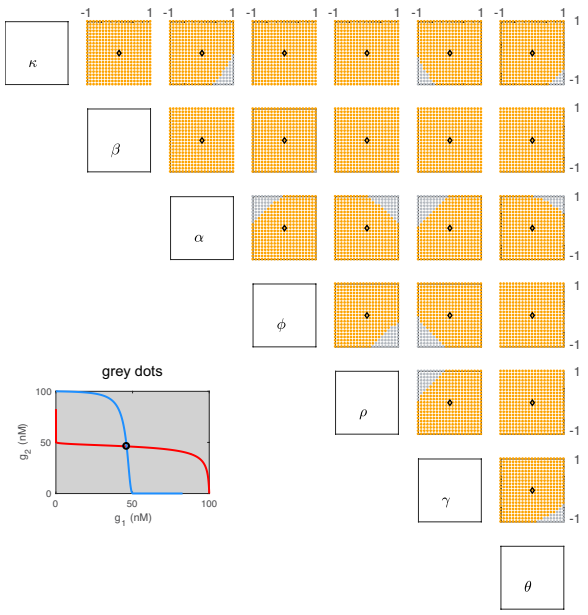

Figure 4.6: **Bifurcation analysis of rate constants of the reactions.** Bistability regions were computed evaluating the Jacobian at each of three equilibria, which were calculated using the expressions at Section 4.3.1. Nominal parameters are in Table 4.1. The grey dots shows a single intersection. However, the algorithm fails to detect the other two equilibrium, an example of it is shown in the figure with a grey background

gRNA. Our numerical results suggest that the regulatory module exhibits a robust and tunable ultrasensitive response. We find that ultrasensitivity is maintained in the presence of a downstream load and in a regime where resources (Cas9) are shared.

The proposed network is bistable in a wide range of parameters, which suggests this architecture is robust. For the circuit to work, it is required that the concentration of the input genes (g_3 and g_4) be less than the concentration of genes that mutually inhibit (g_1 and g_2). Given the robust nature of CRISPR-based gene regulation inside cells, the circuit we described has a potential to be implemented *in vivo*.

Chapter 5

An ultrasensitive biomolecular network for robust feedback control

5.1 Introduction

Fulfilling the promises of synthetic biology to be employed for energy, agriculture and health application will require a precise control of regulation of many molecular processes such as transcription, translation and post-translational modification. Biological cells have evolved feedback pathways so that the concentration of proteins and small molecules remains within a desirable range; negative autoregulation, for instance, has been found in more than half of genes in *E coli* ([87]). Although there has been a great deal of progress in understanding how to harness feedback to build various biomolecular circuits, including

toggle switches, oscillators, and a variety of logic gates, it is still unclear how to design controller circuits in a rational manner that is comparable to feedback controllers in electrical or mechanical systems.

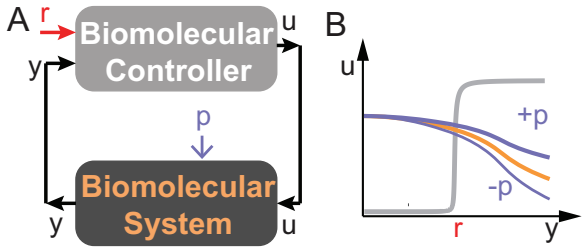

Figure 5.1: **Closed loop molecular network with an ultrasensitive controller** A) Schematic of the interconnection of a biomolecular controller and a biomolecular system; p represents a given parameter perturbation in the system. B) shows an illustration of input-output equilibrium conditions of the controller (in grey) and the system (in orange). The controller ultrasensitive response threshold is tunable by setting the reference signal r, shown in red. Ultrasensitivity of the controller implies that, in a certain regime, perturbations in the input/output curve of the systems have minor influence on the equilibrium point.

In this paper we describe and analyze a molecular controller network that relies on non-cooperative interactions between components. The controller network is used to steer the output of a target system to be controlled in closed loop, as shown in Fig. 5.1 A.

The most important feature of the controller we present is its steady state ultrasensitive response which has a tunable threshold. The threshold is designed to "track" the controller reference input, so that the closed loop equilibrium tracks the reference robustly. Ultrasensitivity is achieved by combining two mechanisms: molecular titration ([20, 28]), rather than cooperativity, and an activation/deactivation cycle of the controller variable, similar to a phosphorylation/dephosphorylation monocycle ([40]). Each of these mechanisms, taken in isolation and modeled with mass action kinetics, are not sufficient to provide highly ultrasensitivity. Titration reactions facilitate the tunability of the response threshold,

and titration together with the activation/deactivation cycle mechanism creates a highly ultrasensitive input/output curve. This ultrasensitive behavior is very similar to zero-order ultrasensitivity when enzymes are saturable and their activities are given by Michaelis-Menten equations ([40]. The controller reaction network is directly implementable using *in vitro* synthetic transcriptional systems, such as negative feedback systems ([43]) to balance production rates. The module, taken as a subsystem in a larger network, can also be used to build oscillatory systems ([26]). We exploit the controller ultrasensitivity to tune the closed loop equilibrium point, and to achieve robustness relative to parameter perturbations, as sketched in Fig. 5.1 B.

Titration reactions *in vivo* without degradation were used recently by [17] to propose an antithetic integral feedback controller, whose reactions are analogous to the first stage of our controller. Our network differs from the anthitetic controller for two reasons: first, it includes an additional activation/deactivation cycle for the controller molecule; second, we take into account degradation (or dilution) reactions that are known to be present in most biochemical and cellular processes. As shown in our manuscript, these processes can disrupt the tracking and adaption properties of the controller ([33]). [66] found that an ultrasensitive network can model osmoregulation behaviors better than proportional and/or integral networks; this suggests that natural circuits may have evolved ultrasensitivity to robustify equilibria as shown in this paper.

In Section 5.2 we describe the controller network in isolation, and we characterize its ultrasensitive behavior. In Section 6.27 we describe the target system to be controlled. Finally, in Section 5.4 we consider the closed loop system and examine the capacity of the

system output to track a reference, as well as its sensitivity with respect to perturbations in the reaction rates and concentration of components. We discuss the reactions chosen to design the controller in relation to a potential *in vitro* implementation with synthetic transcriptional networks [53].

Throughout the paper we consider biomolecular systems that are described by chemical reactions. Species indicated as uppercase letters, concentrations as lowercase letters (e.g. species X has concentration x). Given a set of chemical reactions, we use the law of mass action to derive ordinary differential equation (ODE) models that describe the kinetics of the ensemble of reactions.

5.2 Design of an ultrasensitive molecular controller

The controller network (Fig. 5.2A) consists of a single output species U and two input species, an activator A and an inhibitor I. The output species can be in active form U, or inactive form U^*, and its total concentration is conserved ($u^{tot} = u + u^*$). Active U is assumed to have a regulatory function in downstream reactions, which cannot be performed by U^*. The inputs A and I respectively produce species R_A and R_I, which regulate the active fraction of output U. R_I binds to and deactivates U, forming an inert species U^*. In contrast, species R_A binds to and reactivates U^* by displacing R_I from U^*, yielding a waste complex $R_A \cdot R_I$. In addition, free R_A and R_I bind and mutually titrate forming waste complex $R_A \cdot R_I$. The biomolecular reactions constituting our controller network are:

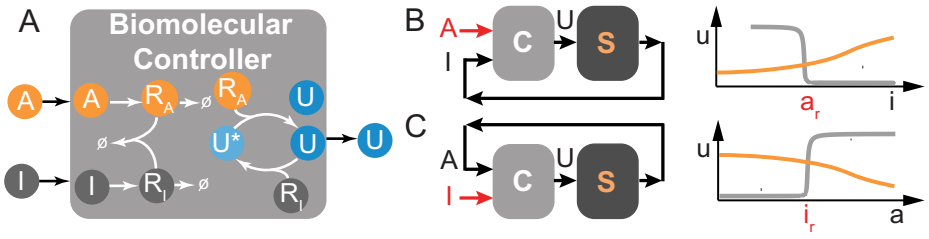

Figure 5.2: **Ultrasensitive network.** A) Schematic summary of the reactions defining the controller network. B) Controller network within a feedback loop, where signal A is kept constant and represents a reference signal, shown in red. C) Controller in a feedback loop where signal A is kept constant and acts as a reference, shown in red. The thresholds a_r and i_s are functions of the reference a and i (in red) and of the parameters of the system.

$A \xrightarrow{\kappa_c} A + R_A$	Production
$I \xrightarrow{\theta_c} I + R_I$	Production
$R_A + R_I \xrightarrow{\gamma_c} R_A \cdot R_I$	Titration
$R_A \xrightarrow{\phi_c} 0$	Degradation
$R_I \xrightarrow{\phi_c} 0$	Degradation
$R_A + U^* \xrightarrow{\alpha_c} U + R_A \cdot R_I$	Reactivation
$R_I + U \xrightarrow{\beta_c} U^*$	Inhibition

Using the law of mass action, we derive the following ODEs that describe the dynamics of the system:

$$\dot{u} = \alpha_c r_A u^* - \beta_c r_I u \tag{5.1}$$

$$\dot{r}_A = \kappa_c A - \alpha_c r_A u^* - \gamma_c r_A r_I - \phi_c r_A \tag{5.2}$$

$$\dot{r}_I = \theta_c I - \beta_c r_I u - \gamma_c r_A r_I - \phi_c r_I \tag{5.3}$$

Fig. 5.2 B and C illustrate the desired interactions of species U, R_A, and R_I, and

how they result in an ultrasensitive response. First, consider the case where the system receives a step input in i. Then, active species u is expected to be quickly converted to its inactive form u^*. However, the presence of a (which produces r_A) has a "buffering" effect: free r_A binds to r_I and titrates it before it can inhibit u (this of course requires that γ_c is fast). Due to this buffering effect, we can think of i as the input to the controller, and of the titrating species a as a "reference" signal: the controller responds only if i exceeds a. A similar reasoning can be followed to explain the behavior of the system when the system receives a step input a: in this case, free r_I acts like a buffer for r_A. We can think of a as the input to the controller, and of the titrating species i as the reference; only when a exceeds i the controller responds. In both cases, the transition point (at which the concentration of u switches from low to high and vice-versa) depends on the concentration of the titrating species.

This reaction network could be experimentally realized using nuceic acids and proteins. Species U could be an RNA polymerase whose activity can repressed using an RNA aptamers (R_I) as those proposed by [67, 69] (species R_I). RNA polymerase activity could be restored via another RNA species (R_A) displacing the aptamer as suggested in [26]. Synthetic templates (A, I) could be used to produce the RNA regulators. Numerical integration of equations (5.1)–(5.3) is done assuming nominal values of parameters (Table 5.1) that are realistic in the implementation context just described.

In the next sections we examine the behavior of the controller network. We derive its steady state input/output response analytically, and then we test numerically the sensitivity of the controller response to parameter perturbations.

Boundedness and monotonicity

The solutions of the biomolecular controller model are bounded. After a state transformation, the Jacobian of ths system is a Metlzer matrix, which is Hurwitz stable, and we can conclude that the input-output equilibrium maps of $u(A)$ and $u(I)$ are monotonically increasing and decreasing. These claims can be demonstrated following the analysis in [26], which are not reported here.

Input-output characterization

We begin by finding an expression for the concentration of input A as a function of the concentrations of input I and output U. (These expressions are more convenient to find relative to deriving the concentration of U as a function of A and I).

$$a(u,i) = \frac{\theta_c}{\kappa_c} i + \frac{\phi_c}{\kappa_c}\left(1 - \frac{\alpha_c u^*}{\beta_c u}\right)\bar{r}_A(u,i), \tag{5.4}$$

where

$$\bar{r}_A(u,i) = \frac{-b_A + \sqrt{b_A^2 - 4a_A c_A}}{2a_A},$$

$a_A = \alpha_c \gamma_c u^*$, $b_A = \alpha_c u^*(\beta_c u + \phi_c)$ and $c_A = -u\beta_c \theta_c I$.

Similarly, we find an expression relating the equilibrium concentration of I as a function of U and A.

$$i(u,a) = \frac{\kappa_c}{\theta_c} a - \frac{\phi_c}{\theta_c}\left(\frac{\alpha_c u^*}{\beta_c u} - 1\right)\bar{r}_I(u,a), \tag{5.5}$$

where

$$\bar{r}_I(u,a) = \frac{-b_I + \sqrt{b_I^2 - 4a_I c_I}}{2a_I},$$

$a_I = \beta_c \gamma_c u$, $b_I = \beta_c u(\alpha_c u^* + \phi_c)$ and $c_I = -\alpha_c u^* \kappa_c A$.

Ultrasensitivity characterization

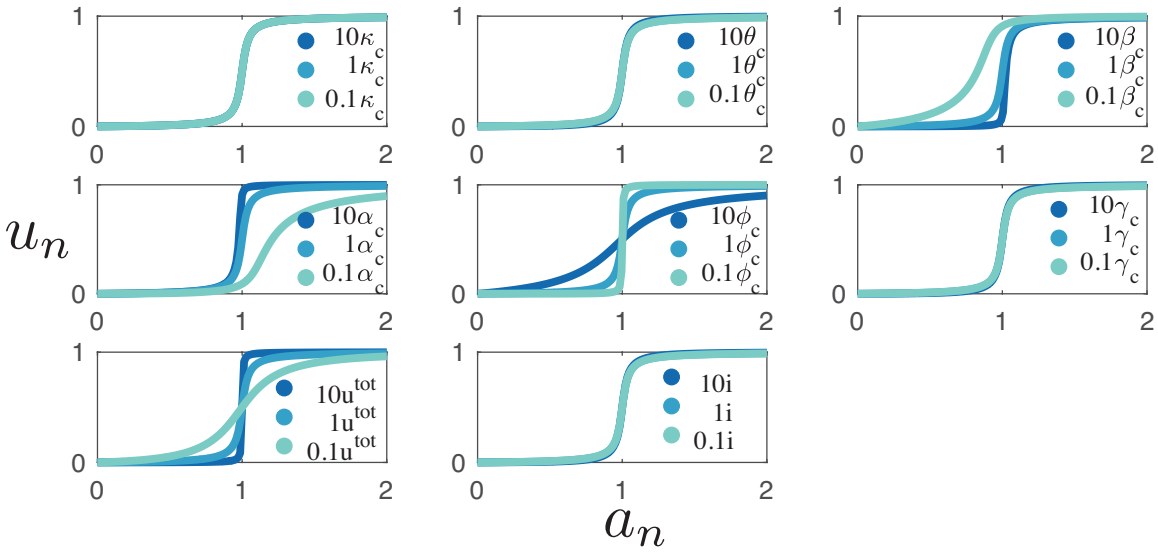

Figure 5.3: **Controller ultrasensistive response.** Input-output equilibrium conditions from equation (5.4) as parameters are varied. Nominal simulation parameters are listed in Table 5.1.

To assess the ultrasensitivity of the input/output curves with respect to parameter variations, we vary individual parameters of the network. We focus on plotting expression (5.4): we fix the concentration of i, and then evaluate $\bar{r}_A(u, i)$ when u varies between 0 and u^{tot}; this allows us to evaluate the map $a(u, i)$ (x axis) versus u (y axis) as shown in Fig. 5.3. We note that if the concentration of i is fixed, we can think of term $i_r = \frac{\kappa_c}{\theta_c} i$ as the threshold of the ultrasensitive response.

The plots in Fig. 5.3 were obtained using normalized concentrations of species $a_n = a(u, i)/i_r$, and $u_n = u/u^{tot}$. The behavior of the input-output expression (5.4) is evaluated as parameters are individually varied.

Table 5.1: Nominal simulation parameters of the controller

Parameter	Description	Value	Other studies
θ_c (/s)	Production	$7.5 \cdot 10^{-4}$	
κ_c (/s)	Production	$5 \cdot 10^{-4}$	Transcription: $10^{-3} - 1$ [91, 22]
β_c (/M/s)	Inhibition	$6 \cdot 10^4$	$10^4 - 10^6$ [53, 99]
α_c (/M/s)	Reactivation	$6 \cdot 10^4$	$10^4 - 10^6$ [53, 99]
γ_c (/M/s)	Titration	$3 \cdot 10^4$	$10^4 - 10^6$ [53, 99]
ϕ_c (/s)	Degradation	$3.85 \cdot 10^{-4}$	$10^{-4} - 10^{-3}$ [52].
$u^{tot}(nM)$	Concentration	500	

We note that curves are very sensitive to the inhibition rate (β_c), the activation rate (α_c), the degradation rate (ϕ_c) and total amount of input (u^{tot}). The input/output curve steepness increases when these parameters are large, with exception for the degradation rate (ϕ_c), which largely reduces the ultrasensitivity.

The last panel of Fig. 5.3 shows the influence of variations of i on the input-output response. Because of how the variables are normalized, the curve transition always occurs at $a_n = 1$: this indicates that the output equilibrium always perfectly tracks the desired threshold, which can be seen as a "reference" in the closed loop system, as we further explain in the next sections. (A non-normalized plot of the input-output response is in Fig. 5.6 B, C, D.)

It is possible to plot (6.13) by defining similar threshold parameters and normalized variables, and we obtain similar results (not shown for brevity).

5.3 Controlled system

We consider an example transcription process as a target system to be controlled. Specifically, we focus on a class of synthetic *in vitro* genetic switches which have been

used to build a variety of autonomous circuits including bistable and oscillatory networks [53, 51, 42].

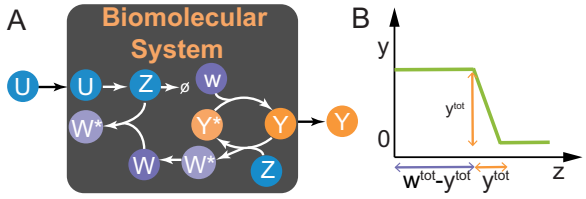

Figure 5.4: **Biomolecular system or process** A) Schematic of a simplify model of a synthetic gene switch with input u and output y. B) An illustration of input/output response with input z and output y.

The target system receives a single input species U and produces an output species Y. As in [53], Y is a synthetic template (genelet) that is activated by a DNA activator molecule W, and deactivated by an RNA inhibitor molecule Z. The input U could be an RNA polymerase transcribing inhibitor Z from a constitutively active template; Z is designed to bind to Y and convert it to inactive Y^* (this occurs by displacement of the activator W). In addition, Z directly binds to and titrates W converting it to inactive species W^*. We assume that inhibited activator W^* spontaneously reverts to its active form W. The total concentrations of Y and W are assumed to be constant, $y^{tot} = y + y^*$ and $w^{tot} = w + y + w^*$. These regulatory interactions are illustrated in Fig. 5.4A, and the

corresponding set of chemical reactions is:

$U \xrightarrow{\kappa_s} U + Z$	Production
$Z + W \xrightarrow{\gamma_s} W^*$	Titration
$Z \xrightarrow{\phi_s} 0$	Degradation
$W^* \xrightarrow{\theta_s} W$	Recovery
$W + Y^* \xrightarrow{\alpha_s} y + W^*$	Activation
$Y + Z \xrightarrow{\beta_s} Y^*$	Inhibition

Using the law of mass action we derive the following ODEs:

$$\dot{y} = \alpha_s w y^* - \beta_s y z \tag{5.6}$$

$$\dot{w} = \theta_s w^* - \alpha_s w y^* - \gamma_s z w \tag{5.7}$$

$$\dot{z} = \kappa_s u - \beta_s y z - \gamma_s z w - \phi_s z \tag{5.8}$$

In earlier work ([28]) we demonstrated analytically that the solutions of ODEs (5.6)–(5.8) are bounded, that the system is structurally stable and monotone, and the input-output map is monotonically decreasing. We find the equilibrium values of u and y are related according to the following expression:

$$u(y) = \frac{\theta_s w^* + \phi_s z}{\kappa_s}, \tag{5.9}$$

$$\text{where} \quad z = \frac{\alpha_s}{\beta_s}\frac{y^*}{y} w, \quad w = \frac{-b_s + \sqrt{b_s^2 - 4a_s c_s}}{2a_s}$$

$a_s = \frac{\alpha_s \gamma_s}{\beta_s}\frac{y^*}{y}$, $b_s = \alpha_s y^* + \theta_s$ and $c_s = -\theta_s(w^{tot} - y)$.

In the next sections, we numerically integrate the system ODEs using the nominal parameters listed in Table 6.1, which are realistic values relative to the proposed circuit

Table 5.2: Nominal simulation parameters of the controlled system

Rate	Description	Value	Other studies
κ_s (/s)	Production	$5 \cdot 10^{-4}$	Transcription: $10^{-3} - 1$ [91, 22]
θ_s (/s)	Recovery	$3 \cdot 10^{-4}$	$10^{-5} - 10^{-2}$ [22, 8]
β_s (/M/s)	Inhibition	$6 \cdot 10^{4}$	$10^{4} - 10^{6}$ [53, 99]
α_s (/M/s)	Reactivation	$6 \cdot 10^{4}$	$10^{4} - 10^{6}$ [53, 99]
γ_s (/M/s)	Titration	$3 \cdot 10^{4}$	$10^{4} - 10^{6}$ [53, 99]
ϕ_s (/s)	Degradation	$3.85 \cdot 10^{-4}$	$10^{-4} - 10^{-3}$ [52]
$y^{tot}(nM)$	Concentration	800	
$w^{tot}(nM)$	Concentration	800	

implementation using transcriptional circuits ([53]).

5.4 Closed loop system

We now analyze the performance of the closed loop system where controller and system are interconnected. The goal is to control the concentration of active template Y as shown in Fig.5.5, following a reference signal R. Because the input/output behavior of this particular system is monotone decreasing (Fig. 5.4), we operate our controller so that the feedback loop counter acts the system response. So we connect variable Y in the feedback loop to serve as input A (activator) for the controller. The controller input I is now considered the reference signal R. We note that if the system to be controlled had a monotonically increasing input-output map, we would have operated the controller in the opposite way, so that input A would be the reference. This suggests that this controller architecture can be adapted to work with systems having very different input-output behaviors; a theoretical characterization of this property is left for future work.

We combine equations (5.1)–(5.3) (controller) and equations (5.6)–(5.8) (controlled

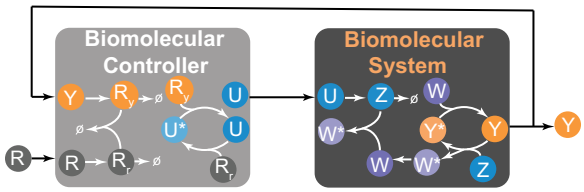

Figure 5.5: **Feedback control system.** Closed loop system between the biomolecular controller and biomolecular system. Where the set point, output and actuator are r, y and u respectively.

system) and obtain the closed loop system equations:

$$
\mathrm{C}\begin{cases}
\dot{u} = \alpha_c r_y u^* - \beta_c r_r u & \text{controller output} \\
\dot{r}_y = \underbrace{\kappa_c y}_{\text{controller input}} - \alpha_c r_y u^* - \gamma_c r_y r_r - \phi_c r_y & \\
\dot{r}_r = \underbrace{\theta_c r}_{\text{external input}} - \beta_c r_r u - \gamma_c r_y r_r - \phi_c r_r &
\end{cases}
$$

$$
\mathrm{S}\begin{cases}
\dot{y} = \alpha_s w y^* - \beta_s y z & \text{system output} \\
\dot{w} = \theta_s w^* - \alpha_s w y^* - \gamma_s z w & \\
\dot{z} = \underbrace{\kappa_s u}_{\text{system input}} - \beta_s y z - \gamma_s z w - \phi_s z &
\end{cases}
$$

The system output is y, as annotated in the equations above, and its external input or reference input is r. We assume $u^{tot} = u + u^*$, $y^{tot} = y + y^*$ and $w^{tot} = w + y + w^*$.

The experimental implementation of these two reaction systems in isolation was discussed earlier. Their interconnection would be immediately feasible: transcriptional circuits and aptamer systems have been characterized in compatible *in vitro* conditions; the RNA polymerase U can be easily used to transcribe RNA species Z from a constitutively active template.

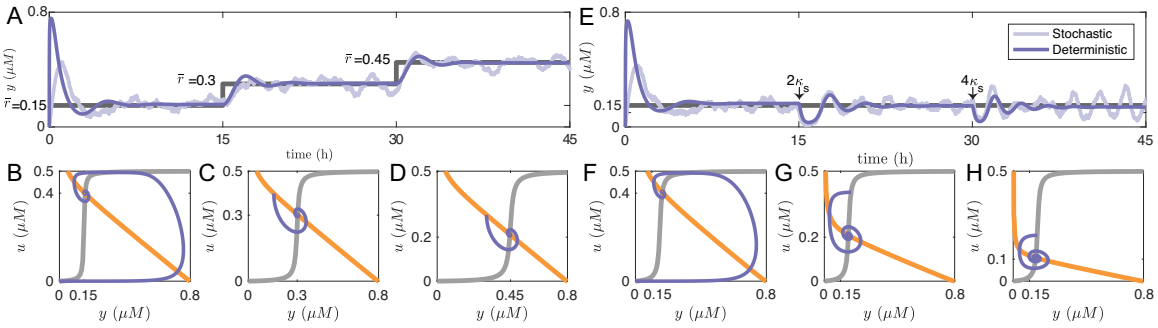

Figure 5.6: **Tracking and adaptation** A) The output y of the closed loop system (purple) tracks three different references ($\bar{r} = 0.15, 0.3$ and $0.45\mu M$, dark gray). B,C and D) show equilibrium conditions as they change as a function of reference changes, where grey corresponds to the controller (5.4), and orange corresponds to the system (5.9). E) Adaptation of the system output in the presence of a step perturbation of the production rate (κ_s) applied at 15 and 30h, where the final values are two and four times its nominal value listed on Table 6.1.

Integral behavior

We now define a rescaled reference signal as $\bar{r} = \frac{\theta_c}{\kappa_c} r$; then, we define the error signal $e = \bar{r} - y$ and variable $e_r = r_r - r_y$. Differentiating, we find that $\dot{e}_r = \dot{r}_r - \dot{r}_y = \theta_c r - \kappa_c y - \phi_c e_r + \dot{u}$. Then, we obtain

$$u(t) = e_r + \phi_c \int e_r dt - \kappa_c \int e dt. \tag{5.10}$$

The expression above includes terms that depend on e_r and on e, which respectively measure the difference between controller internal variables r_r and r_y, and the difference between the output y and the reference $\bar{r}$. If the controller response is ultrasensitive, and the controller is operating in its ultrasensitive regime, then at equilibrium $y \approx r$ (based on the input-output responses we examined earlier). Then, by subtracting the dynamics of $\dot{r}_y$ and $\dot{r}_r$ we find that:

$$\phi_c e_r = \kappa_c e.$$

This implies that, if the controller operates in the ultrasensitive regime, then $e_r \approx 0$, which implies that also $e \approx 0$. These approximations become exact if $\phi_c = 0$. In addition, Fig. 5.3 shows that reducing ϕ_c increases the ultrasensitive response. The closed loop performance of the ultrasensitive controller is examined next.

Reference tracking and disturbance rejection

We recall the definition of the rescaled reference signal $\bar{r} = \frac{\theta_c}{\kappa_c} r$, and that y is the output of the closed loop system. We test the ability of y to track changes in $\bar{r}$ using numerical simulations. Fig. 5.6A shows the response of the output to step-increases in rescaled reference signal $\bar{r} = 0.15, 0.3$ and $0.45 \mu M$. The rescaled reference and the reference input are related as: $\bar{r} = \frac{\theta_c}{\kappa_c} r = 1.5\, r$, given the nominal parameters in Tables 5.1 and 6.1.

The system's output y, shown in purple, closely tracks each reference input (dark gray line). Fig.5.6 B, C and D show the input-output equilibrium conditions of the controller and system at the corresponding reference value: the threshold of the ultrasensitive input/output controller map tracks the reference $\bar{r}$. Fig. 5.6 E shows the behavior of the output in the presence of a step-perturbation of transcription rate κ_s, given a constant reference $\bar{r} = 0.15 \mu M$. The system converges to the reference input rejecting the disturbance; Fig.5.6 F, G and H show input-output equilibrium conditions of the controller and system for different disturbance values on κ_s. The system is able to reject those disturbance in the ultra sensitivity region. Gillespie simulations (light purple color) suggest that the tracking and disturbance rejection of the closed loop system hold also in a stochastic setting.

Sensitivity analysis

1. Sensitivity to variations of system parameters: When the equilibrium of the closed loop system is in the ultrasensitive regime of the controller response, the system transient and stationary responses are robust with respect to parameter variations of the system to be controlled. Numerical sensitivity analysis is shown in Fig. 5.7. The closed loop system transient (Fig. 5.7 A) and equilibria (Fig. 5.7 B) are robust to most parameter variations spanning 0.5 to 2 times the nominal values listed on Table 6.1.

We note that the controller can "saturate" in a certain range of the production rate of Z (κ_s), the recovery rate of W (θ_s), the total concentration of template (y^{tot}) and total concentration of activator (w^{tot}).

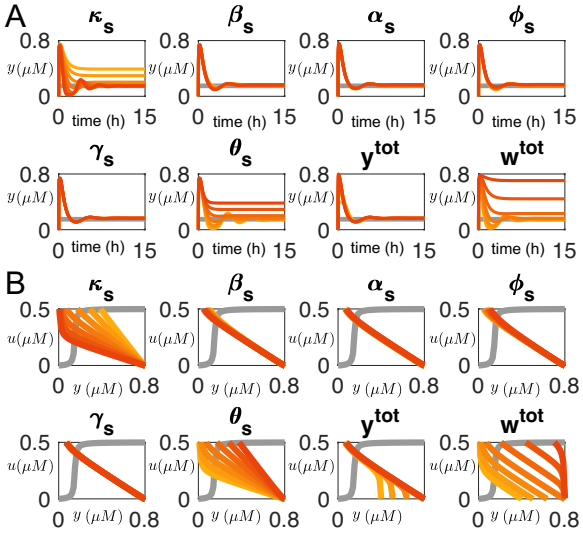

Figure 5.7: **Rejection of system parametric disturbances** A) Output y is shown as parameter values vary from 0.5 to 2 times their nominal values listed on Table 5.1 (yellow to red). B) Input-output equilibrium conditions of the controller (grey) and system (color scale), as the same parameters are varied.

Large θ_s or w^{tot} increase free w, which can bind faster to y^*. To balance this

process, the system increases the demand of controller species u in order to inhibit w. This can cause the controller to reach a saturation point and fail. If y^{tot} is much lower than the reference value, the controller may fail to supply the system's demand of u because there is not enough free y available. (Note that Y is not depleted by the controller reactions.)

2. Sensitivity to variations of controller parameters: We test how changes in the parameters of the biomolecular controller affect the closed loop system behavior. Fig. 5.3 and Fig. 5.8 show that the system is generally very robust to changes in controller parameters. An exception is parameter u^{tot}, which defines the upper bound of the controller's output. By increasing this parameter we improve the robustness of the ultrasensitive response of the controller. In contrast, if u^{tot} is reduced, the controller may saturate and fail to supply enough input U to the system.

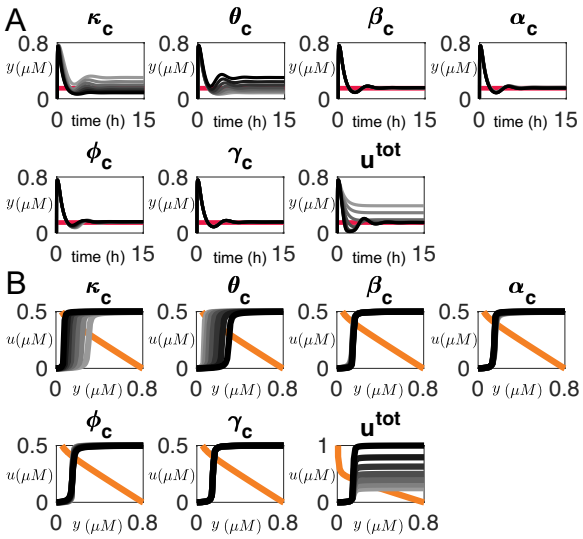

Figure 5.8: **Controller robustness** Top shows y trajectories for different parameter values that varies from 0.5 to 2 times its nominal values listed on Table 5.1 (from gray to black). Bottom shows input-output equilibrium condition of the controller (grey scale) and system (orange).

5.5 Discussion

We presented a biomolecular controller that operates via titration reactions, and showed its closed loop performance when the system to be controlled is an RNA transcription process.

We combine two mechanism, titration and activation/inhibition cycle, to create a highly ultrasensitive behavior. Titration is important for tuning the threshold of the ultrasensitive response and both mechanism are important to raise the highly ultrasensitive response.

This ultasensitive controller overcomes the challenge of designing an integral controller that takes into account degradation and dilution processes [17]. We believe that our studies could be useful to guide experimental implementation of a variety of molecular controllers, beyond the *in vitro* implementation that we suggest here. Ultrasensitivity may be obtained using mechanisms other than molecular sequestration; for instance, [48] showed that phosphorylation cycles have an ultra sensitive response. Many post-translational modification pathway such as phosphorylation, glycosylation, acetylation and ubiquitination could be used to design an ultrasensitive feedback controller for tracking and disturbance rejection.

Chapter 6

An ultrasensitive motif for robust closed loop control of biomolecular systems

6.1 Introduction

The next engineering challenge of our time is to design molecular feedback control networks for complex molecular systems. These controllers will enable us to engineer precise and reliable synthetic circuits for a variety of applications in therapeutics, biological smart materials, metabolic engineering, food industry and agriculture. Feedback promises to mitigate many roadblocks preventing the systematic use of components developed in synthetic biology, which include their nonlinearity, stochasticity, variability and lack of modularity [33].

We recently proposed a biomolecular network that can be used for closed loop feedback control [25]. The main feature of this network is its ultrasensitive response, which is achieved by combining molecular titration [20, 28] (comparator) with a downstream activation/deactivation cycle (on/off switch), which is similar to phosphorylation/dephosphorylation reactions ([40]). One of the limitations of this controller is its "unidirectional" action, in other words the controller can be used to activate or inhibit the target process, but can't generate both regulatory actions in parallel. This limitation, qualitatively illustrated in Fig. 6.1, is common to virtually all molecular feedback controllers proposed in the past. In this paper, we a) characterize the ultrasensitive regime of the controller motif, which we name "Brink Controller" motif, which is enabled by fast titration and switching rates, as well as slow degradation rate, and b) propose to operate two Brink Controllers in parallel to achieve a robust control loop system that can simultaneously manage positive and negative regulation.

An anthitetic feedback controller was recently proposed in [17], which relies on titration reactions but neglects the effects of degradation of components. Relative to the antithetic controller, our Brink Controller motif includes an additional activation/deactivation cycle for the controller molecule, and takes into account degradation (or dilution) reactions that are known to be present in most biochemical and cellular processes. We show that a large degradation rate can in fact reduce the ultrasensitive behavior of the controller.

The paper is organized as follows. In Section 6.2 we formulate our general problem and describe an architecture for a closed loop molecular controller that can manage positive and negative action on the system. In Section 6.3 we introduce the Brink controller motif

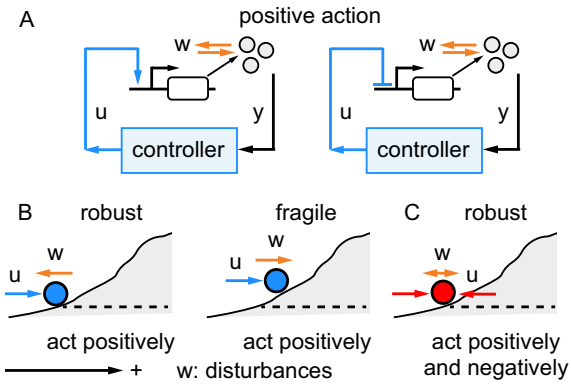

Figure 6.1: A: Tradtional biomolecular control systems have can either upregulate or downregulate the production of a target molecule. This "unidirectional" control action may fail to control the system as desired, as illustrated in panel B: The controller u in blue can act exclusively positively on the target system, failing to maintain the position of the sphere for arbitrary disturbances w. However, the red controller u can act both positively and negatively, the sphere position can be controlled.

and derive conditions guaranteeing its ultrasensitivity. Numerical simulations showing the effectiveness of the closed loop Brink Controllers are in Section 6.4 even in the presence of downstream loads, and we briefly discuss potential biological realizations of the circuit in Section 6.5.

6.2 Architecture of a synthetic molecular controller for homeostasis

In this paper we indicate chemical species with capital letters (e.g. U) and their concentration with the corresponding lowercase letters (e.g. u). Let us consider a biological process where a protein Y is produced at an unknown rate θ and degraded at an unknown rate δ. Our goal is to control its concentration y so that it maintains (at steady state) the same concentration of a reference species R. For this purpose, we can engineer a

biomolecular "controller" $U(R, Y)$ as follows:

$$\dot{y} = \underbrace{\theta_s - \delta_s y}_{process} + \overbrace{u(y, r)}^{\text{controller}}. \tag{6.1}$$

This goal could be achieved by the controller architecture in Fig. 6.2, which operates as the combination of two components as shown equation (6.2). The first controller component u_1 should have a positive action on the process by producing y, while the second controller u_2 should have a negative action by removing y.

$$\dot{y} = \underbrace{\theta_s - \delta_s y}_{process} + \overbrace{\underbrace{u_1(y, r)}_{\text{positive action}} - \underbrace{u_2(y, r)}_{\text{negative action}}}^{\text{controller}}. \tag{6.2}$$

To track the reference r, we require that u_1 is active (non-zero) only when $y < r$, and that u_2 is active only when $y > r$:

$$u_1(y, r) \approx \begin{cases} \alpha_s \,\text{if}\, y < r, \\ 0 \,\text{if}\, y \geq r, \end{cases} \qquad u_2(y, r) \approx \begin{cases} \beta_s \,\text{if}\, y > r, \\ 0 \,\text{if}\, y \leq r. \end{cases} \tag{6.3}$$

The desired "shape" of the response of each controller element is shown in Fig. 6.3 A. If the requirements (6.3) are satisfied, then we claim that y converges to r at steady state and that this is true in a broad parameter range. This claim can be qualitatively supported by sketching equilibrium conditions: Fig 6.3 B shows the combined response of the controllers (orange), overlapped with the equilibrium condition of the process (gray); these equilibrium conditions intersect for $y \approx r$ for a variety of slopes (δ_s, degradation rate) and intercepts (θ_s, production rate) characterizing the process.

A candidate class of controllers that can satisfy the requirements (6.3) is given by Hill-type functions shown in equation (6.4): these functions have a sigmoidal shape, a threshold that depends on r, and a steepness that depends on n.

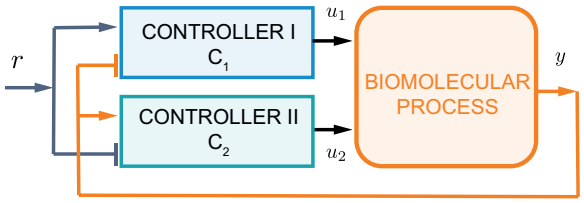

Figure 6.2: **The homeostatic Brink Controller** consists of two Brink controllers in parallel, where controller C_1 has a positive action and C_2 has a negative action on the biomolecular process.

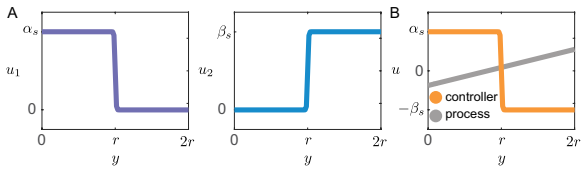

Figure 6.3: **Ultrasensitive controller** A) Shows the input-output equilibrium conditions of u_1 and u_2. B) Illustrate the input-output equilibrium conditions for u in orange, while the grey line represent the input-output equilibrium mapping of the process.

$$u_1 = \alpha_s \frac{r^n}{y^n + r^n}, \quad u_2 = \beta_s \frac{y^n}{y^n + r^n}. \tag{6.4}$$

We can achieve requirements (6.3) as long as these controllers are ultrasensitive (very large n) as shown in Fig. 6.3 A (and there is no basal expression of control signal). The combined candidate Hill-type controller is:

$$u = u_1 - u_2 = (\alpha_s + \beta_s)\frac{r^n}{y^n + r^n} - \beta_s, \tag{6.5}$$

The combined controller u preserves the ultrasensitive behavior of the individual controllers, has positive and negative effects on the process as desired (Fig. 6.3B), and operates in the range $-\beta_s$ to α_s. In the next section, we suggest a chemical reaction network that achieves a fast, ultrasensitive response with a tunable threshold to approximate controllers (6.4).

6.3 Brink Controller: A tunable, ultrasensitive molecular motif

6.3.1 The Brink Controller motif

In this section we describe the Brink Controller motif, shown in detail in Fig. 6.4A, that will be used as a regulatory element to build the homeostatic architecture presented in the previous section. The Brink Controller consists of three species: two inputs, an inhibitor species I and an activator species A, and one output, species U (Fig. 6.4B). Either input I or A can be kept constant (acting as the "reference" signal) while the other is varied (signal to be controlled).

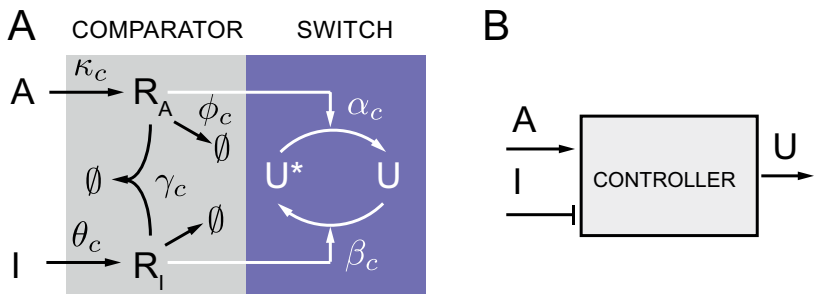

Figure 6.4: **Brink Controller motif** A) Summary of the reactions defining the Brink Controller motif. A stands for activator, I stands for inhibitor and U stands for output. B) Block diagram summarizing the inputs and the output of the controller.

The inhibitor I produce species R_I, which can bind and inhibit U by forming a complex U^*. This new species U^* is to be considered inactive. The activator A produces species R_A, which can reactivate U^* by removing R_I from the complex Y^*, thereby converting U^* back to U. Species R_A and R_I bind to each other to produce a waste complex which does not interfere with the rest of the circuit. In addition, R_A and R_I degrade at a

constant rate.

$A \xrightarrow{\kappa_c} A + R_A$	Production
$I \xrightarrow{\theta_c} I + R_I$	
$R_A + R_I \xrightarrow{\gamma_c} R_A \cdot R_I$	Titration
$R_A \xrightarrow{\phi_c} 0$	Degradation
$R_I \xrightarrow{\phi_c} 0$	
$R_A + U^* \xrightarrow{\alpha_c} U + R_A \cdot R_I$	Reactivation (switch on)
$R_I + U \xrightarrow{\beta_c} U^*$	Inhibition (switch off)

We assume the total concentration of species U is constant:

$$u^{tot} = u + u^* \tag{6.6}$$

(As a reminder, in this paper we indicate chemical species with capital letters (e.g. U) and their concentration with the corresponding lowercase letters (e.g. u).)

Using the law of mass action (and the mass conservation equality), we obtain the following model for the Brink Controller module:

$$\dot{r}_A = \kappa_c a - \alpha_c r_A u^* - \gamma_c r_A r_I - \phi_c r_A, \tag{6.7}$$

$$\dot{r}_I = \theta_c i - \beta_c r_I u - \gamma_c r_A r_I - \phi_c r_I, \tag{6.8}$$

$$\dot{u} = \alpha_c r_A u^* - \beta_c r_I u. \tag{6.9}$$

Within the Brink Controller module we can identify two subsystems: a comparator and a switch (Fig. 6.4 A). The comparator reactions rely on molecular titration, whose purpose is to ensure that only the most abundant species beween I and A is propagated

to the downstream reactions. The switch reactions shift the balance betwen U and U^*, depending on the output of the comparator subsystem.

6.3.2 Ultrasensitivity and tunability conditions

We seek to design a Brink Controller module with an ultrasensitive input-output steady state response. In this section, we will derive analytical conditions to achieve such behavior in the system.

First, we consider the case where I is kept constant and acts as a reference input to the module, while A can vary. We derive equilibrium conditions by setting equations (6.7)-(6.9) equal to zero. Finding the controller output u as a function of a and i is a long and tedious procedure. However, we can easily express a as a function of i and u in closed form:

$$\bar{a}(\bar{u}, i) = \frac{\theta_c}{\kappa_c} i + \frac{\phi_c}{\kappa_c} \left(1 - \frac{\alpha_c \bar{u}^*}{\beta_c \bar{u}}\right) \bar{r}_A(\bar{u}, i), \tag{6.10}$$

where

$$\bar{r}_A(\bar{u}, i) = \frac{-b_A + \sqrt{b_A^2 - 4a_A c_A}}{2a_A},$$

and $a_A = \alpha_c \gamma_c u^*$, $b_A = \alpha_c \bar{u}^* (\beta_c \bar{u} + \phi_c)$ and $c_A = -\bar{u} \beta_c \theta_c i$. Equation (6.10) describes the input-output steady state mapping of the model (6.7)-(6.9) and can be rewritten as:

$$\bar{a}(\bar{u}, i) = k_a(i) + \Delta(\bar{u}, i), \tag{6.11}$$

with $k_a(i) = \frac{\theta_c}{\kappa_c} i$ and $\Delta(\bar{u}, i) = \frac{\phi_c}{\kappa_c} \left(1 - \frac{\alpha_c \bar{u}^*}{\beta_c \bar{u}}\right) \bar{r}_A(\bar{u}, i)$. Expression (6.11) is useful because it allows us to clearly break down $a(\bar{u}, i)$ as the sum of a threshold $k_a(i)$ depending on input i, and of an additional term $\Delta(\bar{u}, i)$.

If the input/output relationship between a and u is ultrasensitive, then we should observe a regime for $a \approx k_a(i)$ where small changes in a correspond to large changes in u. Therefore we focus on term $\Delta(\bar{u}, i)$, and we ask if there are conditions that guarantee $\Delta(\bar{u}, i)$ to be small, for arbitrary values of $u \in [0, u^{tot}]$. Within term $\Delta(\bar{u}, i)$, the factor $\bar{r}_A$ (defined earlier) is small if $b_A^2 \gg -4a_A c_A$, *i.e.* if:

$$\frac{\beta_c}{\gamma_c}\bar{u} \gg 4\frac{\theta_c}{\alpha_c}\frac{i}{\bar{u}^*}. \tag{6.12}$$

Because titration rates γ_c are usually fast (large magnitude), condition (6.12) is satisfied if also the switching rates α_c and β_c are fast.

In addition, term $\Delta(\bar{u}, i)$ is small if ϕ_c/κ_c is small. This fraction is the ratio between degradation and production rates of r_a: if the degradation rate is very small, it promotes ultrasensitive behavior.

To summarize, to obtain ultrasensitivity we require fast titration and fast switching rates. In addition, the threshold of the ultrasensitive response $\kappa_a = \frac{\theta_c}{\kappa_c} i$ can be tuned linearly with the input i. A slow degradation rate ϕ_c also contributes to promote utrasensitivity.

Our derivations are supported by the numerical simulation of expression (6.12) in Fig. 6.5, which was done using the parameters reported in Table 6.1. The x axis of this plot uses a threshold-normalized input $a_n = \frac{a(u,i)}{\kappa_a}$. The nominal values of titration rate γ_c and switch rates α_c and β_c are chosen to be in a realistic range for nucleic acid networks, and are in the same order of magnitude. Ultrasensitivity is not drastically affected if we change γ_c within one order of magnitude of the nominal value; however, variations of α_c and β_c in the same range make the transition less sharp. A small degradation rate ϕ_c helps improve

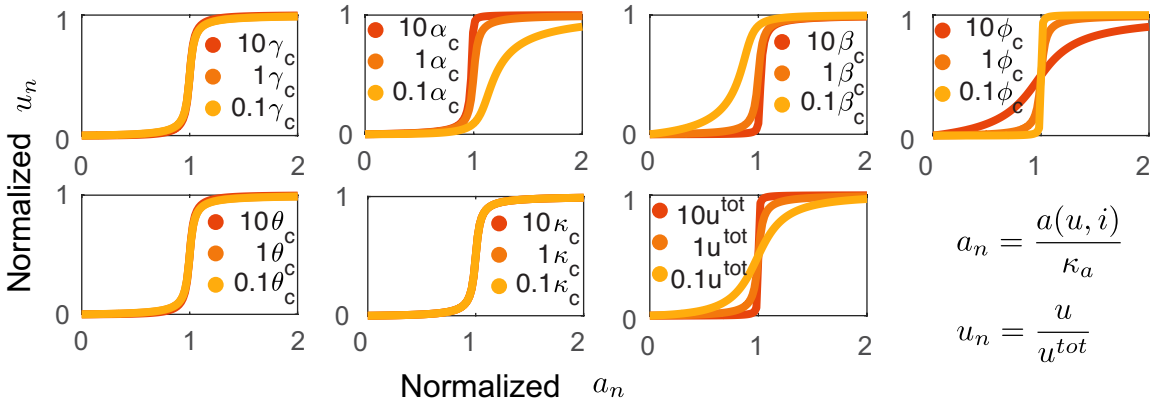

Figure 6.5: **Ultrasensitive characterization** Input-output equilibrium conditions behavior of our controller module from equation (6.10) as parameters are changed. Nominal parameters are in Table 6.1.

ultrasensitivity. Changes in θ_c and κ_c primarily affect the threshold κ_a, however because our plot uses a threshold-normalized input these effects are not visible.

We follow the same steps to find the input-output mapping when the inhibitor i is varied while the activator a is constant, and determines the threshold for the input/output mapping. In this case we obtain:

$$\bar{i}(\bar{u}, a) = \frac{\kappa_c}{\theta_c} a - \frac{\phi_c}{\theta_c} \left(\frac{\beta_c \bar{u}}{\alpha_c \bar{u}^*} - 1 \right) \bar{r}_I(\bar{u}, a), \tag{6.13}$$

where

$$\bar{r}_I(u, a) = \frac{-b_I + \sqrt{b_I^2 - 4 a_I c_I}}{2 a_I}, \tag{6.14}$$

with $a_I = \beta_c \gamma_c \bar{u}$, $b_I = \beta_c \bar{u}(\alpha_c \bar{u}^* + \phi_c)$ and $c_I = -\alpha_c \bar{u}^* \kappa_c a$. As before, it is convenient to write equation (6.14) as:

$$\bar{r}_I(u, a) = k_i(a) + \Delta(\bar{u}, a).$$

To identify the ultrasensitive regime, we examine term $\Delta(\bar{u}, a)$ and in particular from factor

r_I we derive conditions:

$$\frac{\alpha_c}{\gamma_c}\bar{u}^* \gg 4\frac{\kappa_c}{\beta_c}\frac{a}{\bar{u}}. \tag{6.15}$$

As earlier, we require values of γ_c, β_c and α_c for ultrasensitive response. The threshold k_i can be tuned linearly by the concentration of a, similarly to the case considered earlier. Numerical analysis (not reported for brevity) shows a dependence of ultrasensitivity on parameters that is analogous to what shown in Fig. 6.5.

6.3.3 Approximated input-output mapping

In this section, we approximate the input-output ultrasensitive response of the Brink Controller motif with an equivalent Hill function; specifically we find expressions for equivalent threshold and Hill coefficient as a function of the Brink Controller reaction rates. This approximation is convenient because it shows that our motif can operate within a homeostatic controller as outlined in Section 6.2 (in the limit for very large Hill coefficient). For the Brink Controller motif where the inhibitor I is kept constant, while the activator concentration is varied, we approximate the input-output steady state as:

$$\bar{u} \approx u^{tot}\frac{a^n}{a^n + \kappa_a^n}, \tag{6.16}$$

where the threshold $\kappa_a = \frac{\theta_c}{\kappa_c} i$ was defined in expression (6.11).

The ultrasensitive region can be approximated linearly as the maximum slope S of the Hill function as shown in Fig. 6.6. The maximum slope of equation (6.16) is the derivative of u with respect to a evaluated at κ_a. We obtain that

$$S_{max,H} = \frac{d\bar{u}}{da}_{|a=k_a} = u^{tot}\frac{n}{4\kappa_a}. \tag{6.17}$$

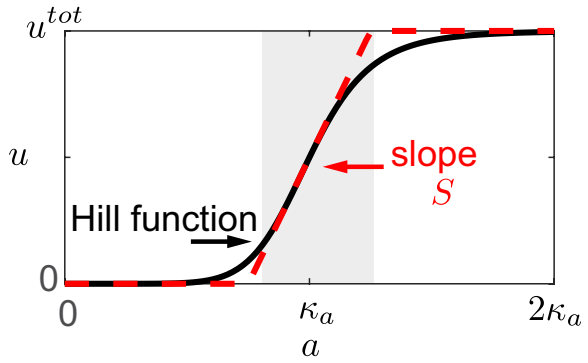

Figure 6.6: A Hill function can be linearly approximated in the transition region with its maximum slope.

The slope of equation (6.10) can be approximated as the change of input a that induces a change from L% (low) to H% (high) fraction of the output u^{tot}. The maximum slope occurs when at the half-max value of u^{tot}, thus $L = H = 0.5$. We can write:

$$\begin{aligned} S_{max,BC} &= \lim_{L,H\to 0.5} \frac{Hu^{tot} - Lu^{tot}}{a(Hu^{tot}) - a(Lu^{tot})} \\ &\approx \frac{1}{4}\frac{(u^{tot})^2}{(1+\frac{\alpha_c}{\beta_c})}\frac{\alpha_c}{\phi_c\kappa_a}. \end{aligned} \tag{6.18}$$

First, from equation (6.10) we find that r_A is the solution of a second order polynomial, $a_A r_A^2 + b_A r_a + c_A = 0$. We normalized the coefficients by a_A and we obtain

$$a_n = 1, \quad b_n = \frac{\beta_c u + \phi_c}{\gamma_c}, \quad c_n = -\frac{\beta_c \theta_c u}{\alpha_c \gamma_c u^*} i \tag{6.19}$$

To obtain an ultrasensitive response, we found that α_c, β_c and γ_c must be large with respect to the other parameters. Then, b_n is larger than c_n.

We recall that:

$$r_A = \frac{-b_n + \sqrt{b_n^2 - 4c_n}}{2}$$

We now expand with Taylor series the function:

$$\sqrt{x^2+a}-x=\frac{a}{2x}-\frac{a^2}{8x^3}+\frac{a^3}{16x^5}-\frac{5a^4}{128x^7}+O(x^{-9}).$$

When x is very large we can neglect infinitesimal terms:

$$\sqrt{x^2+a}-x\approx\frac{a}{2x}.$$

Because we assume b_n is much larger than c_n, and ϕ_c is smaller than $\beta_c u$, we approximate:

$$r_A\approx\frac{-4c_n}{4b_n}=\frac{\beta_c u\theta_c i}{\alpha_c u^*(\beta_c u+\phi_c)}i\approx\frac{\theta_c i}{\alpha_c u^*}$$

Next, we approximate the change in steady state input a corresponding to changes in the output u between two values H (high) and L (low) as follows:

$$\begin{aligned}a(H)-a(L) &\approx \frac{\phi_c}{\kappa_c}\left(\frac{1}{L}-\frac{\alpha_c}{\beta_c H}-\frac{1}{H}+\frac{\alpha_c}{\beta_c L}\right)\frac{\theta_c i}{\alpha_c u^{tot}}\\ &\approx \frac{\phi_c}{\alpha_c}\frac{H-L}{HL}\left(1+\frac{\alpha_c}{\beta_c}\right)\frac{\kappa_a}{u^{tot}}\end{aligned}$$

Then the slope of the transition can be approximated as:

$$S=\frac{Hu^{tot}-Lu^{tot}}{a(Hu^{tot})-a(Lu^{tot})}\approx HL\frac{(u^{tot})^2}{(1+\frac{\alpha_c}{\beta_c})}\frac{\alpha_c}{\phi_c\kappa_a}.$$

Then, by equating the maximum slope expressions (6.17) and (6.18), we find an approximated relationship between the equivalent Hill coefficient n and the reaction rates of the Brink Controller motif:

$$n=\frac{1}{(1+\frac{\alpha_c}{\beta_c})}\frac{\alpha_c}{\phi_c}u^{tot}. \tag{6.20}$$

Similar steps can be followed for equation (6.13), taking into account a Hill function of the form:

$$\bar{u}=u^{tot}\frac{\kappa_i^m}{i^m+\kappa_i^m}, \tag{6.21}$$

whose threshold is now defined as $\kappa_i = \frac{\kappa_c}{\theta_c} a$. Then, the slope of the equation (6.21) is

$$S_{max,H} = \frac{du}{di}_{|_{i=\kappa_i}} = -u^{tot} \frac{m}{4\kappa_i} \tag{6.22}$$

Likewise, the approximated slope of equation (6.13) is computed as

$$S_{max,BC} \approx \frac{(u^{tot})^2}{(1 + \frac{\beta_c}{\alpha_c})} \frac{\beta_c}{\phi_c \kappa_i}. \tag{6.23}$$

We find the Hill exponent m,

$$m = \frac{1}{(1 + \frac{\beta_c}{\alpha_c})} \frac{\beta_c}{\phi_c} u^{tot}. \tag{6.24}$$

To summarize, we derived a Hill-type approximation of the input-output mapping of the Brink Controller motif, and related the Hill function parameters to the controller reaction rates. Consistently with the conditions found in the earlier section, large values of α_c and β_c, and small values of ϕ_c improve ultrasensitivity (a large value of γ_c is also required for the slope approximation justified in Appendix **??**).

6.4 Results: The homeostatic Brink Controller

We now describe the full implementation of the Homeostatic Brink Controller, shown in Fig. 6.2, where two Brink Controllers operate in parallel. Controller 1 has a positive action on the system, and is active when the reference r is larger than y; Controller 2 has a negative action on the system, and is active when the reference r is smaller than y. The ODEs describing the closed loop system are:

$$\text{C1}\begin{cases}\dot{r}_r = \kappa_c r - \alpha_c r_r u_1^* - \gamma_c r_r r_y - \phi_c r_r, \\ \dot{r}_y = \theta_c y - \beta_c r_y u_1 - \gamma_c r_r r_y - \phi_c r_y, \\ \dot{u}_1 = \alpha_c r_r u_1^* - \beta_c r_y u_1, \end{cases} \tag{6.25}$$

$$\text{C2}\begin{cases}\dot{r}_y = \theta_c y - \alpha_c r_y u_2^* - \gamma_c r_y r_r - \phi_c r_y, \\ \dot{r}_r = \kappa_c r - \beta_c r_r u_2 - \gamma_c r_y r_r - \phi_c r_r, \\ \dot{u}_2 = \alpha_c r_y u_2^* - \beta_c r_r u_2, \end{cases} \tag{6.26}$$

$$\text{S}\begin{cases}\dot{y} = \underbrace{\theta_s}_{\text{production}} - \underbrace{\delta_s y}_{\text{degradation}} + \underbrace{\alpha_s u_1}_{\text{C1 action}} - \underbrace{\beta_s u_2}_{\text{C2 action}}. \end{cases} \tag{6.27}$$

We rewrite the last equation as $\dot{y} = \theta_s - \delta_s y + u$. Where $u = \alpha_s u_1 - \beta_s u_2$. The equilibrium condition of biomolecular process is:

$$u = g(y) = \delta_s y - \theta_s. \tag{6.28}$$

Now, we assume that a) each brink controller converges to steady state much faster than the process, and b) we approximate the input-output mapping of each brink controller with an equivalent Hill function. We obtain the following expressions:

$$u_1 = u_1^{tot}\frac{\bar{r}^n}{y^n + \bar{r}^n} \qquad \text{and} \qquad u_2 = u_2^{tot}\frac{y^n}{y^n + \bar{r}^n}, \tag{6.29}$$

where n and m can be approximated respectively using expressions (6.20) and (6.24). We then define a scaled reference $\bar{r} = \frac{\kappa_c}{\theta_c} r$, and we find the overall equilibrium condition of the controller:

$$u = f(y) = (\alpha_s + \beta_s)\frac{\bar{r}^n}{y^n + \bar{r}^n} - \beta_s. \tag{6.30}$$

Using the parameters in Table 6.1, in Figs. 6.7 and (6.8) we numerically integrate equations (6.25), (6.26), and (6.27) (purple), and we plot the approximated equilibrium condition (6.30) (orange) as well as the system equilibrium condition (6.28) (gray). Fig. 6.7 shows that the controller rejects parametric disturbances, and therefore maintains the desired reference (homeostasis); Fig. 6.8 shows that the system succssfully tracks changes in the reference. Both simulations show that the ultrasensitive regime of the controller is successfully approximated with steep Hill functions in the (realistic) parameters we picked (which satisfy the fast titration/fast switching requirements described in the previous sections).

It is worth noting that a more realistic *actuation* mechanism for the controllers is:

$$\dot{y} = \underbrace{\theta_s}_{\text{production}} - \underbrace{\delta_s y}_{\text{degradation}} + \underbrace{\alpha_s \frac{u_1}{u_1+\kappa_1}}_{\text{C1 action}} - \underbrace{\beta_s \frac{u_2}{u_2+\kappa_2}}_{\text{C2 action}}.$$

In this case, the controller equilibrium conditions become:

$$u = f(y) = (\bar{\alpha}_s + \bar{\beta}_s)\frac{\bar{r}^n}{y^n + \bar{r}^n} - \bar{\beta}_s,$$

where $\bar{\alpha} = \alpha \frac{u_1^{tot}}{u_1^{tot}+\kappa_1}$ and $\bar{\beta} = \beta \frac{u_2^{tot}}{u_2^{tot}+\kappa_2}$. The results of numerical analysis in this case, with $\kappa_1 = \kappa_2 = 500$ nM do not significantly differ from the simulations in Figs. 6.7 and 6.8 (not shown).

6.4.1 Loading effects on the controller

The Brink Controller outputs may be depleted by the downstream circuits (load) which could cause retroactivity effects on the controller [32]; we have neglected this issue

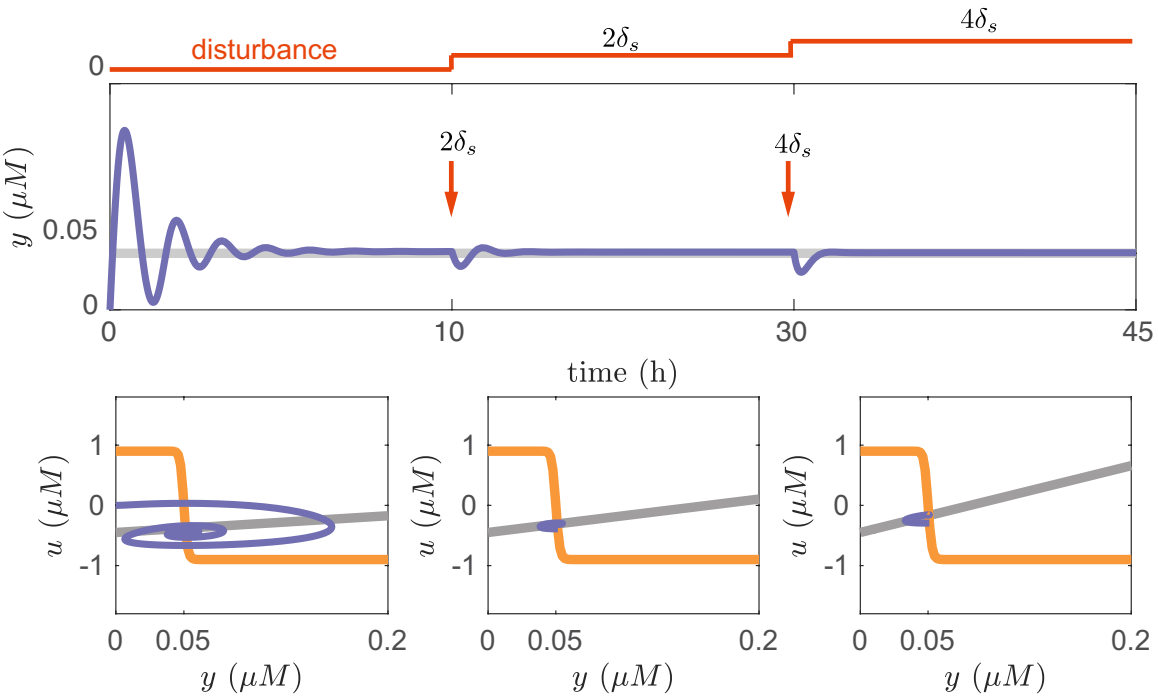

Figure 6.7: **Homeostasis behavior** Top: Time response of the closed loop system under different disturbances (disturbances rejection). Bottom: Nullclines of the controller and the process under different constant disturbances.

in the previous sections. If U drives a downstream process by binding and unbinding to a target, this can be taken into account as:

Downstream process

$U + E \underset{\kappa^-}{\overset{\kappa^+}{\rightleftharpoons}} C$	association/dissociation with the load E

Then, equation (6.9) becomes

$$\dot{u} = \alpha_c r_A u^* - \beta_c r_I u + \underbrace{\kappa^- c - \kappa^+ u e}_{\text{loading}} \tag{6.31}$$

If we assume that association/dissociation (κ^+/κ^-) are fast with respect to the time scale of the module, at steady state we find that $c = \frac{e}{e+\kappa_M} u$, where $\kappa_M = \frac{\kappa^+}{\kappa^-}$. We define the effective load on the system as $\lambda = e/\kappa_M$. Then, we update equation (6.6).

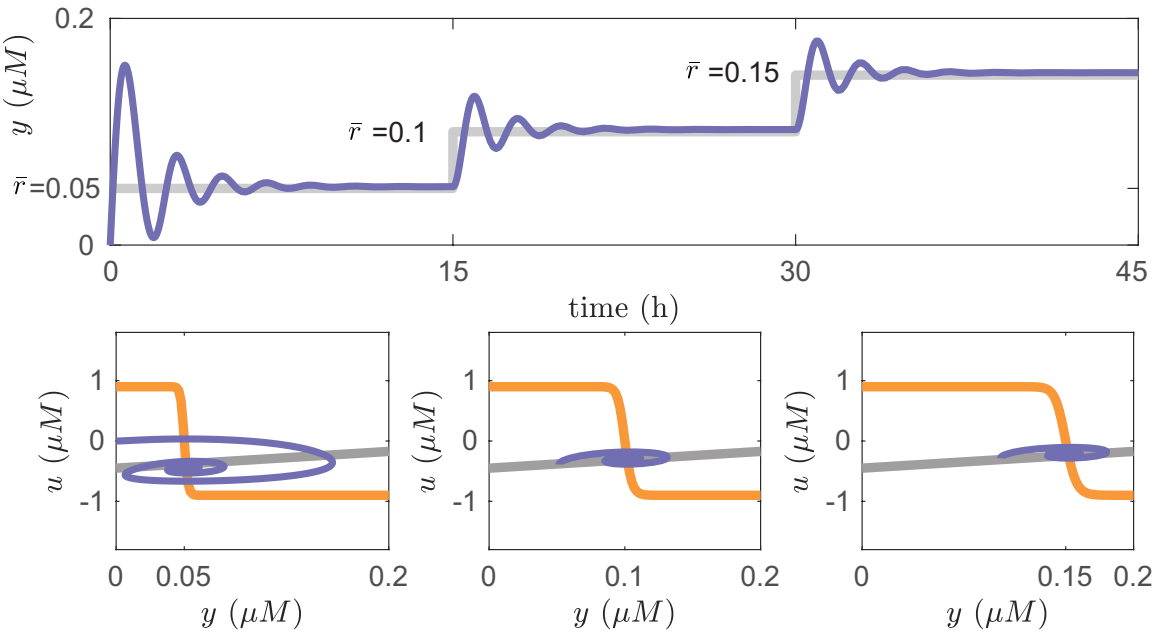

Figure 6.8: **Precise tracking** Top: Tracking of different reference of Homeostasis Brink Controller. Bottom: Nullclines of the controller and process at different references, $r = 0.1$, 0.2 and $0.3\mu M$ ($\bar{r} = 0.05$, 0.1, 0.15 μM).

$$u^{tot} = u + u^* + \frac{\lambda}{1+\lambda}u \tag{6.32}$$

The analytical conditions for the Brink Controller under a load are similar to equation (6.12) and (6.15). In other words, under fast binding/unbinding assumptions, loading effects do not significantly affect the input-output ultrasensitive response of the module characterized in isolation.

We plot the input/output response of the Brink Controller motif as a function of the effective load λ in Fig. 6.9; the results show that the presence of a load does not affect ultrasensitivity. This suggest that the proposed controller mechanism could be coupled to more complex networks and maintain the ultrasensitivity observed when the circuit is in

Table 6.1: Nominal simulation parameters of the controlled system

Parameter	Description	Value	Other studies
θ_c (/s)	Production	10^{-3}	$10^{-3} - 1$ [91, 22]
κ_c (/s)	Production	$5 \cdot 10^{-4}$	$10^{-3} - 1$ [91, 22]
β_c (/M/s)	Inhibition	$6 \cdot 10^{4}$	$10^{4} - 10^{6}$ [54, 99]
α_c (/M/s)	Reactivation	$6 \cdot 10^{4}$	$10^{4} - 10^{6}$ [54, 99]
γ_c (/M/s)	Titration	$3 \cdot 10^{4}$	$10^{4} - 10^{6}$ [54, 99]
ϕ_c (/s)	Degradation	$3.85 \cdot 10^{-4}$	$10^{-4} - 10^{-3}$ [52].
$u_1^{tot}(nM)$	Concentration	500	
$u_2^{tot}(nM)$	Concentration	500	
θ_s (/s)	Production	$1.25 \cdot 10^{-4}$	$10^{-3} - 1$ [91, 22]
δ_s (/s)	Degradation	$3.85 \cdot 10^{-4}$	$10^{-4} - 10^{-3}$ [52].
$\alpha_s(/s)$		$5 \cdot 10^{-4}$	$10^{-3} - 1$ [91, 22]
$\beta_s(/s)$		$5 \cdot 10^{-4}$	$10^{-3} - 1$ [91, 22]

isolation.

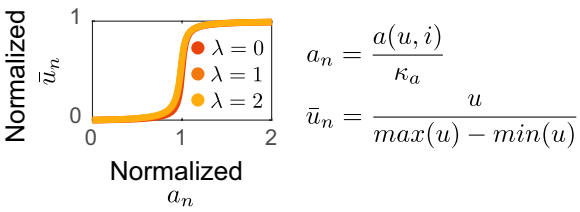

Figure 6.9: **Loading analysis** shows that the presence of a fast binding/unbindign load does not significantly affect ultrasensitivity of the input-output mapping of the Brink Controller.

6.5 Biological implementation of the Brink Controller

We will describe how we can implement the Homeostasis Brink Controller using nucleic acids nanotechnology and the CRISPR/Cas system. The predictability of nucleic acids Watson-Crick base pair interactions of RNA and DNA enables the rational design of strand interactions based on their well understood thermodynamic properties. Using principles of strand displacement and toehold mediated branch migration, nucleic acid nanotechnology

has enabled the rational design of sensors and many dynamic and logic networks [98] using computational tools. RNA-based regulation *in vivo* has significant advantages over traditional protein-based regulation, including low metabolic burden (avoiding resource-intensive translation), portability (RNA based regulators are found in different bacterial kingdom and are often not host-specific), and reduced delays (RNA degradation is fast and offer short time response).

CRISPR based systems are a powerful tool for gene editing and gene regulation at will inside the cell. The system consists of a DNA endonuclease enzyme (Cas9 [84] and Cfp1 [96]), which bind to DNA targets that depend on a Cas-binding guide RNA (gRNA). The Cas9/gRNA complex recognizes precisely the target DNA and localizes the enzyme on the target. A catalytically inactive form of Cas9 [72] is called dead Cas9 (dCas9) strongly binds to the target DNA (without cleaving) and can be used to regulate promoter activity.

The combination of tools from nucleic acids nanotechnology and the CRISPR system has the potential to provide a rapidly expandable array of orthogonal, programmable regulators with sophistiated logic functions. We briefly speculate on two possible implementations of our Brink Controller motif using these tools.

One strategy is based on strand displacement of gRNA from Cas9, and is shown in Fig. 6.10 A. Inactive species U^* could be implemented as dCas9, which can be activated by a guide RNA R_A, forming an active complex U. Another RNA R_I, complementary to the RNA R_A, could inactivate U by displacing R_A from the complex U; this may be done, for example, using "displacement" domains, or toeholds. Inputs A and I could be transcription factors or synthetic plasmids responsible for the production of RNA R_A and

R_I. Displacement of the guide-RNA from dCas9 was experimentally tested *in vivo* in [57].

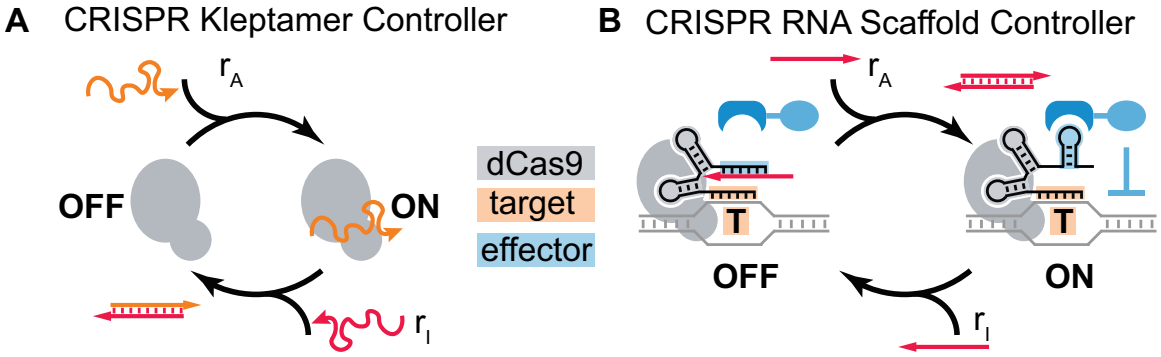

Figure 6.10: **CRISPR-based feedback controllers.** A) dCas9 directed regulation, controller by guide-RNA (r_A) and kleptamer (r_I). B) dCas9-effector fusion proteins. The guide-RNA is extended with additional domain to recruit RNA-binding protein.

An alternative implementation of the Brink Controller is shown in Fig.6.10 B and relies on RNA scaffolds. A CRISPR RNA scaffold [95] recruits proteins independently from the gene target and regulates the downstream gene by either activating or inhibiting it. We suggest that the RNA scaffold could be engineered to include a toehold that enables RNA removal to control the activity of the scaffold and therefore regulate gene expression. CRISPR RNA scaffolds have been implemented in different hosts such as bacteria, yeast, and mammalian cells.

6.6 Conclusion

We have presented a strategy to build a homeostatic biomolecular controller architecture that relies on the motif we name Brink Controller. We require that this controller converges fast and has an ultrasensitive input/output response. We discuss derive conditions to achieve ultrasensitivity, and in particular we require fast titration rates and fast

switching of the controller reactions. We derive a simple Hill-type approximation of the Brink Controller input/output mapping. Using numerical simulations we demonstrate that by combining two Brink Controllers (respectively having a positive and a negative action on the system) we can obtain a robust homeostatic system that tracks a desired reference. Finally, we discussed potential implementations of the Brink Controller motif.

Bibliography

[1] Biomolecular Design (BIOMOD) Competition 2014 - Breaking RNA team (UC Riverside).

[2] D. Angeli and E.D. Sontag. Monotone control systems. *IEEE Transactions on Automatic Control*, 48(10):1684–1698, 2003.

[3] D. Angeli and E.D. Sontag. Oscillations in I/O monotone systems. *IEEE Transactions on Circuits and Systems: Special Issue on Systems Biology*, 55:166–176, 2008.

[4] David Angeli, James E Ferrell, and Eduardo D Sontag. Detection of multistability, bifurcations, and hysteresis in a large class of biological positive-feedback systems. *Proceedings of the National Academy of Sciences of the United States of America*, 101(7):1822–1827, 2004.

[5] Mariette R Atkinson, Michael A Savageau, Jesse T Myers, and Alexander J Ninfa. Development of genetic circuitry exhibiting toggle switch or oscillatory behavior in *Escherichia coli*. *Cell*, 113(5):597–607, 2003.

[6] Attila Becskei and Luis Serrano. Engineering stability in gene networks by autoregulation. *Nature*, 405(6786):590–593, 2000.

[7] Clare A Beelman and Roy Parker. Degradation of mRNA in eukaryotes. *Cell*, 81(2):179–183, 1995.

[8] Clare A Beelman and Roy Parker. Degradation of mrna in eukaryotes. *Cell*, 81(2):179–183, 1995.

[9] David Bikard, Wenyan Jiang, Poulami Samai, Ann Hochschild, Feng Zhang, and Luciano A Marraffini. Programmable repression and activation of bacterial gene expression using an engineered crispr-cas system. *Nucleic acids research*, 41(15):7429–7437, 2013.

[10] F. Blanchini, E. Franco, and G. Giordano. A structural classification of candidate oscillatory and multistationary biochemical systems. *Bulletin of Mathematical Biology*, 76(10):2542–2569, 2014.

[11] F. Blanchini and S. Miani. *Set-theoretic methods in control*. Systems & Control: Foundations & Applications. Birkhäuser, Basel, 2015.

[12] Franco Blanchini and Elisa Franco. Structurally robust biological networks. *Bio Med Central Systems Biology*, 5(1):74, 2011.

[13] Franco Blanchini, Elisa Franco, and Giulia Giordano. A structural classification of candidate oscillators and multistationary systems. *bioRxiv doi:10.1101/000562*, 2013.

[14] Franco Blanchini, Elisa Franco, and Giulia Giordano. Structural conditions for oscillations and multistationarity in aggregate monotone systems. In *Proceedings of the IEEE Conference on Decision and Control (to appear), available at: https://users.dimi.uniud.it/~franco.blanchini/aggreg_mon.pdf*, 2015.

[15] Franco Blanchini, Christian Cuba Samaniego, Elisa Franco, and Giulia Giordano. Design of a molecular clock with RNA-mediated regulation.

[16] Franco Blanchini, Christian Cuba Samaniego, Elisa Franco, and Giulia Giordano. Design of a molecular clock with rna-mediated regulation. In *Decision and Control (CDC), 2014 IEEE 53rd Annual Conference on*, pages 4611–4616. IEEE, 2014.

[17] Corentin Briat, Ankit Gupta, and Mustafa Khammash. Antithetic integral feedback ensures robust perfect adaptation in noisy bimolecular networks. *Cell systems*, 2(1):15–26, 2016.

[18] Nicolas E Buchler and Frederick R Cross. Protein sequestration generates a flexible ultrasensitive response in a genetic network. *Molecular Systems Biology*, 5:272, 2009.

[19] Nicolas E. Buchler and Matthieu Louis. Molecular titration and ultrasensitivity in regulatory networks. *Journal of Molecular Biology*, 384(5):1106–1119, 2008.

[20] Nicolas E Buchler and Matthieu Louis. Molecular titration and ultrasensitivity in regulatory networks. *Journal of molecular biology*, 384(5):1106–1119, 2008.

[21] David Chen and Adam P Arkin. Sequestration-based bistability enables tuning of the switching boundaries and design of a latch. *Molecular systems biology*, 8(1), 2012.

[22] Huiyi Chen, Katsuyuki Shiroguchi, Hao Ge, and Xiaoliang Sunney Xie. Genome-wide study of mRNA degradation and transcript elongation in escherichia coli. *Molecular systems biology*, 11(1):781, 2015.

[23] Le Cong, F Ann Ran, David Cox, Shuailiang Lin, Robert Barretto, Naomi Habib, Patrick D Hsu, Xuebing Wu, Wenyan Jiang, Luciano A Marraffini, et al. Multiplex genome engineering using crispr/cas systems. *Science*, 339(6121):819–823, 2013.

[24] Christian E Cuba, Alexander R Valle, Giancarlo Ayala-Charca, Elizabeth R Villota, and Alberto M Coronado. Influence of parameter values on the oscillation sensitivities of two p53–Mdm2 models. *Systems and synthetic biology*, 9(3):77–84, 2015.

[25] Christian Cuba Samaniego and Elisa Franco. An ultrasensitive biomolecular network for robust feedback control. In *IFAC World Congress 2017*, 2017, in press.

[26] Christian Cuba Samaniego, Giulia Giordano, Franco Blanchini, and Elisa Franco. Stability analysis of an artificial biomolecular oscillator with non-cooperative regulatory interactions. *Journal of Biological Dynamics*, page xxx, 2016.

[27] Christian Cuba Samaniego, Giulia Giordano, Franco Blanchini, and Elisa Franco. Stability analysis of an artificial biomolecular oscillator with non-cooperative regulatory interactions. *Journal of biological dynamics*, 11(1):102–120, 2017.

[28] Christian Cuba Samaniego, Giulia Giordano, Jongmin Kim, Franco Blanchini, and Elisa Franco. Molecular titration promotes oscillations and bistability in minimal network models with monomeric regulators. *ACS synthetic biology*, 5(4):321–333, 2016.

[29] Christian Cuba Samaniego, Sho Kitada, and Elisa Franco. Design and analysis of a synthetic aptamer-based oscillator. In *American Control Conference (ACC), 2015*, pages 2655–2660. IEEE, 2015.

[30] Subramanian Hari Cuba Samaniego, Christian and Elisa Franco. Design of a biomolecular bistable network using the crispr/cas system. In *2017 IEEE Conference on Control Technology and Applications*, 2017, in press.

[31] Tal Danino, Octavio Mondragon-Palomino, Lev Tsimring, and Jeff Hasty. A synchronized quorum of genetic clocks. *Nature*, 463(7279):326–330, 2010.

[32] D. Del Vecchio, A.J. Ninfa, and E.D. Sontag. Modular cell biology: Retroactivity and insulation. *Molecular Systems Biology*, 4:161, 2008.

[33] Domitilla Del Vecchio, Aaron J Dy, and Yili Qian. Control theory meets synthetic biology. *Journal of The Royal Society Interface*, 13(120):20160380, 2016.

[34] Andrew D. Ellington and Jack W. Szostak. In vitro selection of RNA molecules that bind specific ligands. *Nature*, 346:818–822, 1990.

[35] Michael B Elowitz and Stanislas Leibler. A synthetic oscillatory network of transcriptional regulators. *Nature*, 403(6767):335–338, 2000.

[36] Michael B. Elowitz and Stanislas Leibler. A synthetic oscillatory network of transcriptional regulators. *Nature*, 403(6767):335–338, 2000.

[37] German A. Enciso. *Monotone input/output systems, and applications to biological systems*. PhD thesis, Graduate School – New Brunswick, Rutgers, The State University of New Jersey, 2005.

[38] James E Ferrell. Self-perpetuating states in signal transduction: positive feedback, double-negative feedback and bistability. *Current opinion in cell biology*, 14(2):140–148, 2002.

[39] James E Ferrell and Sang Hoon Ha. Ultrasensitivity part i: Michaelian responses and zero-order ultrasensitivity. *Trends in biochemical sciences*, 39(10):496–503, 2014.

[40] James E Ferrell and Sang Hoon Ha. Ultrasensitivity part i: Michaelian responses and zero-order ultrasensitivity. *Trends in biochemical sciences*, 39(10):496–503, 2014.

[41] E. Franco, G. Giordano, P.-O. Forsberg, and R. M. Murray. Negative autoregulation matches production and demand in synthetic transcriptional networks. *ACS Synthetic Biology*, 3:589–599, 2014.

[42] Elisa Franco, Eike Friedrichs, Jongmin Kim, Ralf Jungmann, Richard Murray, Erik Winfree, and Friedrich C. Simmel. Timing molecular motion and production with a synthetic transcriptional clock. *Proceedings of the National Academy of Sciences*, 108(40):E784–E793, 2011.

[43] Elisa Franco, Giulia Giordano, Per-Ola Forsberg, and Richard M Murray. Negative autoregulation matches production and demand in synthetic transcriptional networks. *ACS synthetic biology*, 3(8):589–599, 2014.

[44] Teruo Fujii and Yannick Rondelez. Predator–prey molecular ecosystems. *ACS nano*, 7(1):27–34, 2012.

[45] E. Fung, W. W. Wong, J. K. Suen, T. Bulter, S.-G. Lee, and J. C. Liao. A synthetic gene-metabolic oscillator. *Nature*, 435:118–122, 2005.

[46] Timothy S Gardner, Charles R Cantor, and James J Collins. Construction of a genetic toggle switch in *Escherichia coli*. *Nature*, 403(6767):339–342, 2000.

[47] A Goldbeter. *Biochemical Oscillations and Cellular Rhythms: The Molecular Bases of Periodic and Chaotic Behaviour*. Cambridge University Press, 1997.

[48] Albeter Goldbeter and DE Koshland. Ultrasensitivity in biochemical systems controlled by covalent modification. interplay between zero-order and multistep effects. *Journal of Biological Chemistry*, 259(23):14441–14447, 1984.

[49] Josef Hofbauer. An index theorem for dissipative semiflows. *Journal of Mathematics*, 20(4), 1990.

[50] Martin Jinek, Alexandra East, Aaron Cheng, Steven Lin, Enbo Ma, and Jennifer Doudna. Rna-programmed genome editing in human cells. *Elife*, 2:e00471, 2013.

[51] J. Kim and E. Winfree. Synthetic *in vitro* transcriptional oscillators. *Molecular Systems Biology*, 7:465, 2011.

[52] Jongmin Kim, Ishan Khetarpal, Shaunak Sen, and Richard M Murray. Synthetic circuit for exact adaptation and fold-change detection. *Nucleic acids research*, page gku233, 2014.

[53] Jongmin Kim, Kristin S White, and Erik Winfree. Construction of an *in vitro* bistable circuit from synthetic transcriptional switches. *Molecular systems biology*, 2(1), 2006.

[54] Jongmin Kim, Kristin S White, and Erik Winfree. Construction of an in vitro bistable circuit from synthetic transcriptional switches. *Molecular systems biology*, 2(1):68, 2006.

[55] Paul A Krieg and DA Melton. In vitro RNA synthesis with SP6 RNA polymerase. *Methods in enzymology*, 155:397–415, 1987.

[56] Tina Lebar, Urban Bezeljak, Anja Golob, Miha Jerala, Lucija Kadunc, Boštjan Pirš, Martin Stražar, Dušan Vučko, Uroš Zupančič, Mojca Benčina, Vida Forstnerič, Rok Gaber, Jan Lonzarić, Andreja Majerle, Alja Oblak, Anže Smole, and Roman Jerala. A bistable genetic switch based on designable DNA-binding domains. *Nat Commun*, 5:5007, 2014.

[57] Young Je Lee, Allison Hoynes-O'Connor, Matthew C Leong, and Tae Seok Moon. Programmable control of bacterial gene expression with the combined crispr and antisense rna system. *Nucleic acids research*, page gkw056, 2016.

[58] Azi Lipshtat, Adiel Loinger, Nathalie Q Balaban, and Ofer Biham. Genetic toggle switch without cooperative binding. *Phys Rev Lett*, 96(18):188101, May 2006.

[59] Vahid Mardanlou, Christian Cuba Samaniego, and Elisa Franco. A bistable biomolecular network based on monomeric inhibition reactions. In *Decision and Control (CDC), 2015 IEEE 54th Annual Conference on*, pages 3858–3863. IEEE, 2015.

[60] Vahid Mardanlou, Christian Cuba Samaniego, and Elisa Franco. A bistable biomolecular network based on monomeric inhibition reactions. In *Decision and Control (CDC), 2015 IEEE 54th Annual Conference on*, pages 3858–3863. IEEE, 2015.

[61] Vahid Mardanlou, Claire H. Tran, and Elisa Franco. Design of a molecular bistable system with RNA-mediated regulation.

[62] William T Mcallister, Hans Küpper, and Ekkehard KF Bautz. Kinetics of transcription by the bacteriophage-T3 RNA polymerase in vitro. *European Journal of Biochemistry*, 34(3):489–501, 1973.

[63] Deepak Mishra, Phillip M Rivera, Allen Lin, Domitilla Del Vecchio, and Ron Weiss. A load driver device for engineering modularity in biological networks. *Nature biotechnology*, 32(12):1268–1275, 2014.

[64] FJM Mojica, C Ferrer, G Juez, and F Rodríguez-Valera. Long stretches of short tandem repeats are present in the largest replicons of the archaea haloferax mediterranei and haloferax volcanii and could be involved in replicon partitioning. *Molecular microbiology*, 17(1):85–93, 1995.

[65] Kevin Montagne, Raphael Plasson, Yasuyuki Sakai, Teruo Fujii, and Yannick Rondelez. Programming an in vitro DNA oscillator using a molecular networking strategy. *Molecular Systems Biology*, 7(1):–, 2011.

[66] Francesco Montefusco, Ozgur E Akman, Orkun S Soyer, and Declan G Bates. Ultrasensitive negative feedback control: a natural approach for the design of synthetic controllers. *PLoS One*, 11(8):e0161605, 2016.

[67] Yusuke Mori, Yoshikazu Nakamura, and Shoji Ohuchi. Inhibitory RNA aptamer against SP6 RNA polymerase. *Biochemical and Biophysical Research Communications*, 420(2):440–443, 2012.

[68] Alec AK Nielsen and Christopher A Voigt. Multi-input CRISPR/Cas genetic circuits that interface host regulatory networks. *Molecular systems biology*, 10:11, 2014.

[69] Shoji Ohuchi, Yusuke Mori, and Yoshikazu Nakamura. Evolution of an inhibitory RNA aptamer against T7 RNA polymerase. *FEBS open bio*, 2012.

[70] Adrien Padirac, Teruo Fujii, and Yannick Rondelez. Bottom-up construction of *in vitro* switchable memories. *Proceedings of the National Academy of Sciences*, 109(47):E3212–E3220, 2012.

[71] Lei S Qi, Matthew H Larson, Luke A Gilbert, Jennifer A Doudna, Jonathan S Weissman, Adam P Arkin, and Wendell A Lim. Repurposing crispr as an rna-guided platform for sequence-specific control of gene expression. *Cell*, 152(5):1173–1183, 2013.

[72] Lei S Qi, Matthew H Larson, Luke A Gilbert, Jennifer A Doudna, Jonathan S Weissman, Adam P Arkin, and Wendell A Lim. Repurposing crispr as an rna-guided platform for sequence-specific control of gene expression. *Cell*, 152(5):1173–1183, 2013.

[73] Francesco Ricci, Alexis Vallée-Bélisle, and Kevin W Plaxco. High-precision, in vitro validation of the sequestration mechanism for generating ultrasensitive dose-response curves in regulatory networks. *PLoS computational biology*, 7(10):e1002171, 2011.

[74] D. Richeson and J. Wiseman. A fixed point theorem for bounded dynamical systems. *Illinois Journal of Mathematics*, 46(2):491–495, 2002.

[75] D. Richeson and J. Wiseman. Addendum to: "A fixed point theorem for bounded dynamical systems" [*Illinois J. Math.* 46(2):491–495, 2002]. *Illinois Journal of Mathematics*, 48(3):1079–1080, 2004.

[76] Christian Cuba Samaniego and Elisa Franco. A minimal biomolecular frequency divider. In *Decision and Control (CDC), 2015 IEEE 54th Annual Conference on*, pages 1277–1282. IEEE, 2015.

[77] Christian Cuba Samaniego, Giulia Giordano, Jongmin Kim, Franco Blanchini, and Elisa Franco. Molecular titration promotes oscillations and bistability in minimal network models with monomeric regulators. *ACS Synthetic Biology*, 5(4):321–333, 2016.

[78] Christian Cuba Samaniego, Sho Kitada, and Elisa Franco. Design and analysis of a synthetic aptamer-based oscillator. In *American Control Conference (ACC), 2015*, pages 2655–2660. IEEE, 2015.

[79] Maximilian Schlosshauer and David Baker. Realistic protein–protein association rates from a simple diffusional model neglecting long-range interactions, free energy barriers, and landscape ruggedness. *Protein science*, 13(6):1660–1669, 2004.

[80] Gideon Schreiber, Gilad Haran, and H-X Zhou. Fundamental aspects of protein–protein association kinetics. *Chemical reviews*, 109(3):839–860, 2009.

[81] E.H. Snoussi. Necessary conditions for multistationarity and stable periodicity. *Journal of Biological Systems*, 6:3–9, 1998.

[82] E.D. Sontag. Molecolar systems biology and control. *European Journal of Control*, 11:396–435, 2005.

[83] R Srzednicki. On rest points of dynamical systems. *Fundamenta Mathematicae*, 126(1):169–81, 1985.

[84] Samuel H Sternberg, Sy Redding, Martin Jinek, Eric C Greene, and Jennifer A Doudna. Dna interrogation by the crispr rna-guided endonuclease cas9. *Nature*, 507(7490):62–67, 2014.

[85] Jesse Stricker, Scott Cookson, Matthew R. Bennett, William H. Mather, Lev S. Tsimring, and Jeff Hasty. A fast, robust and tunable synthetic gene oscillator. *Nature*, 456(7221):516–519, 2008.

[86] Stanley Tabor and Charles C Richardson. A bacteriophage T7 RNA polymerase/promoter system for controlled exclusive expression of specific genes. *Proceedings of the National Academy of Sciences*, 82(4):1074–1078, 1985.

[87] Denis Thieffry, Araceli M Huerta, Ernesto Pérez-Rueda, and Julio Collado-Vides. From specific gene regulation to genomic networks: a global analysis of transcriptional regulation in *Escherichia coli*. *Bioessays*, 20(5):433–440, 1998.

[88] R. Thomas. On the relation between the logical structure of systems and their ability to generate multiple steady states or sustained oscillations. In Jean Dora, Jacques Demongeot, and Bernard Lacolle, editors, *Numerical Methods in the Study of Critical Phenomena*, volume 9 of *Springer Series in Synergetics*, pages 180–193. Springer Berlin Heidelberg, 1981.

[89] Marcel Tigges, Tatiana T. Marquez-Lago, Jorg Stelling, and Martin Fussenegger. A tunable synthetic mammalian oscillator. *Nature*, 457(7227):309–312, 2009.

[90] Tsz-Leung To and Narendra Maheshri. Noise can induce bimodality in positive transcriptional feedback loops without bistability. *Science*, 327(5969):1142–1145, 2010.

[91] Ulla Vogel and Kaj Frank Jensen. The RNA chain elongation rate in escherichia coli depends on the growth rate. *Journal of bacteriology*, 176(10):2807–2813, 1994.

[92] Maximilian Weitz, Jongmin Kim, Korbinian Kapsner, Erik Winfree, Elisa Franco, and Friedrich C. Simmel. Diversity in the dynamical behaviour of a compartmentalized programmable biochemical oscillator. *Nature Chemistry*, 6(4):295–302, 04 2014.

[93] A. T. Winfree. *The Geometry of Biological Time*. Springer-Verlag, New York, NY, 1980.

[94] Bernard Yurke and Allen P. Mills. Using DNA to power nanostructures. *Genetic Programming and Evolvable Machines*, 4:111–122, 2003.

[95] Jesse G Zalatan, Michael E Lee, Ricardo Almeida, Luke A Gilbert, Evan H Whitehead, Marie La Russa, Jordan C Tsai, Jonathan S Weissman, John E Dueber, Lei S Qi, et al. Engineering complex synthetic transcriptional programs with crispr rna scaffolds. *Cell*, 160(1):339–350, 2015.

[96] Bernd Zetsche, Jonathan S Gootenberg, Omar O Abudayyeh, Ian M Slaymaker, Kira S Makarova, Patrick Essletzbichler, Sara E Volz, Julia Joung, John van der Oost, Aviv Regev, et al. Cpf1 is a single rna-guided endonuclease of a class 2 crispr-cas system. *Cell*, 163(3):759–771, 2015.

[97] D. Y. Zhang, A. J. Turberfield, B. Yurke, and E. Winfree. Engineering entropy-driven reactions and networks catalyzed by DNA. *Science*, 318:1121–1125, 2007.

[98] David Yu Zhang and Georg Seelig. Dynamic DNA nanotechnology using strand-displacement reactions. *Nature Chemistry*, 3(2):103–113, 2011.

[99] David Yu Zhang, Andrew J Turberfield, Bernard Yurke, and Erik Winfree. Engineering entropy-driven reactions and networks catalyzed by dna. *Science*, 318(5853):1121–1125, 2007.